ISAS - INTERNATIONAL SCHOOL
FOR ADVANCED STUDIES

Compact Radio Sources. Beaming and shocks in jets

Thesis submitted for the degree of
"Magister Philosophiae"

Astrophysics Sector

Candidate:

José A. Acosta Pulido

Supervisors:

Prof. John Miller
Prof. Massimo Calvani

Academic Year 1987/88

TRIESTE

SISSA - SCUOLA
INTERNAZIONALE
SUPERIORE
I STUDI AVANZATI
TRIESTE
Strada Costiera 11

Acknowledgements

First of all I should thank my supervisors John Miller and Massimo Calvani for many helpful advises during the elaboration of this thesis. I think it was very hard for them try to understand my sentences and put them in a readable fashion. I am also indebted them for putting me to study this problem.

I also thank to Ewa Szuszkiewicz and Sanjiv Kumar for valuable comments on some parts of the text.

Undoubtedly, I should thank my colleagues of the Astrophysics Sector for solving me a lot of problems, very especially Mauro Orlandini ("il mostro di Latex"), Marco Bruni ("Mongo è bell-llissimo"). Roberto Scaramella gave me a precious program (he knows which), some graphs are made with its results.

At last, but not least, Armando Pisani and Antonella Diviacchi gave me the energy to stay in Trieste and enjoy the life simultaneously with the work.

Contents

Introduction 1

1 About compact radio sources 5
- 1.1 Introduction . . . 5
- 1.2 Morphology . . . 6
  - 1.2.1 Structural variations (Superluminal motion) . . . 7
- 1.3 Radio Spectrum . . . 10
- 1.4 Continuum spectrum . . . 11
- 1.5 Radio Variability . . . 12
- 1.6 Polarization . . . 14

2 Semidynamical Models of relativistic jets 17
- 2.1 Kinematical consequences of relativistic motion . . . 17
  - 2.1.1 Observed emission . . . 18
- 2.2 Inhomogeneous models of radio sources . . . 19
  - 2.2.1 A simple ballistic jet model . . . 20
  - 2.2.2 Two inhomogeneous jet models . . . 21
  - 2.2.3 Unresolved jet . . . 25
  - 2.2.4 Application of the two models to observations of BL Lac objects . . . 29

3 Statistical properties of the relativistic beaming hypothesis 32
- 3.1 Unified beaming models . . . 32
- 3.2 Source counts are not as precise . . . 38
- 3.3 Other interesting statistical results . . . 45
  - 3.3.1 Misalignments . . . 48
  - 3.3.2 Linear size of relativistically beamed sources . . . 49
  - 3.3.3 Independent evidences for relativistic motions . . . 51
  - 3.3.4 Infrared, Optical and Ultraviolet properties . . . 54
  - 3.3.5 Asymmetry in the polarization properties . . . 55

4 Shocks as the origin of radio variability **58**
4.1 Introduction 58
4.2 Adiabatically evolving structures 59
4.2.1 Comparison with observations 65
4.3 A piston driven shock 66
4.3.1 Observations 66
4.3.2 The model 70
4.3.3 Extension of the model to other sources 76
4.4 High frequency outbursts. Flare models 77
4.4.1 Observations 77
4.4.2 The flare evolution model 77
4.5 Modelling flows with shock waves. Calculating the spectrum 82

Appendices:

A Synchrotron radiation **86**
A.1 Synchrotron emission 86
A.1.1 Synchrotron self-absorption 87
A.1.2 Polarization of the synchrotron radiation 88
A.2 Compton scattering 89
A.2.1 Compton spectrum 90

B Emission from relativistically moving emitting sources **92**
B.1 Beaming Effect 92
B.2 Doppler effect 92
B.3 Lorentz transformations of the radiation field 93

Bibliography **96**

Introduction

The interpretation of the emission from radio galaxies and quasars as incoherent synchrotron radiation was already well established in the mid-1960's. The model was able to explain the characteristic radio spectra of the radio sources and the variations of the flux on times scales of years. Using arguments like equipartition of magnetic energy density and electron energy density it is possible to estimate the linear size of those sources and this resulted to be around 1 milliarcsecond. However the discovery of rapid variability in sources like 3C 273 presented considerable problems with the synchrotron theory. The short variability time scales indicates that the dimensions of the source are very small and hence the very high radiation energy density is present in the source as it is derived from the total output luminosity. This high energy density has catastrophical consequences for the existence of the source, the scattering of the radio photons by the same emitting electrons arises enormously the X-ray flux and the energetic losses for the electrons are drastics.

A satisfactory explanation of this question was presented by Rees (1967), who proposed that this problem could be alleviated if the sources were relativistically expanding. In that case the observed time scales do no correspond to the real time scales of the source, they are shorter than those in the frame of the source.

However the confirmation to this prediction came few years later, from the recent developments of Very Long Baseline Interferometry (VLBI) techniques, which allow to map the radio sources with an angular resolution of milliarcseconds ($\equiv$ m.a.s.).

Let us expend few words on the resolution capability of VLBI. The angular resolution achieved by these measurements reaches 1 m.a.s. at an observing wavelenght of 6 cm. In terms of linear resolution 1 m.a.s. ranges from a fraction of *pc* in nearby galaxies to few *pc* in most quasars. This means that we are looking at regions close to the central object; thus the narrow and broad emission line regions are well resolved with VLBI

observations, but we are still a little far from the central nucleus.

Moreover we consider that the processes occuring at the inner engine will be rather complicated and matter of other studies. We will only treat with processes which occur in the resolved structure without making any reference to their internal origin (see appendix on Phinney'85 for a justification of this point).

When the first VLBI observations (Cohen et al, 1971) reported that motions at speeds larger than that of the light were occuring in compact sources, it was realized that the relativistic expansion model could also account for the observed rapid motions if the axis of the source was oriented in a small angle with the line of sight.

However this interpretation was not accepted inmediatly and a proliferation of different models arose. They proposed that motions were not real but simply an illusion due to properly phase flux variations in stationary components. Moreover the one-sideness appearance of the source was proposed to be a real effect, the sources were supposed to be intrinsically one side.

It seems that now the observational evidence for superluminal motions is well established and the current model is the twin relativistic beam model (Blandford and Königl (1979)). In this model two similar antiparallel jets are escaping from the central source and the fact that we see only one side is a pure relativistical beaming effect and not an intrinsic asymmetry.

From the time of the discovering of the first superluminal sources up to now, the number of these has increased to roughly 25 sources with confirmed superluminal motions. Most of the brightest radio sources which have been observed with VLBI techniques show rapid separation motions between the components. This force us to believe that relativistic motions instead of being a rare phenomenon are rather common between radio sources.

Evidently there is a statistical problem with this hypothesis: if we select a complete sample of radio sources only a small number of those should have the special orientations requirements to show superluminal motions and relativistic beaming. Unfortunately there are two main problems to test this thesis. First, the choice of a sample free of orientation bias is a difficult task and it still is a motive of controversy. Second, the fraction of sources which present relativistic beaming in a supposed unbiased sample is model dependent and then looking at the statistics of radio sources it is not easy to rule out any model.

On the other hand there is a class of extragalactic sources identified by the properties of high variability and polarization of the radiation at optical frequencies, they are called *blazars* (Angel and Stockman, 1980). The superluminal sources are in general showing blazars properties, which is easily interpreted in a relativistic jet model if we consider that variability time scales are compressed by the motion of the emitting source and then

those that otherwise will be normal sources appear to be specially variable sources.

One of the most intriguing problems concerns to explain with a unique model the different time scales and amplitudes of the flux density variations observed in these particularly active sources. It is notorious the efforts of some groups (*e.g.* Bregman et al 1986, 1988) making sistematically simultaneous observations over a very large range of frequencies, from radio to X-rays. In the sources where relativistic beaming of the flux is believed to be important and perhaps dominant in the total observed radiation, it will be interesting to study the emission processes having place in the jet.

By the way the jet is imagined as a supersonic outflow which interacts with the enviroment and undergoes expansions and compressions, apart from the perturbations which come from the inner engine. Hence shock waves and rarefaction waves could be present in the propagation of the jet. For us it is interesting to identify these perturbations of the flow as the cause of the emission variability, shocks are enhancements of the brightness and rarefactions are invisible zones in the edges. The structure of the shock fronts could be important if we like to know the emission properties inside the jet. Moreover if the shocks are identified with the moving components we see on VLBI maps, their orientation and kinematics would determine the relativistic enhancement of the flux and the observed motions. Therefore the conclusion is that the shocks, if they are responsible of the emission, could modify substantially the observational consequences derived from more simple ballistic jet models.

These are the reasons why we believe interesting to study flows with shock waves propagating through them, as models for extragalactic jets. The ideal treatment of the problem should be done with magnetohydrodynamics, but since this complicates the problem and still we have no clear indications of the conditions in the medium in which jet propagates neither the conditions in the jet itself, an approximative treatment could be sufficient for the moment.

The plan of this work covers only a small part of this problem and it does not aim to be an extensive review but rather a starting point for future work.

In the first chapter we will give an insight to the observational status of the compact radio sources with emphasis on the more general features observed in this class of objects. The more impressive obsevations are coming from the radio band, in the sense that we have the higher resolution and hence well defined morphologies and variations of it. This motivates to construct jet models which are not homogeneous (the observed morphology is not homogeneous), with directional variations of the relevant parameters for emission quantities. We will describe what are the predictions of these models in the second chapter, moreover we will try to compare with obser-

vations to check the validity of them.

In the third chapter we will look at the statistical problems of the relativistic beaming hypothesis. The attempts to identify unbeamed populations of radio sources and what are their results compared with the observed statistics are mentioned. In the second part of this chapter we will examine how statistics of beamed sources changes with the model assumed for the emitting source. In the last part of this chapter we will consider other statistical studies which could help to establish the relativistic beaming hypothesis. Finally in the last chapter we will present works considering how shocks waves will modulate the emission of the jet. These models are not dynamically exact, they rather approximate features, shock fronts, concerning mainly the propagation through the jet.

Chapter 1

About compact radio sources

1.1 Introduction

At present the radio observations of extragalactic radio sources are able to distinguish between three different emission regions :

- diffuse emission coming from more or less symmetric radio lobes which straddles the central parent object
- narrow, rather well collimated beams, and hot spots in the line joining the central object and the outer lobes
- finally, the compact central source, which is in general coincident and well identified with a galactic nucleus or a quasar.

The jets are considered as channels which fairly efficiently transport energy from the central engine to the outer lobes, solving the problem of the large observed radio luminosities ($10^{45} ergs/sec$ between 10 MHz. and 100 GHz.), and the energetic requirements (as much as 10^{61} ergs) in relativistic particles and magnetic fields derived from equipartition arguments. Moreover these jets should be supersonic outflows at least in the inner parts since the conditions of the external medium are not perturbing the innnermost parts of the jet. Blandford and Rees (1974) considered a simple model in which the acceleration of the flow is occuring through a nozzle. The model consider a central source of hot particles with high internal energy, surruounding the central object exists a plasma which has steeper pressure and density gradients in one direction. This favours the formation of a channel with a nozzle such that when the flow passes through it becomes supersonic.

There are many variations on this overall scheme of the radio structure and there have been general reviews on extended sources and large scale structure of the jets, collimation problems, interaction with the medium (see

the extensive reviews of Begelman, Blandford and Rees, 1984 and Bridle and Perley, 1984). However this thesis will be centred on the compact central source, identified with the active nucleus, and more specifically on the intrinsic compact radio sources, sources whose emission angular size is a few arcseconds, identified with BL Lac objects or OVV's. [1] In general all of them show high surface brightness, strong polarization and variability on time scales from months to years and predominantly flat or inverted radio spectra, at higher frequencies the spectrum steepens.

1.2 Morphology

Extensive surveys of compact radio structures have been made by several groups (Pearson, Readhead, 1988 and previous references; Eckart et al., 1985; Romney et al., 1984). A rough classification of the observed structures as *very compact*, *core–jet*, *compact double* or *complex* can be made (Porcas, 85), with the hope of differentiating real properties of the sources.

More specifically, Pearson and Readhead classify the sources into 6 groups:

- *Very compact sources*: these sources are only barely resolved and 95% of their flux density is in an unresolved core; they are associated with quasars and BL Lac objects exclusively, showing high variability and polarization.

- *Asymmetric sources (core–jets)*: these are characterized by a strong compact component at one end of a lower brightness linear feature. The core has a flat spectrum while the linear feature has a steeper, optically thin spectrum. They show variability, but not as violent as in the previous category.

- *Symmetric sources or Compact Doubles*: these objects consists of two components of almost equal brightness, the separation between them usually being larger than the extension of the asymmetric sources. The spectrum is steep at high frequencies with a smooth hump, peaking at around 1–5 GHz. They show low polarization and variability is almost absent. Remarkably they do not show any extended structure at the arcsecond scale.

- *Central components of classical double sources*: in general, these show good alignment between the central structure and the outer lobes.

[1] BL Lac objects are characterized by the absence of emission lines in their spectrum. OVV's(Optically Violent Variables) are quasars, which show high percentage of polarization and strong variability.

In most cases they are very weak and VLBI measurements are not available. However in those cases where small scale structure has been resolved interesting features appear (*e.g* superluminal motion, core-jet structure with two-sided ejection).

- *Steep spectrum compact (SSC)*: these show a steep spectrum, usually flat at high frequencies, where the core dominates, and a low frequency turnover near 100 MHz. The m.a.s.(m.a.s.≡milliarcsecond) structure is complex with a compact, flat-spectrum core and a central jet (dominating the emission) with steep spectrum and polarization. The large scale structure is misaligned, by as much as 90° in the case of 3C 216. The general belief is that they are intrinsically small and strongly interact with the ambient medium.

- *Unclassified sources*: these show complex structure, which can not be identified unambiguously with any of the previous categories.

The sources of interest in this thesis are the ones which manifest considerable variability, since in these the relativistic effects are thought to be important and the special orientation of the emitting sources combined with high velocities will be able to explain the peculiar *superluminal motion.*[2]

1.2.1 Structural variations (Superluminal motion)

Using VLBI monitoring of strong, compact radio sources, superluminal motion has been found by the same authors (Pearson and Readhead), for every category in the previous classification, except for that of compact double sources.

The observed superluminal motion is simply modelled by a blob moving away, at relativistic velocity from a stationary core. The apparent transverse velocity of separation is

$$v_{app} = \frac{v \sin\theta}{1 - \frac{v}{c}\cos\theta}$$

where θ is the angle between the jet axis and the line of sight and v is the velocity of the blob.

For a measured apparent transverse velocity, v_{app}, we can take combinations of the orientation angle and the velocity besides there is a value of θ, θ_{min} which minimizes v and hence γ. On the other hand there is a limit in the value of the velocity, v cannot exceed c and this puts a limit on the angle θ with the line of sight, θ_{max}. These two values of the angle gives

[2]Measured at two different times the angular separation of two components, the apparent transverse velocity is greater than the speed of light.

us an indication of the possible orientation of the source such that exhibits that superluminal motion.

This model implies a preferred orientation of the sources which show this apparent motion; moreover the radiation emitted by these sources is Doppler boosted, so that we will preferentially see radiation coming from sources pointing towards us.

While some superluminal sources are one-sided, many are found to have two-sided large scale structure. Extensive studies of the ocurrence of superluminal motion indicate that it is probably a rather common phenomenon, appearing in various very different scenarios, including those in which one will expect to find no special relativistic effects (*e.g.* in the nucleus of sources which are supposed to be oriented close to the plane of the sky, almost perpendicular to our line of sight).

There are several questions that should be answered, to clearly identify the cause of motion observed in these sources, for example:

- are the features which we see real blobs, strong shocks, or something else?
- do successive features follow the same path from the core?
- are all of them accelerated to the same velocities?

The answer to these questions would come from the natural improvement of the techniques of observation, a higher dynamic range, or better from a well established set of observations.

Let us look at one example. A very well studied superluminal source is 3C 345, Unwin et al. (1983) presented observations made at different times (see fig 1.1). Looking at the displacements of the components they found an apparent tranverse velocity of about 15c. With the usual relativistic jet model they constrained the angle of the axis with the line of sight to a maximum value $\theta \sim 7°$ and a minimum Lorentz factor $\gamma \sim 6$. The emission from the nucleus is dominant and so there is no obvious correlation between the flux density history and the evolution of the components or morphological changes, *i.e* in principle we can not expect to detect new superluminal events from the total flux variations.

An important fact is that the components, and the nucleus change spectral index with time (see fig 1.2b). Any model must be able to explain these details: the steepening of the spectra for the knots suggests radiation losses. However the time scale for synchrotron losses is 10^6 years. Moreover a simple model of adiabatic losses in a homogeneouos sphere (*i.e.* a power law) can not fit the observed decrease in flux density (see fig 1.2a).

The conclusion is that an homogeneous simple model is turning out to be inadequate to explain all of the observed features (*e.g.* the observed

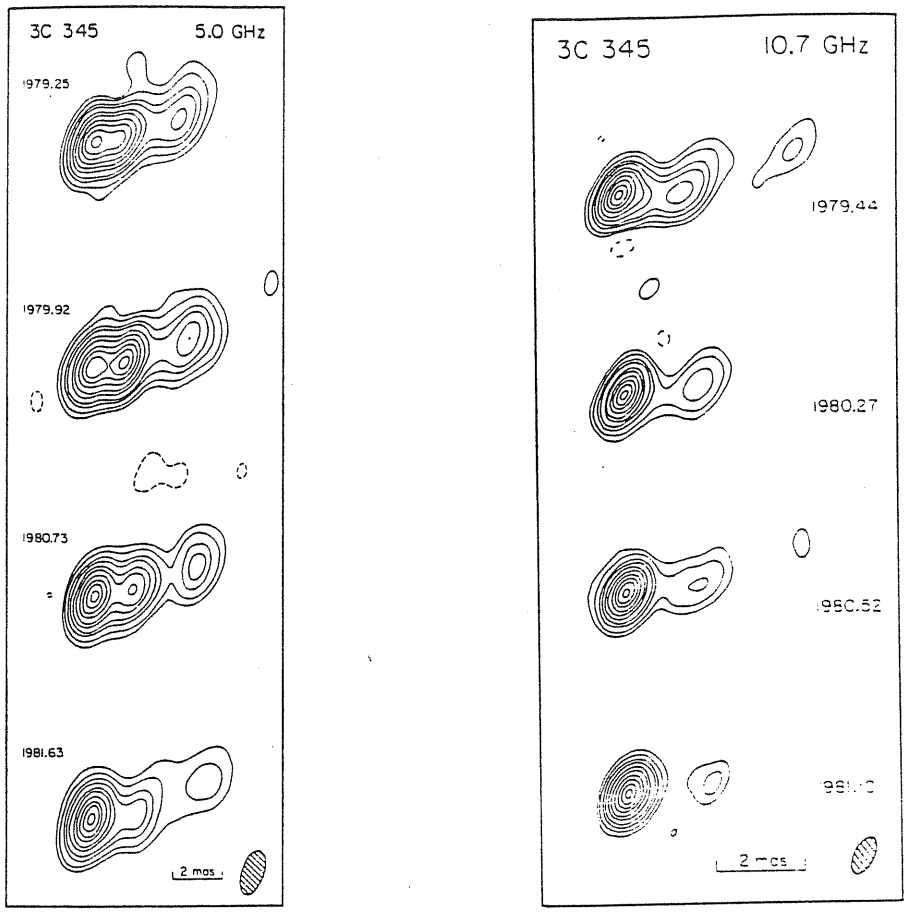

Figure 1.1: VLBI maps at differents times, from Unwin et. al. 1983

variation of the flux density and the variation of the spectral index of the components).

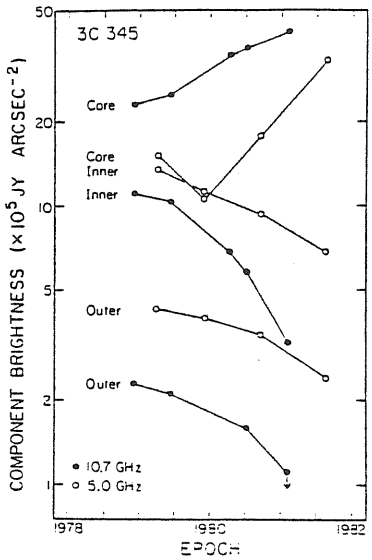

Figure 1.2a Variations of the peak brightness of the different components , from Unwin et al.(1983)

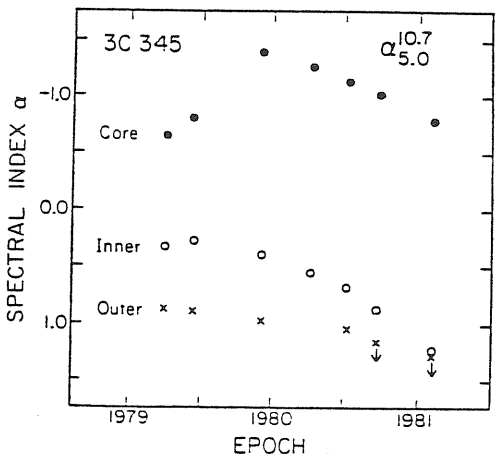

Figure 1.2b Evolution of the spectral index ($S_\nu \propto \nu^{-\alpha}$), from Unwin et al.(1983)

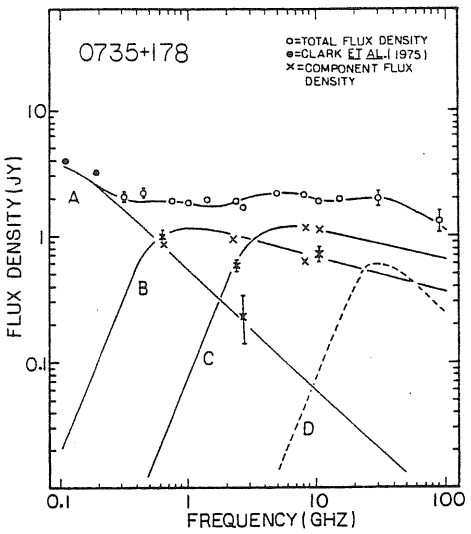

Figure 1.3: "Cosmic Conspiracy", from Cotton et al. (1980)

Unwin et al'83 proposed non homogeneous emitting knots, when they are moving along the jet the characteristics of the emission will change because the conditions are changing. In the chapter 4 we will introduce models in which changes of spectral index are present.

A very extended survey of superluminal sources has been made by Porcas(1986) and Pearson and Readhead(1988). They include possible candidates and also sources with confirmed subluminal behaviour.

1.3 Radio Spectrum

Compact radio sources have flat, undulating or inverted radio spectra.

The flattening of the spectra can be interpreted in terms of spatial inhomogeneities, different parts of the spectrum becoming opaque at different wavelengths so that in superposition, they broaden the self-absorption cutoff [3]; however the coincidence of producing a flat spectrum is rather fortuitous, and this is called "Cosmic Conspiracy".

Cotton et al. (1980) modelled the flat spectrum of the source $0735+178$ by adding four sub-components which have peaks at different frequencies (see fig 1.3). This confirms that the flat spectrum can be obtained by combining non-homogeneous self-absorbed subcomponents.

The tendency is to believe that long wavelength emission is dominated by radiation coming from the outer regions, where there is less self-absorption because self-absorption of the synchrotron emission occurs at higher density of electrons, or at lower frequencies.

In the small scale structure it is possible to distinguish between a flat

[3] A self-absorbed synchrotron spectrum is a peaked spectrum at the frequency ν_m, below this frequency, an inverted spectrum is seen $S_\nu \propto \nu^{2.5}$, above this frequency there is the usual synchrotron spectrum $S_\nu \propto \nu^{-\alpha}$, with $\alpha \sim 0.7$

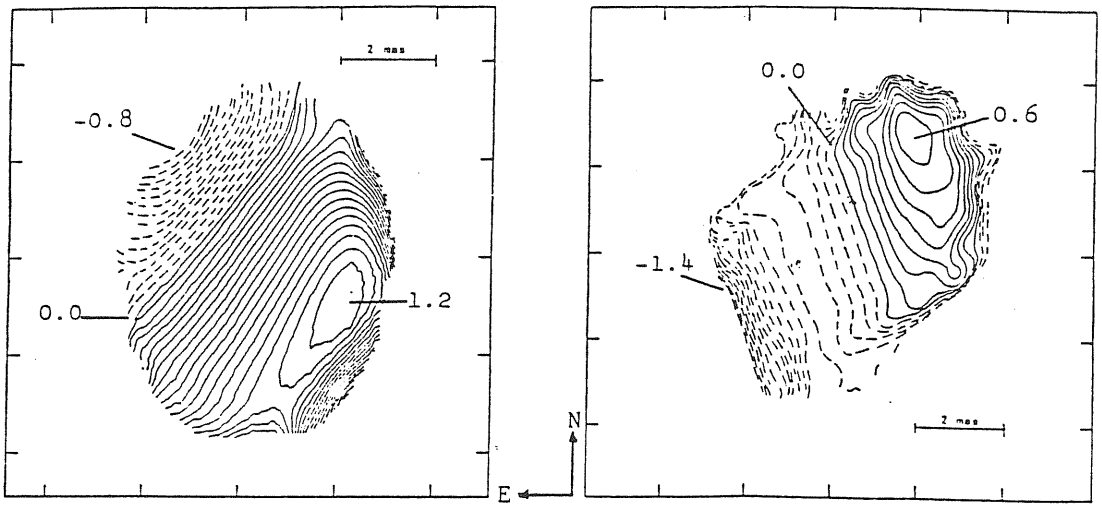

Figure 1.4: Mapping of the spectral index, from Marcaide et al. (1984)

spectrum bright nucleus and a low surface brightness jet showing a steep spectrum.

Spectral index mapping of m.a.s. structure may give a lot of information, but at present only few sources have been mapped in this fashion. It is difficult to obtain spectral index maps by using the VLBI technique. There are several problems in doing this. The sources cores are strongly variable so that observations must be made quasi simultaneously at the different radio frequencies. The lack of absolute position information makes difficult to combine maps at different time expositions and moreover the resolution of VLBI is a decreasing function with the increasing wavelenght. The chance to make spectral radio maps is given when there are two objects very close and it is possible to take one as reference.

Marcaide and Shapiro (1984) made maps for the two close quasars $1038+528A,B$, which showed the typical structure of core-jet sources: an inverted spectrum core component at one end of the structure and an extended component with spectral index steepening with increasing distance from the core (see fig 1.4)

1.4 Continuum spectrum

The understanding of the continuum spectrum of the core of radio sources is an important point. Some theories make predictions about other than radio frequencies regions of the spectrum and this should be checked with observations.

Since the spectrum shows strong variability the observations at different

frequencies should be made simultaneously. This supposse a strong effort to combine all the observations at the different ranges, however it has been carried for more than ten objects (see Bregman, 1985).

In order to known what is the dominant mechanisn in the production of energy is also important to look at the power emitted at different regions (νF_ν).

Let us first distinguish between the different spectrum observed for different classes of active nuclei, but we will only consider those in which non thermal process are dominant. Generalizing we could divide the objects in normal radio quasars and blazars.

Radio quasars are characterized by the high emission at radio frequencies with a smooth curved spectrum extending from 10^9 to 10^{14} Hz. They show the UV bump, probably associated with an accretion disk. The X-rays emission could be connected with the infrared component. The power is roughly equally emitted from infrared to X-rays.

Blazars have a flat spectrum at radio wavelenghts and an extended curved spectrum from 10^9 to 10^{15} Hz, more curved than the radio quasars. The UV bump is weakly observed. The X-rays are stronger than the extrapolation from UV frequencies. The power is concentrated at infrared frequencies.

Since blazars are more interesting for this work I give a more detailed description. The characteristic radio spectra of these sources is extended up to several tens or few thousands of GHz. Above this frequency the spectrum is steepen to a spectral index around 1. From 100-1 μm the spectrum could steep again to an spectral index in the range 1 to 1.5. In the optical to ultraviolet sometimes it is observed spectral indices of order 3. An exponential fall off is observed in different regions of the spectrum ranging from the infrared, in red quasars, to UV, in some BL Lacs.

An extended study of the average spectral indices in different spectral regions for radio selected and X-rays selected blazars can be found in Ghisellini et al. (1986). An important result is that X-rays selected quasars are showing flatter spectra than radio selected quasars in all frequencies ranges.

1.5 Radio Variability

The observed time scales for the variation of the flat spectrum radio sources are of the order of months to years, indicating that emission comes from small regions $l \lesssim c\,\Delta t_{var}$, so if $\Delta t_{var} \sim 4\ months$, then $l \sim 0.1pc.$ ($1pc. \sim 3light - years$). This region is still three orders of magnitude larger than the *Schwarzschild* radius of a possible central black hole ($\sim 10^9 M_\odot$).

Conventionally, variability is separated into two different ranges of radio frequencies:

- high frequency variability ($> 1GHz.$)
- low frequency variability ($< 1GHz.$)

At high frequency, the variability is characterized by variations of the flux density in the range of 20% to 50%, and by superposition of events in a short time (single outbursts are rare). The variations are larger at higher frequencies. This can be explained qualitatively in terms of an adiabatically expanding sychrotron emitting cloud.

On the other hand, at low frequencies the variability time scales are usually shorter, but the variations are larger in amplitude. The short timescales are in conflict with the inverse Compton problem, when the energy density of the radiation is sufficiently high the synchrotron photons are scattered by high energy electrons which lose their energy, producing an excess of X-ray emission, thus that unless new energetic electrons are supplied, the source dies. With moderate Lorentz factors, relativistically expanding models lower the brightness temperature below the limit of $10^{12^o}K$, which is the usual limit for the inverse Compton problem.[4]

In general three classes of variability are observed (Padrielli et al., ??):

- variability only at low frequencies ($\lambda \sim 1m.$): the optical counterparts of these objects are galaxies and QSO's. [5]
- variability at high and low frequencies, but uncorrelated, and with a minimum at around 2.5 GHz.
- correlated variability in both frequencies ranges.

[4]The Compton limit is obtained by assuming that the Compton catastrophe occurs when the inverse Compton scattering power exceeds the synchrotron emitted power

$$\frac{P_{Comp}}{P_{synch.}} \lesssim 1$$

and

$$\frac{P_{Comp.}}{P_{synch.}} = \frac{U_{synch.}}{U_B}$$

so that

$$\frac{kT_b\nu_s^3}{c^3} \lesssim \frac{B^2}{8\pi}$$

and ν_s is taken to be the maximum of the synchrotron spectrum.

T_b is found to be independent of ν_s and B and the value is $T_b \lesssim 10^{12^o}K$.

[5]There is some evidence that low frequency variability could be attributed to interstellar scintillation (resulting from slow variations in the refractive index of the interstellar medium), as is the case for pulsars, Sieber (1982). This mechanism only works for sufficiently compact sources.

BL Lac objects show variability over the whole range of frequencies, starting at higher ones with higher amplitudes, and propagating down to lower frequencies with decreasing amplitude.

1.6 Polarization

Significant (sometimes exceeding 10%) and variable polarization is found in most compact radio sources, especially in OVV's and BL Lac objects.

Detailed observations of the variations of linear polarization are difficult, since the degree of polarization is only a few percent of the total flux, whereas the time scale appears to be much shorter than for variations of the total flux.

In some cases the polarization angle remains constant, but in many cases it changes in a rather random way.

However a smooth and monotonic change in polarization angle is seen in some of these events. The BL Lac object $0235+16$ underwent an outburst in late 1975; during the decay the polarization angle rotated through an angle of $\sim 130\ ^\circ$ (Ledden and Aller, 1978). BL Lacertae also showed changes in the polarization angle, during outbursts in 1981–1983 (Aller,Aller and Hughes, 1985). The object OJ 287 showed a rapid variation of polarization angle simultaneously in the optical and radio frequencies, during February 1986 (Kikuchi et al., 1988). The swing in the polarizxation angle occurred at radio wavelenght before than at optical. They also found that the maximum rate of variation occurs associated with a minimum of the degree of polarization. The same behaviour has been observed in other BL Lac object ON 325(Barbieri et al., 1988).

Faraday rotation is ruled out as a possible cause in most cases because the variation is independent of the frequency. Rotation of the magnetic field may be the most straighforward explanation, as proposed initially by Blandford and Königl (1979). The behaviour described above is consistent with this model but also with a two components model (Björnsson, 1982).

However the most promising model to account for the smooth polarization swings is the model developed by Königl and Choudhuri (1985) in which a shock front is propagating down in a helical (*i.e.* non axisymmetrical) configuration of the magnetic field.

When the viewing angle is small the propagation of the shock will produce a rotation of the polarization angle. The swing in polarization angle is highly non uniform when the viewing angle is close to $\cos\theta = \beta_{postshock}$, this could explain the more common observed erratic behaviour of the polarization.

This model predicts also an oscillation of the degree of polarization and the minimum coincides with the maximum jump in the polarization angle.

Measurements of polarization at VLBI scales reveal the sources as resolved into a low polarization flat-spectrum core and a more highly polarized steep-spectrum jet; the orientation of the polarization vector is seen to be parallel to the source in the core and perpendicular to it in the jet. From the work of Roberts and Wardle(1985) some clues emerge about the polarization structure and hence magnetic field structure, (see fig 1.5) in the compact radio sources:

The observations show that the cores of the quasar 3C 345 and the galaxy 3C 120 are substantially less polarized than the jet part. This is reflected in a displacement of the centroids in the I and P maps. [6] In 3C 345 they noticed a change in the orientation of the polarization, from perpendicular to the jet close to the core, to alignment with the jet in the outer parts. In 3C 120 (a superluminal source, with extended structure), the polarization is concentrated in the jet component; however most of the polarization seen at arcsecond structure is missing. The BL Lac object OJ287 has a highly polarized core and strongly variable structure (see the two different time maps shown in fig1.5).

This overall behaviour is expected from a synchrotron source where the jet is optically thin. Then the polarization vector is perpendicular to the magnetic field. Whereas in the optically thick, self-absorbed core, the polarization is very low, the residual component being that parallel to the magnetic field, in which direction there is a smaller optical depth (we should remember that absorption of the synchrtron radiation occurs preferentially in the direction of the magnetic field).

[6]The Stokes parameters, I and P, represent total and polarized flux density, respectively.

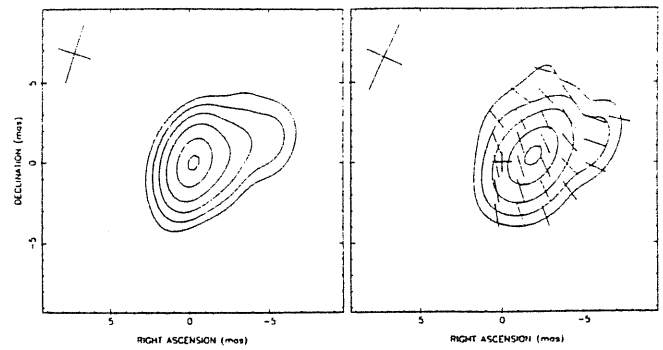

3C 345 at 5 GHz, epoch 1981.9

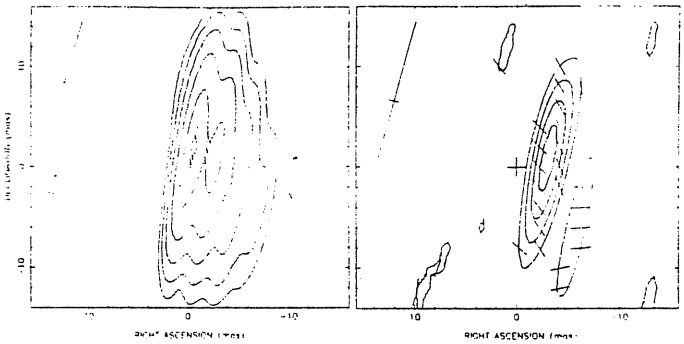

3C 120 at 5 GHz, epoch 1982.9.

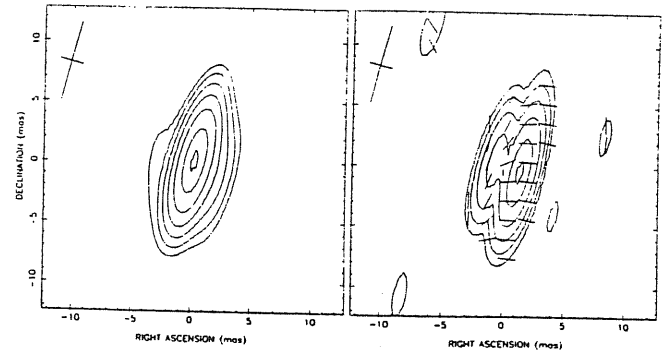

OJ 287 at 5 GHz, epoch 1981.9.

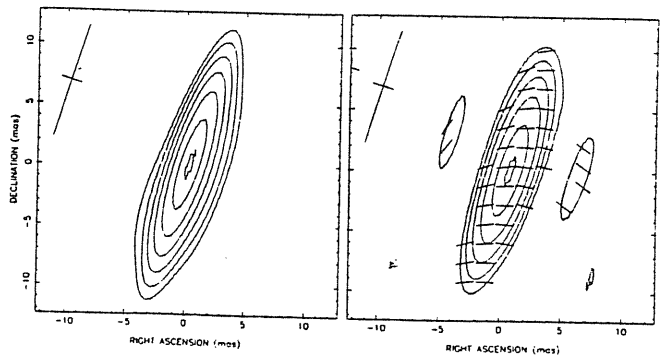

OJ 287 at 5 GHz, epoch 1982.9.

Figure 1.5: VLBI maps of I and P Stokes parameters. Left, total intensity map;right, complex polarization map (from Roberts and Wardle,1986)

Chapter 2

Semidynamical Models of relativistic jets

In this chapter we will present simple models of relativistic jets. We will consider the emission coming from these jets but we will forget about the considerations of the dynamical support for these models. Therefore our basic model is an outflow of plasma with a certain magnetic field emitting incoherent synchrotron radiation. The velocity of the flow will be considered constant and the orientation of the jet is critical for producing the Doppler boosting of the radiation and the observed relativistic motions.

First of all, let us look at the implications of having a stream of emitting fluid moving in a direction close to our line of sight with relativistic speed.

2.1 Kinematical consequences of relativistic motion

Suppose a source which is moving with a velocity v in a direction making an angle θ with the direction of the observer. Then the observed velocity is given, as in the previous chapter, by the expression:

$$v_{obs} = \frac{v \sin\theta}{1 - \frac{v}{c}\cos\theta}$$

If we consider v as a fixed value, there is an angle for which v_{obs} shows a maximum, this value corresponds to $\cos\theta = v/c$ or $\sin\theta = 1/\gamma$. But this maximum will exceed the value of c only for values of $v > c/\sqrt{2}$, hence a minimum bulk Lorentz factor $\gamma = \sqrt{2}$ is needed to produce superluminal motion.

Alternatively what we obtain from observations is the value of v_{obs} and a minimum value of v may be desiderable because the acceleration mechanisms which are operating in the more internal parts of the jet could be

inefficient. This minimum value occurs when $\cot\theta = v_{obs}c$ and the value of $\gamma = \sqrt{1 + v_{obs}/c}$.

On the other hand an upper limit to the value of the angle with the line of sight can be obtained when $v \rightarrow c$ and for a known value of v_{obs} this angle is given by: $\cot(\theta/2) = v_{obs}/c$.

2.1.1 Observed emission

The flux emitted by a source which is moving with respect to an observer will undergo changes in the frame of the observer, if that source is moving with a relativistic velocity. That changes should be computed using the appropiate Lorentz transformations. An standard derivation can be found in Rybicki, Lightman (1970) (see also appendix B); for us is sufficient to consider how the basic quantities change:

Suppose a reference frame K' which is moving with a velocity β with respect to a rest frame K (quantities with the prime are in the prime reference frame). Then the radiation reaching the observer is emitted at an angle θ with the direction of motion in the frame K. The basic quantities determining the radiation field are then transformed as follows:

- Specific intensity
$$I'_{\nu'} = \left(\frac{\nu}{\nu'}\right)^3 I_\nu$$
- Emission coefficient
$$j'_{\nu'} = \left(\frac{\nu}{\nu'}\right)^2 j_\nu$$
- Absorption coefficient
$$k'_{\nu'} = \left(\frac{\nu}{\nu'}\right)^{-1} k_\nu$$

where $\mathcal{D} = \nu'/\nu$ is the Doppler factor given by the expression $\mathcal{D} \equiv 1/\gamma(1 - \beta\cos\theta)$.

For the case of an optically thin synchrotron emission the flux density we receive is given by the expression

$$S_{obs}(\nu) = \mathcal{D}^{3+\alpha} S(\nu);$$

deriving this expression one should consider that the flux for the optically thin case is proportional to the emissivity and moreover the synchrotron power law spectrum is assumed. This expression has strong implications on the appearance of the source. If we have a source with two antiparallel

jets, oriented very close to our line of sight the flux of the side approaching to us will be enhanced by a factor

$$R(\theta) = \left[\frac{(1+\beta)}{(1-\beta)}\right]^{3+\alpha}$$

with respect to the side which is receding.

Anyhow, the boosting of the radiation will change depending on the model which is adopted for the kinematics of the emitting material.

For instance, in the case of an optically thin plasma flowing in volume which is at rest in the observer frame, the flux is transformed as transforms the emissivity, so that the flux will change as:

$$S_{obs}(\nu) = \mathcal{D}^{2+\alpha} S(\nu).$$

In the appendix B this is considered in more detail (or see Lind and Blandford, 1985).

2.2 Inhomogeneous models of radio sources

The classical homogeneous model of a radio source consists of a spherical source in which all the quantities are considered to be uniform in the whole extension of the source (Jones,O'Dell and Stein 1974); this model in general needs to strech out the parameters to rather unlikely values.

A realistic model of compact radio sources adopt the presence of a jet; naturally the relevant quantities, magnetic field, electron energy density and number density are considered to vary along the jet. These are inhomogeneous models of jets.

The inhomogeneuos models have the problem of the high number of parameters which are not easily constrained.

Several inhomogeneous models of jets have been proposed, among others Marscher (1977,1980), Blandford and Königl (1979), Königl (1981), Reynolds(1982), Ghisellini, Maraschi and Treves (1985). The differences between these models are basically in the adopted geometry, the assumed energy distribution of the electrons, the maximum energy and in some cases in the dynamical models underlying the bulk motion of the flow, *e. g.* the models presented by Reynolds (1982) consider the acceleration of the jet flow solving consistently the dynamics equations.

The main goal of these models is to explain the differences between the observed spectra and the expected spectrum for a single power law energy distribution of emitting electrons. By the way these models try to explain the different variability timescales occurring at different spectral regions, indicating which different zones are responsible of the emission in each region of the spectrum.

2.2.1 A simple ballistic jet model

The first simple jet model I will consider was proposed by Blandford and Königl (1979). This model solved in a very natural way the problem of having a stationary core and outer components moving with relativistic velocities but with the flux boosted by the same Doppler factor.

The radio emission is originated by synchrotron electrons which are locally accelerated within the jet.

In this model a narrow collimated beam of emitting material will be oriented in a small angle, close to our line of sight. The magnetic field is varies as r^{-1} being r the distance along the jet. Moreover equipartition of the magnetic density energy with the electron energy density is assumed and then the running of the electron energy density is fixed.

The electrons will undergo synchrotron losses, larger losses at higher frequencies, such that they will emit up to a frequency ν_b an optically thin synchrotron spectrum. This frequency is estimated to be directly proportional to the distance r from which the flux is observed. Above this frequency for that distance the spectrum steepens to a spectral index close to unity, due to synchrotron losses.

The observed brightness temperature has a maximum value which is independent of the frequency. And it is localized at a radius r_{max} which is inversely proportional to the frequency. At radii less than this value for the same frequency the spectrum becomes optically thick. Therefore this radius should be the radius of the core at that observing frequency [1]. The corresponding angular size for 3C 345 is estimated by the formula $r_{max}/D \sim 1.8\nu_9^{-1} m.a.s.$, which is consistent with the observations.

The maximum observed flux is also independent of the frequency because at a given frequency the flux is $S_{obs} \propto r_{max}^2 \nu^2 T_{max}$. Therefore the spectrum will be flat up to a frequency ν_b such which is the maximum emitted frequency for that radius, r_b. Above this frequency the spectrum steepens and is dominated by the emission coming from distances nearly less than r_b.

In this way this model proposes that we will see an optically thick core with flat spectrum and at outer distances, where the jet becomes optically thin, the moving components appear. But both regions the core and the jet are Doppler boosted by the same Doppler factor and hence they will have similar enhancement of the flux.

[1] They noted that this radius is frequency dependent and furthermore it has the same dependency that the resolution of the observations using interferometric techniques. Therefore if at a given VLBI frequency the core is not resolved it could not be resolved at higher frequencies

2.2.2 Two inhomogeneous jet models

The aim of this section is to explain how inhomogeneous models work and what are their predictions about variability time scales and integrated spectra. For this reason I selected two of the models mentioned previously. The two rather simple models I will describe are: as first model, the one presented by Blandford and Königl (1979) and in a subsequent paper by Königl (1981), the second model is described in Ghisellini, Maraschi and Treves (1985). In spite ot their simplicity they include the main observed features of inhomogeneous models.

Both models assume an impose motion of the flow, characterized by a constant bulk velocity v_j. The emission coming from the jet is assumed to be incoherent synchrotron radiation and in adittion inverse self-Compton scattering will contribute at higher frequencies, X-rays.

A narrow, axially symmetric jet is considered oriented within an angle θ with the line of sight. We take a coordinate R determines the distance through the jet while the coordinate r is giving the transverse width of the jet.

In the first model the geometry will be assumed to be conical; instead in the second model a parameter ϵ is determining the shape of the beam,

$$r \propto R^{\epsilon}$$

the only constrain to the value of this parameter is that the jet is supposed to be collimated, hence ϵ should be less than or equal to 1.

The magnetic field is assumed to vary with r as

$$B(r) = B(r_o)(r_o/r)^m = B(R_o)(R_o/R)^{\epsilon m}$$

The distribution of the particle energy is assumed to be a power law for the relativistic electrons within a range of energy comprissed between $\gamma_{e_{min}}$ and $\gamma_{e_{max}}$:

$$N(\gamma_e) = K_e \gamma_e^{-\alpha_e}$$

For energies above the maximum value $\gamma_{e_{max}}$ the energy distribution and the spectrum will have a cutoff or steepening to higher slopes, when synchrotron or adiabatic losses are important.

The number distribution of electrons is also assumed to vary as a power law with the radius r:

$$K_e(R) = K_e(R_o)(r_o/r)^n = K_e(R_o)(R_o/R)^{\epsilon n}$$

In the first model an estimation of the maximum energy of the electrons is made by equating the synchrotron cooling time to the expansion time

along the jet axis, which is assumed to be comparable to the reacceleration time scale. Then

$$t_{synch} \sim 3 \times 10^7 \gamma_j \mathcal{D}_j^{\alpha} \nu_9^{-\alpha} B^{-(1+\alpha)} sec$$

and

$$t_{exp} \sim 10^8 R \beta_j sec$$

which yields

$$\nu_{b_9} \simeq 0.07 (\gamma_j \beta_j)^{1/\alpha} \mathcal{D}_j B_o^{-(1+\alpha)/\alpha} R^{-k_b},$$

where

$$k_b = \frac{1 - \epsilon m(1+\alpha)}{\alpha}$$

and R is measured in pc.

For the first model $\epsilon = 1$ and assuming a magnetic field which is predominantly parallel to the jet axis (*i.e.* $m = 1$), a conventional spectral index $\alpha = 0.5$, k_b takes the value -1, such that the high frequency cutoff is increasing with the radius.

An estimation of the maximum electron energy is obtained by taking the energy of the electrons which radiates at the frequency ν_b

$$\gamma_{e_b}^2 = \frac{\nu_b}{\nu_B}$$

where $\nu_B \propto B$ and then

$$\gamma_{e_b}^2 \propto \frac{R}{R^{-m}} \propto R^{(1+m)}$$

However in the second model the maximum electron energy is given by

$$\gamma_{e_b}(R) = \gamma_{e_b}(R_o)(R_o/R)^{ee}$$

with $e > 0$.

Then the maximum frequency produced by optically thin synchrotron emission is:

$$\nu_b(R) = \nu_b(R_o)(R_o/R)^{\eta},$$

where $\eta = \epsilon(2e + m)$.

There is a significant difference in these two assumptions: in the first case an excess of high energy electrons is found at the outer radii, because the magnetic field is weaker in the outer regions and hence the electrons will radiate less energy in form of synchrotron emission. However in the second case the higher energy electrons are found in the inner radii and this is assumed a priori.

The validity of one assumption against the other will depend on the acceleration mechanism of the electrons and whether this is expected to be

more efficient in the base of the jet as for the second model or everywhere in the jet has the same efficiency as for the first model.

The locally emitted synchrotron spectrum will be characterized by an optically thin part, with an spectral index α_o, related to the index of the electron distribution function by the expression $\alpha_e = 2\alpha_o + 1$.

This will be extended down from the frequency $\nu_{s_m}(R)$ which corresponds to the maximum in the spectrum. At this frequency the optical depth to synchrotron self-absorption is almost equal to unity. Below the frequency $\nu_{s_m}(R)$ the source becomes optically thick and then the spectrum rises with the frequency as $\nu^{5/2}$.

There will be a high frequency cutoff corresponding to the frequency ν_{s_h} where the synchrotron losses produce a steepening in the power law energy distribution of the electrons, by changing the spectral index from α_e to $\alpha_e + 1$, hence at frequencies higher than ν_{s_h} the spectrum changes spectral index from α_o to $\alpha_o + 1/2$.

This steeper spectrum extends up to the frequency ν_{e_u} which corresponds to the characteristic emission frequency of the electrons having the maximum energy of the electron energy distribution. This maximum energy could be estimated from the maximum attainable values with the acceleration mechanism. At frequencies higher than the ν_{e_u} the spectrum falls off exponentially as for the emission of a single electron.

The local volume emissivity and absorption coefficient for synchrotron process can be written for a radius R as

$$\epsilon^s_\nu(R) = c_1(\alpha_o) k_o B_o^{1+\alpha_o} \nu^{-\alpha_o} (R_o/R)^{\epsilon(n+m(1+\alpha_o))}$$

$$k^s_\nu(R) = d_1(\alpha_o) k_o B_o^{3/2+\alpha_o} \nu^{-(\alpha_o+5/2)} (R_o/R)^{\epsilon(n+m(3/2+\alpha_o))},$$

where B_o and K_o are the magnetic field and the electron number density at a radius R_o (in general taken as 1 pc). The constants $c_1(\alpha_o)$ and $d_1(\alpha_o)$ are tabulated in Blumenthal and Gould (1970).

If the source is supposed to be oriented towards us forming an angle θ with the line of sight and the emitting material is moving with a velocity β_j, then the observed flux density (for an optically thin source) will be a function of $\epsilon'(\nu')$ where $\nu = \nu' \mathcal{D}$ is the observed frequency and $\mathcal{D}$ is the Doppler factor.

$$S_{obs}(\nu) \propto \mathcal{D}^2 \epsilon(\nu/\mathcal{D}).$$

The frequency at which the spectrum becomes optically thick can be approximately calculated by the expression

$$e^{\tau_m} = 1 + \tau_m \frac{(2\alpha_o + 5)}{5}$$

and the slab approximation has been used (*i.e.* $\tau_m = 2r/\sin\theta\ k^s_\nu(R)$).

The result is a radial dependence of the self-absorbed frequency with R like:

$$\nu_m^s(R) = \nu_m^s(R_o)(R_o/R)^{k_m}$$

where

$$k_m = \frac{2\epsilon}{5+2\alpha_o}(n + m(3/2+\alpha_o) - 1)$$

and

$$\nu_m^s(R_o) = \left[\frac{2d_1(\alpha_o)k_o B_o^{3/2+\alpha o} a R_o^{\epsilon}}{\sin\theta\tau_m(\alpha_o)}\right]^{2/(5+2\alpha_o)}$$

In the case that relativistic effects due to the orientation could be important the estimation is given by the same expression except with the change on $\nu_m^s(R_o)$ given by:

$$\nu_m^s(R_o) = [\nu_m^s(R_o)]_{old}\, \mathcal{D}_j^{(\alpha_o+3/2)/(\alpha_o+5/2)}$$

Let us now consider the first order inverse-Compton scattering of the emitted synchrotron photons. This will be calculated assuming a local approximation, the photon which will be scattered are coming from a region very close to the point where we are calculating the spectrum. Moreover the scattered photons are supposed to be monoenergetic, this is the also called δ function approximation.

The initial synchrotron photon have a frequency $\nu_s^{'}$, in the rest frame of the source, the frequency of the scattered photon is $\nu_c^{'} = \gamma_e^2\nu_s^{'}$ (suposing an isotropic electron distribution) in the Thomson regime ($\gamma_e^2 h\nu_s^{'} \lesssim m_e c^2$) and $\nu_c^{'} = \gamma_e m_e c^2$ in the Klein-Nishina regime ($\gamma_e^2 h\nu_s^{'} \gtrsim m_e c^2$).

The emissivity due to scattering in the Thomson limit is given by

$$\epsilon_c^T(\nu_c) \approx k_e\sigma_T(aR^{\epsilon})\epsilon_s(\nu_c)\int_{\gamma_{min}}^{\gamma_{max}} \gamma^{2(\alpha_o-\alpha_e)-1}d\gamma\ ,$$

which is valid for the range of frequencies:

$$\gamma_{e_{min}}^2\nu_{s_{min}} \lesssim \nu_c \lesssim min\left\{\gamma_{e_{max}}^2\nu_{s_{max}}; \gamma_{e_{max}}m_e c^2/h; \left(\frac{m_e c^2}{h}\right)^2/\nu_{s_{min}}\right\},$$

where

$$\gamma_{min} = max\left\{\gamma_{e_{min}}; (\nu_c/\nu_{s_{max}})^{1/2}; \frac{h\nu_c}{m_e c^2}\right\},$$

and

$$\gamma_{max} = min\left\{\gamma_{e_{max}}; (\nu_c/\nu_{s_{min}})^{1/2}\right\}.$$

In the Klein-Nishina regime ($\gamma_e^2 h\nu_s' \gtrsim m_e c^2$) the emissivity is given by

$$\epsilon_c^{KN}(\nu_c) \approx \frac{3}{8} k_e \sigma_T r \epsilon_s(\nu_c) \left(m_e c^2/h\right)^{2(\alpha_e+1)} \nu_c^{\alpha_s-2\alpha_e-1} \times \tag{2.1}$$

$$\times \left[\frac{\nu^{-(\alpha_s+1)}}{\alpha_s+1}\left(\frac{\alpha_s+3}{2(\alpha_s+1)} + \ln\left\{\left[\frac{h}{m_e c^2}\right] 2\nu\nu_c\right\}\right)\right]_{\nu_{max}}^{\nu_{min}}, \tag{2.2}$$

which is valid for the range:

$$max\left\{\gamma_{e_{min}}\frac{m_e c^2}{h}; \left(\frac{m_e c^2}{h}\right)^2/\nu_{s_{max}}\right\} \lesssim \nu_c \lesssim \gamma_{e_{max}} m_e c^2/h,$$

where

$$\nu_{min} = max\left\{\nu_{s_{min}}; \left(\frac{m_e c^2}{h}\right)^2/\nu_c\right\}$$

and

$$\nu_{max} = \nu_{s_{max}}.$$

The synchrotron self-Compton spectrum extends between the frequencies $\nu_{c_m} = \gamma_{e_{min}}^2 \nu_{s_m}$ and $min\{\nu_{c_{max}}; \nu_{KN}\}$ where $\nu_{c_{max}} \equiv \gamma_{e_{max}}^2 \nu_{s_{max}}$, $\nu_{KN} \equiv \gamma_{e_{max}} m_e c^2/h$ and with a break occuring at $\nu_{c_b} = \gamma_{e_b}^2 \nu_{s_b}$ where $\gamma_{e_b}^2 = \nu_{s_b}/\nu_B$.

2.2.3 Unresolved jet

The next step is to integrate the emissivity through the whole jet, taking into account the variations of the relevant quantities.

For the first model there exists a radius in which the optically thin part of the spectrum is only marginally observed. The existence of this radius arises from the different dependences on the radius for the maximum frequency and the cutoff frequency. The frequency corresponding to the maximum of the flux increases with decreasing radii. However the high frequency cutoff decreases with decreasing radius. Therefore there should be a minimum radius for which the optically thin spectrum dissapears when the radius is decreasing and then the cutoff frequency becomes very close to the maximum frequency. This radius is called R_M. An estimation of this radius is obtained putting equal the maximum frequency to the turnover frequency. For this model the value of this radius with the typical values of the parameters one has from observations is of the order of $\sim 100pc$. And the frequency at which this occurs is called ν_M and it is of the order of 100 MHz.

This radius R_M represents the radius of the optically thick core in the original model of Blandford and Königl (1979).

However in the second model this radius could not exist, because both the frequency ν_{s_m} which corresponds to the maximum in the spectrum and

the cutoff frequency ν_{s_b} decreases with radius and could not coincide for any value of R.

Let us come back to our initial purpose of integrating the flux. If we want to obtain the flux emitted by the jet we should evaluate the integral :

$$S_{ob}(\nu) = \frac{\mathcal{D}^2}{4\pi D^2} \int_{R_{min}(\nu)}^{R_{max}(\nu)} \epsilon\,(\nu/\mathcal{D})\,\pi r^2 dR\ ,$$

where $R_{max}(\nu)$ and $R_{min}(\nu)$ should be calculated as the upper and lower limits, respectively, which contributes to the optically thin part of the spectrum .

This integral can be written as:

$$S_{ob}(\nu) \propto \frac{\mathcal{D}^{2+\alpha_o}}{4\pi D^2} \nu^{-\alpha_o} R_o^{\epsilon(n+m(1+\alpha_o))} \int_{R_{min}(\nu)}^{R_{max}(\nu)} R^{\epsilon(2-n-m(1+\alpha_o))} dR$$

$$\propto \left[R^{\zeta}\right]_{R_{min}(\nu)}^{R_{max}(\nu)}\ ,$$

with $\zeta = 1 + \epsilon\,[2 - n - m(1 + \alpha_o)]$ and we have used the parametrizations for the emissivity mentioned above. Whether the contribution to the flux density comes from the minimum or maximum radius depends on the sign of the exponent ζ.

In the first model the reasonable values of $m \sim 1$ and $n \sim 2$ yield $\zeta < 0$, hence the minimum radius will dominate in this case.

In this model one can estimate the shape of the spectrum based on the considerations made by defining the frequency ν_{s_M}. For frequencies below ν_{s_M} the spectrum will be dominated by emission coming from a radius R such that the maximum of its local spectrum is localized at that frequency ν, this radius is given by the expression $R = (\nu_s/\nu_{s_M})^{-1/k_m} R_M$, k_m has the same meaning as before and R_M is the radius defined above. The maximum radius is the maximum radius of the jet.

For frequencies above the value ν_{s_M} the spectrum is dominated by the emission coming from a radius R such that the frequency ν corresponds to its high frequency cutoff, this radius is given by the expression $R = (\nu_s/\nu_{s_M})^{-1/k_b} R_M$, k_b is the same as defined before.

With these presciptions it is possible to estimate the integrated flux density and this is given by two power laws:

$$S_{obs}(\nu) = \begin{cases} S_{obs}(\nu_{s_M})\,(\nu_s/\nu_{s_M})^{-\alpha_{s_1}} & \nu_{s_M}\,(R_u/R_M)^{-k_m} \lesssim \nu_s \lesssim \nu_{s_M} \\ S_{obs}(\nu_{s_M})\,(\nu_s/\nu_{s_M})^{-\alpha_{s_2}} & \nu_{s_M} \lesssim \nu_s \lesssim \nu_{s_M}\,(R_u/R_M)^{k_b} \end{cases},$$

being

$$\alpha_{s_1} = (4 + m - 5k_m)/2k_m$$

$$\alpha_{s_2} = \alpha_o - k_s/k_b, \quad k_s = (1 + \alpha_o)m + n - 3$$

For the case when $m \sim 1$, $n \sim 2$ then $\alpha_{s_1} \sim 0$, $\alpha_{s_2} \sim 1$.

Therefore the result is a flatening of the optically thick part of the spectrum and a steepening of the optically thin part, this is an important effect of the inhomogeneity in the emitting source. This is basically the same result obtained by Blandford and Königl (1979), except that more generalized.

In the second model we consider two different geometries: a conical geometry with $\epsilon = 1$ and an elongated parabolic geometry with $\epsilon \lesssim 0.5$.

In the conical case, for the usual values of m and n, ζ is negative and most of the flux will be produced in the inner radius. The spectrum above $\nu_{s_m}(R_o)$ is optically thin and most of the flux is coming from the radius R_o, up to the frequency $\nu_{s_b}(R_o)$. Below the frequency $\nu_{s_m}(R_o)$ the outer parts of the jet begin to dominate and the integrated spectrum can be approximated by a power law with spectral index $\alpha_{thick} = \alpha_o + \zeta/k_m$, which is again a flatter spectrum at low frequencies and an optically thin steep spectrum at high frequencies.

In the parabolic geometry, for $\epsilon \lesssim 0.5$, positive values of ζ appear for the usual values of m and n. Hence the outer regions will dominate the integrated spectrum. For frequencies between $\nu_{s_m}(R_{max})$ and $\nu_{s_b}(R_{max})$ the emission will come mostly from R_{max} with an spectral index α_o. For frequencies higher than $\nu_{s_b}(R_{max})$ the inner radii will contribute considerably and the result will be a power law with spectral index $\alpha_{thin} = \alpha_o + \zeta/\eta$. The overall spectrum is a power law with a break at high frequencies corresponding to the maximum frequency at the maximum radius.

The main differences between the two models are related to the different variability time scales that one should associate to each region of the spectrum depending on the region of the jet which produces it. With the simple prescription that larger variability time scales are associated with outer regions.

In the first model up to the frequency ν_{s_M} the variability time scale tends to decrease, above ν_{s_M} the variability time scale tends to increase again. However in the second model a monotonic behaviour is observed, the variability time scale always tends to increase with decreasing frequency.

Let us now calculate the spectrum at high energies. In a similar way to the integration of the synchrotron spectrum, the shape of the inverse self-Compton scattering spectrum can be predicted.

In the first model the spectrum extends from the frequency $\nu_{c_m}(R_{max})$ up to the frequency $min\left\{\nu_{c_{max}}(R_M); \nu_{KN}\right\}$. In the range $\nu_{c_m}(R_{max}) \lesssim \nu_c \lesssim \nu_{c_m}(R_M)$, where $\nu_{c_m}(R_M) = \gamma_e^2 \nu_{s_M}$, the dominat emission comes from the radius $R = \left(\nu_{c_m}/\nu_{c_M}\right)^{-1/k_m} R_M$. The observed flux density can be approximated by:

$$S_{obs}(\nu) = S_{obs}(\nu_{c_M}) \left(\nu_c/\nu_{c_M}\right)^{-\alpha_{c_1}} \quad ,$$

where $\alpha_{c_1} = \alpha_o - k_c/k_m$, being $k_c = k_s + n - 1$. The values $m \sim 1, n \sim 2, \alpha_o \sim 0.5$ yield $k_c \sim 3/2$ and $\alpha_{c_1} \sim -1$.

This part of the spectrum is the Compton equivalent to the optically thick integrated synchrotron spectrum.

For frequencies in the range $\nu_{c_M} \lesssim \nu_c \lesssim \nu_{c_b}(R_M)$ the spectrum is dominated by the Compton scattered optically thin part of the spectrum (*i.e* with spectral index α_o), coming from the radius R_M.

In the range $\nu_{c_b}(R_M) \lesssim \nu_c \lesssim \nu_{c_b}(R_{max})$ the flux will be dominated by the emission coming from the radius $R = (\nu_{c_b}/\nu_{c_b}(R_M))^{1/(m-2k_b)} R_M$ and the spectral index is approximately given as: $\alpha_{c_2} = \alpha_o + k_c/(m - 2k_b)$.

For higher frequencies the spectrum will steepen when the Klein-Nishina regime is reached.

In the second model (in the Thomson regime[2]) a similar result is obtained for the integrated spectrum and it is depending on the sign of the parameter l:

$$S_{obs}(\nu_c) \propto \nu_c^{-\alpha_o} \left[(R/R_o)^l\right]_{R_{min}(\nu_c)}^{R_{max}(\nu_c)} ,$$

where $l = 1 + \epsilon[3 - 2n - m(1 + \alpha_o)]$ and $R_{max}(\nu_c)$, $R_{min}(\nu_c)$ are the limits of the region which contributes to the flux at the frequency ν_c. The values of $R_{max}(\nu_c)$ and $R_{min}(\nu_c)$ are estimated from the limits of the synchrotron spectrum and the electron energy distribution and their variation with radius consistent with the self-Compton scattering process (see Appendix in Ghisellini et al. 1985 for a determination of these values).

The parameter l determines which region from the source will dominate the observed emission: for a conical geometry ($\epsilon = 1$) and with the usual values of $m \sim 1$ and $n \sim 2$, l is negative and the inner regions will dominate the total emission; whereas for an elongated parabola ($\epsilon \lesssim 0.5$) and the same conditions as before, l is positive and hence the outer regions will be dominant, but negative values are not very far and could be reachable.

Still in the Compton spectrum the two models mantain the difference in the variability time scale associated with different regions, however some spread in frequency is introduced and different regions can contribute at the same frequency:

For the first model it is easy to see that up to the frequency $\nu_{c_M} = \nu_{c_m}(R_M)$ the variability time scale will decrease with the frequency. Between ν_{c_M} up to the frequency $\nu_{c_b}(R_M)$ the variability will be correlated, the flux varies at the same time, because the emission is coming from the same region. Above the frequency $\nu_{c_b}(R_M)$ the variability time scale will decrease with increasing frequency, due to the fact that the radiation is produced at inner radii.

[2]The expression for the Klein-Nishina regime is similar but with a different power law $p = l + \eta(\alpha_o + 1)$.

Instead in the second model the two considered geometries show different possibilities. For the conical geometry the most probable value for l is negative and hence inner regions will dominate and variability time scales will increase with the frequency. But other regions could contribute apreciable, because the spreading in frequency due to the scattering process mixes emission from nearby zones.

In the case of a parabolic geometry the situation is still more difficult because positive and negative values of l are reasonable.

2.2.4 Application of the two models to observations of BL Lac objects

BL Lac objects are usually considered to be beamed sources, oriented very close to the line of sight, so that the non thermal radiation originated in the relativistic jet will dominate the whole spectrum and the previous models could be tested.

The spectra of BL Lac objects are rather flat in the radio band up to a frequency of the order of hundreds of GHz ($\sim 10^{11} Hz$) where there is a break extended to the infrared with an spectral index of order of unity.

For larger frequencies, in the ultraviolet region the spectrum is steeper, with an index of the order of 1.5.

In the X-rays two bands may be distinguish: below 5 keV a soft spectrum is generally observed; above 5 keV a hard spectrum is detected with an spectral index close to the flat spectrum. The soft component could be interpreted as the tail of the synchroton emission and the hard component as the self-Compton scattered emission.

At γ-rays the spectrum is found to be steep, with the spectral index around unity.

The first model is applied to the source Mrk 421 which shows a flat spectrum without break below 90 GHz. A steep infrared spectrum with spectral index $\alpha \gtrsim 0.8$ is assumed. The UV and soft X-ray spectrum have spectral indices around unity; and the hard X-ray spectrum was observed to have a variability $\lesssim 1 yr$.

A model with a optically thin synchrotron spectrum, $\alpha_o = 0.5$, is appropiate to fit this source with the spectral indices $\alpha_{s_1} \simeq 0$, $\alpha_{s_2} \simeq 0.8$ and the frequencies $\nu_{s_M}, \nu_{s_b}(R_{max})$ and $\nu_{s_{max}}(R_{max})$ to be 10^{12} Hz, 10^{15} Hz and 10^{17} Hz, respectively. With these observables the first model could be especified, the values of the parameters for this object are $m = 1.25; n = 1.65; R_M = 2.3 \times 10^{-2} pc.; R_{max} \sim 10 pc.$

The flux density variability of the hard X-ray component should be correlated with the high frequency radio component, because they are supposed to be produced in the same region, close to the radius R_M. Whereas

the soft X-ray component should show less variability with larger times scales, because it is radiation coming from outer radius.

A correlation of the outburst at hard X-rays with radio outbursts is observed but not with the optical band indicating that emission regions are different.

However the second model when is applied to BL Lac objects advocates for two geometries in the source: A conical jet in the outer part which explains the flat part of the spectrum and for higher frequencies behaves with a spectral index α_o. A parabolic geometry to account for the steep spectrum at higher frequencies. The joining region will be responsible for the optically thin spectrum localized in the infrared region. So the spectrum will be flat with spectral index $\alpha_{thick} \sim 0$ up to 10^{12} Hz, from 10^{12} Hz to 10^{14} Hz the optically thin spectrum is found with spectral index α_o and it will change again at $10^{14} - 10^{15} Hz$ to the spectral index $\alpha_o + \Delta\alpha$.

The second model was applied to two sources and it is found that one case Pks 2155-304 could be explained by a model with Doppler factor $\mathcal{D} \equiv 1$, however in the case of Pks 0537-441 relativistic effects should be taken into account in the outer region, the one with conical geometry which produces the flat radio spectrum[3]; whereas the parabolic zone is not affected by beaming.

This fact seems to claim that a model with bulk acceleration of the flow should be considered.

Ghisellini(1987) considered a simple model including acceleration of the flow (he assumed a simple power law dependence, the bulk Lorentz factor increases with R), in this case the integral which is giving the observed emission contains the Doppler factor:

$$S_{obs} \propto \int_{R_{min}(\nu)}^{R_{max}(\nu)} r^2 \epsilon(\nu) \mathcal{D}^{2+\alpha} dR \ ,$$

but $\mathcal{D}$ is depending on R, so that the shape of the spectrum will depend on the viewing angle.

Moreover it is found that the flux density at the maximum frequency emitted by parabolic regions is nearly isotropic for low values of the bulk Lorentz factor:

$$\frac{S_{obs}\,(\nu_b, 0^\circ)}{S_{obs}\,(\nu_b, 90^\circ)} = \gamma^{2(2+\alpha_o)} \ .$$

Therefore only at lower frequencies the beaming effects will be important because the emission at those frequencies is dominated by the outer regions of the source where the bulk Lorentz factor should be larger.

[3]This is made because the extension of the radio source as derived from the variability time scale at 5 GHz is very small and it produces an excess of self-Compton scattering.

For the conical geometry the acceleration of the flow may do that radiation from outer regions will be dominant so that the flat spectrum is no longer present. Then a third region should be considered, where the bulk Lorentz factor becomes constant and the flat spectrum is produced there.

This model with bulk acceleration is applied to blazars and some interesting features are drawn.

From the study of the average spectral index at different regions of the spectrum of blazars two main conclusions can be obtained (Maraschi, 1987):

- objects which are selected in the X-rays surveys have spectral indices which are flatter than those of the radio selected objects .
- the two classes of objects have the same X-ray luminosities despite they appear in two different surveys.

Maraschi (1987) proposed that X-rays selected objects are randomly oriented objects, whereas the radio selected ones are relativistically beamed, since both classes of objects have similar X-ray luminosities they should appear with the same probability at X-rays surveys but they do not hence they are less frequent. Moreover the steeper spectrum for radio selected objects is understood because radio emission is more Doppler boosted than higher frequencies emission.

This is correctly interpreted with the previous model, the high energy part of the spectrum is not relativistically beamed and is produced in the inner regions so that variability time scales are expected to be relatively short. Instead in the low energy part, radio frequencies are relativistically beamed and these sources will produce the radiation mainly in the outer parts with relatively large variability time scales.

Chapter 3

Statistical properties of the relativistic beaming hypothesis

One of the most strong arguments against the beaming hypothesis is based on the statistics of radio sources, because there is a predominancy of strong cores sources against weak core sources. If the cores of superluminal source or sources presenting evidence for relativistic beaming, are oriented close to our line of sight and the emitted flux is amplified by relativistic motion, it is natural to ask where are the unbeamed sources, those which are not oriented directly towards us.

From the simple ballistic jet model the amplification of the flux is confined to a cone of semiaperture $1/\gamma$, thus for each beamed source we will expect to find about γ^2 sources which are not oriented in our direction and hence do not show any relativistic beaming effect.

3.1 Unified beaming models

However the identification of the unbeamed sources is not an easy task and this is the main goal of the so called *unified beaming models.*

The most extended models may be summarized in two extreme positions. From chronological order of appearance, the first model was proposed by Scheuer and Readhead (1979). In this model the unbeamed compact radio sources are identified with the radio quiet quasars (optically selected quasars). The second model was proposed by Orr and Browne (1982). However in this model the unbeamed compact radio sources are the steep-spectrum core sources, lobe-dominated quasars and galaxies, whereas the flat spectrum sources will be the beamed sources. Radio quiet quasars in the Orr and Browne'82 model have a wide distribution of alignments, to distinguish between aligned or misaligned source one should look at the spectrum.

There seems to be strong evidence against the first proposal that radio quiet quasars are the counterpart of the relativistic beamed sources: the number of weak radio sources should increase with decreasing flux according to the law $S^{-1/2}$ (Scheuer and Readhead, 1979) and this is not observed; moreover the emission from radio loud quasars originates in some cases from extended regions, which is not well interpreted as the result of relativistic beaming. However the discovery of extended weak steep spectrum haloes around the compact core of the flat spectrum sources strongly supports the second model to be a righter interpretation.

At this point it seems convenient to introduce the simple model developed by Orr and Browne (1982) in order to quantify the statistical predictions of these models. This model is largely based on the previous model of Scheuer and Readhead (1979), so I will expound only the second model to avoid being redundant.

The basic assumption of the model concerns to the simplified structure of a quasar[1]. Each quasar consists of a relativistically moving central core which emits a flat spectrum , with two extended lobes which are not relativistically beamed and emit a steep spectrum. In summary a beamed part in the core emission and an unbeamed part in the extended emission.

A parameter related to the degree of relativistic beaming is defined in the following way:

$$R \equiv \frac{flux\ density\ of\ the\ core\ component}{flux\ density\ of\ the\ extended\ component} .$$

This quantity depends on the angle which the axis of the core source forms with our line of sight. When the source is oriented whithin the plane of the sky we are looking at the source with the lowest degree of beaming, in this case the value of R is called R_T, this is a lower limit of R.

With the assumption of a flat spectrum for the core component the value of the parameter R is given by the expression:

$$R = R_T \frac{1}{(1 - v/c\cos\theta)^{2+\alpha}} \ (\alpha \sim 0) ,$$

where a optically thin continuous jet model is assumed hence the quantity which should be Lorentz transformed is the emissivity. The spectral index is taken to be close to 0 because it corresponds to the observed flat spectrum of the core emission.

Now the distribution function of values of R can be obtained for a randomly oriented sample by the formula:

$$dP(R) \propto d(\cos\theta) ,$$

[1]Generalization to radio galaxies is done in a later paper by Morisawa and Takahara (1987).

where we have taken the probability as the fraction of solid angle in which the source is contained. This probability distribution is usually given by logarithm interval of R as:

$$P(R) \propto (R_T/R)^{1/2} .$$

To assign a value to the parameter R_T we shall look at a sample selected at low frequency, where the steep spectrum component will dominate and hence should be almost randomly oriented.

The best fit to this unbiased sample will give a value of the parameter R_T and γ.

The next step is to consider the variation of the R parameter with the frequency. It is enough to consider the variation of the transverse value of R, R_T. Consider the value at two different frequencies then the expression giving the frequency dependency is:

$$R_T(\nu) = R_T(\nu_o) \left(\frac{\nu}{\nu_o}\right)^{-(\alpha_{cc}-\alpha_{ext})} (1+z)^{-(\alpha_{cc}-\alpha_{ext})},$$

where a correction for redshift have been included in the same way. This expression is strictly valid only in the range where the spetrum remains a power law (*i.e.* where the spectrum is optically thin).

Assuming for simplicity $\alpha_{cc} = 0$ and $\alpha_{ext} = 1$ the resulting expression is

$$R_{nu}^{(z)} = R_{T\nu_o} \left(\frac{\nu}{\nu_o}\right) (1+z).$$

Moreover we will consider an expression which relates the spectral index of the overall spectrum, which is an observable quantity, with the parameter R. The overall spectrum is a sum of two contributions: the flat core component plus the steep unbeamed extended component, then the ratio of the flux at two different frequencies is:

$$\frac{S_{\nu_2}}{S_{\nu_1}} = \frac{\left(\frac{1}{R_{\nu_2}}+1\right)(C.\,C.)_{\nu_2}}{\left(\frac{1}{R_{\nu_1}}+1\right)(C.\,C.)_{\nu_1}},$$

in this case considering that the core component has a flat spectrum the resulting expression is:

$$\frac{S_{\nu_2}}{S_{\nu_1}} = \frac{\nu_1/\nu_2 + R_{\nu_1}}{1+R_{\nu_2}}$$

At this stage it is possible to use the model to predict the number of flat spectrum quasars with only one parameter to adjust with the observations, this parameter is the bulk Lorentz factor, γ.

If we consider a flux limited sample of quasars the steep spectrum component has a limit depending on the value of R_ν and is given by

$$S_{\nu_{steep}} > \frac{S_o}{1+R_\nu},$$

where S_o is the flux density limit.

Suppose that we have a number counts for steep-spectrum sources, number of sources which exceeds the value of the flux S, given by the expression

$$N(> S_{steep}) \propto S_{steep}^{-\delta}.$$

A redshift distribution function $\rho(z)$ should be assumed if one likes to account for evolutionary effects in the parent population. This function is assumed for simplicity independent of the flux.

Therefore the number of quasars which have a ratio of the core to the extended emission in the range R_ν to $R_\nu + dR_\nu$ in a flux limited sample ($S_\nu \geq S_o$) is given by:

$$N(R_\nu) \propto \left(\frac{S_o}{1+R_\nu}\right)^{-\delta} \int_0^{z_{max}} \rho(z) P(R_\nu) dz.$$

In the figure 3.1 we show the distribution of expected values for $R_{5\mathrm{GHz}}$ and the tendency in which quasars selected at higher frequencies have higher values of the parameter R, indicating that they are really core dominated sources. Therefore the conclusion is that flux limited samples have selection effects, at high frequencies we preferentially select beamed sources.

To obtain the number of flat spectrum quasars one must integrate the number counts between the values of R_ν which gives an overall flat spectrum:

$$N_{fs} = \int_{R_\nu^{min}}^{R_\nu^{max}} N(R_\nu) dR_\nu$$

where R_ν^{min} is the minimum value to produce an overall flat spectrum and depends on the definition of overall flat spectrum, in general a flat overall spectrum is consider to be with the spectral index compressed between the values $0 \lesssim \alpha \lesssim 0.5$, and this condition is such that:

$$R_{\nu_1} > \left(\frac{\nu_1}{\nu_2}\right)^{0.5}.$$

And the value for R_ν^{max} is the corresponding to $R_T(\nu, z_{max})(1-\beta)^{-2}$. Orr and Browne'82 studied the fraction of quasars with flat spectrum and the result is that the best fit for the different samples is with an average value of $\gamma = 5$ and $R_T = 0.024$ at 5GHz.

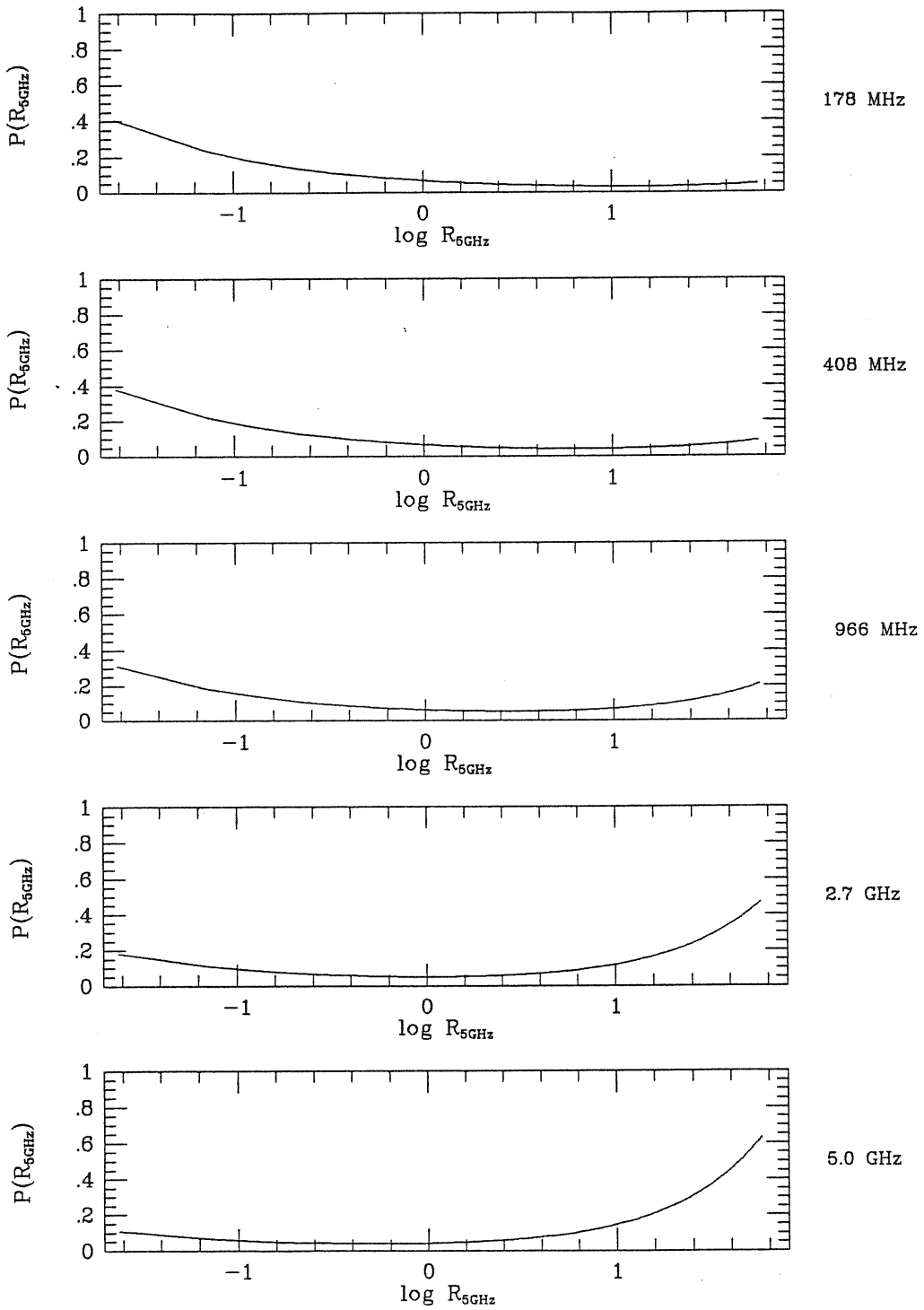

Figure 3.1: The expected probability of finding quasars with a ratio R at 5 GHz for samples selected at different frequencies.

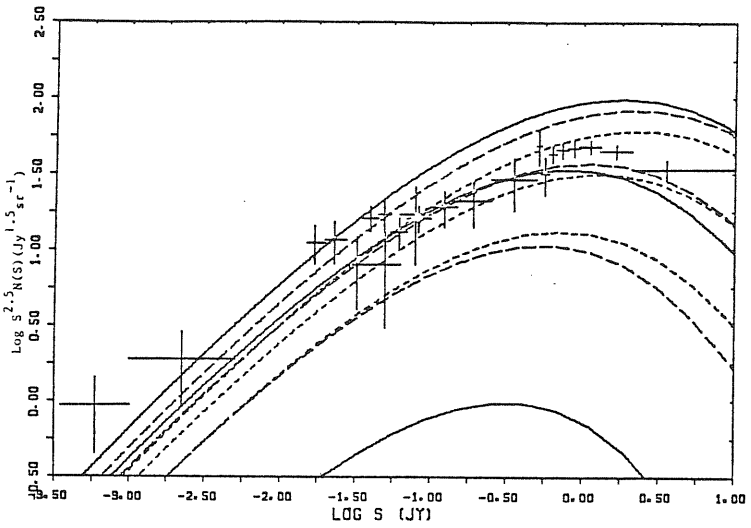

Figure 3.2: Normalized source counts at 5 GHz for flat spectrum sources. The predictions are indicated by: solid lines ($R_T = 0.024$ and $\gamma = 2, 3$ and 4) , dashed lines ($R_T = 0.012$ and $\gamma = 3, 4$ and 5) and dotted lines ($R_T = 0.006$ and $\gamma = 4, 5$ and 6); from Morisawa and Takahara (1987).

A second application of the model was to explain the source counts of flat spectrum sources and the best fit for the model was very close to a value of the bulk Lorentz factor $\gamma = 5$, however the fit is not able to reproduce the observations in great detail, they atribute this fail to the limitation of such simple model and perhaps to uncertainties in the data.

In a similar way the fraction of flat spectrum quasars as a function of the redshift can be obtained. The quasars with high redshift have large values of R_T and therefore a slight excess of high redshift objects would be expected in flux limited samples because they will receive more Doppler boosting.

In a more recent paper Morisawa and Takahara (1987) took the idea of Orr and Browne'82 and extended the result to radio galaxies.

In a first step the luminosity function for steep spectrum radio sources, corresponding to the supposed unbeamed sources, is computed based on well established luminosity functions, normalized source counts and redshift distribution in a more serious way than in the previous model.

The result is that the source counts agree with the expected ones from the model for sets of values γ, R_T (*e.g.* $\gamma \sim 3.2$ with $R_T \sim 0.024$; $\gamma \sim 5.5$ with $R_T \sim 0.006$). We conclude that the value of γ should be larger than 3 because R_T is the minimum limit in the R distribution and R_T must be always smaller than 0.024. For an illustration see the figure 3.2.

The reason for the disagreement with the values obtained by Orr and Browne(1982) ($R_T \sim 0.024$ and $\gamma \sim 5$) could be explained because radio

galaxies have weaker cores than quasars and need lower values of R_T for the same value of γ.

This fact naturally drove us to consider a model with two different populations one for radio galaxies and one for quasars.

The result is, with the prescription of a population of quasars with $\gamma \sim 5$ and $R_T \sim 0.024$, that a good agreement with observations of flat spectrum source counts is found above 1 Jy whereas below 1 Jy the model predictions are lower than the observed values, then the radio galaxies population will contribute there to the source counts. A minimum value of $\gamma \sim 2$ is required to avoid values of R_T larger than those of the quasars and therefore the conclusion is that relativistic beaming could be also claimed for the core of radio galaxies.

Morisawa and Takahara'87 showed that the redshift distribution of steep and flat spectrum radio sources coincide when the sample is limited by a low flux, however when they deal with bright sources the redshift distribution for steep spectrum sources is spread in a range of z values, while the flat spectrum are concentrated in a narrower range of redshift, at higher values.

This fact was also pointed out by Kapahi and Kulkarni (1986) as an additional support to the unified scheme of Orr and Browne (1982).

3.2 Source counts are not as precise

In spite of the relative success (but see also de Ruiter et al., 1986) of the unified model, it has been showed by Lind and Blandford (1985) that different jet models can give similar statistical predictions and therefore the statiscal arguments can not be used as precise probes to discern the right model.

In their work, Lind and Blandford (1985) considered various different models of relativistic beaming. All the models they considered are kinematically exact but the velocity fields are not solution of the full dynamical equations.

Simple models like a plasmoid moving away from the nucleus, continuous uniform jet or propagating patterns along the channel of a stationary jet are considered for statistical purposes. Moreover flows with plane and oblique shocks propagating down in the jet are inspected from the statistical point of view.

For each of these models they calculated the distribution of sources with the flux exceeding a certain value is calculated.[2]

[2]The quantities S (flux density) and R (ratio of core component to extended component) are strictly related and both can be used to account for the degree of beaming

Now let us consider in more detail each one of the models.[3]

One of the more simple models one can imagine is an spherical blob moving at an angle θ to the line of sight, supposing the plasmoid is optically thin, the observed flux is given by the expression:

$$S_\nu \propto \mathcal{D}^{3+\alpha} \int j'_{\nu'}(\nu) dV',$$

where $j'_{\nu'}(\nu)$ and dV' are the emissivity and the element of volume in the rest frame of the plasmoid, respectively.

The probability to observe a plasmoid with flux exceeding S is proportional to the factor $\cos\theta$ which is giving the degree of beaming. Therefore

$$dP(S) \propto d\cos\theta$$

and integrating we obtain the probability for an *infinite lifetime blob* to have a flux exceeding the value S:

$$P(S) \propto \left[\left(\frac{S_{max}}{S}\right)^{1/(3+\alpha)} - 1\right].$$

In this case the lifetime of the blob was assumed to be infinite. If one considers that the blob could have a finite lifetime then the time interval we will observe the source will modify the probability of observing it. The time that an obsever will see the source is given by the expression $dt_o = (1/\mathcal{D})d\tau$, where $d\tau$ is the lifetime interval measured in the blob frame. The observer will see the source less frequently than in the previous case. And the probability of observing the blob will decrease by a factor $dt_o/d\tau$:

$$dP(S) \propto \frac{dt_o}{d\tau} d(\cos\theta)$$

and integrating we obtain the probability to observe the *finite lifetime blob* with a flux exceeding the value S, as it is given by:

$$P(S) \propto \left[\left(\frac{S_{max}}{S}\right)^{2/(3+\alpha)} - 1\right]$$

The range of validity of these formulae is between $S_{max}(1-\beta)^{3+\alpha}$ and S_{max} where S_{max} corresponds to the value of the observed flux when the source is pointing directly towards the observer.

The next model to consider is a chain of blobs which merge together to form a continuous jet; this should be the case of a flow in a continuous stream.

[3] A more detailed explanation of the Lorentz transformation of the specific intensity, emissivity and absorptivity is given in the appendix B.

Therefore in this case the frame of the jet appears stationary to the observer, the Doppler boosting will only come from the comoving emitting plasma frame passing to the rest frame of the jet:

$$S_\nu \propto \mathcal{D}^{2+\alpha} \int j''_{\nu''}(\nu) dV \propto (1 - \beta \cos\theta)^{-(2+\alpha)}.$$

The probability to observe a source with flux density in excess of S for a *continuous jet* will be given as:

$$P(S) \propto \left[\left(\frac{S_{max}}{S} \right)^{1/(2+\alpha)} - 1 \right],$$

valid in the range between $S_{max}(1-\beta)^{2+\alpha}$ and S_{max}.

Now let us consider the opposite case then an exciting pattern which is propagating through an stationary plasma, this is also called *illuminating pattern.*

In this case the Lorentz transformation from the emitting plasma to the pattern frame is Doppler boosted by the inverse Doppler factor which transforms from the pattern frame to the observer frame. Then the observed flux is obtained as:

$$S_\nu \propto \mathcal{D} \int_0^{x'} j''_{\nu''} e^{-\mathcal{D} \int_0^{l'} k''(\nu) ds'} dl'$$

and the optical depth is proportional to $\mathcal{D}$ then the exponential will take value close to unity for small values of the opacity, hence the flux density is proportional to $\mathcal{D}$.

The probability to observe a source, in the case of an *illuminating pattern* with the flux exceeding the value S is given by:

$$P(S) \propto \left[\left(\frac{S_{max}}{S} \right)^{2} - 1 \right],$$

which is valid in the range between $S_{max}(1-\beta)$ and S_{max}.

But the most important results concern the flows which include shock fronts. We will consider two cases plane shocks perpendicular to the direction of the flow and oblique shocks forming an angle with the direction of the flow.

Let us consider first the plane perpendicular shock, for simplicity we will assume that the emission is uniform and limited to a conical volume behind the shock front (see figure 3.3 .a). [4]

[4] A free expansion region is assumed to be present behind the shock, since the jet is expected to be in pressure equilibrium ahead the shock. This region will tend to expand rather quickly and the density will diminish considerably, when this occurs the emission will decay. Hence a good approximation to the emitting region is a cone limited by two rarefactions waves propagating towards the centre of the jet (see figure 3.3 .a.

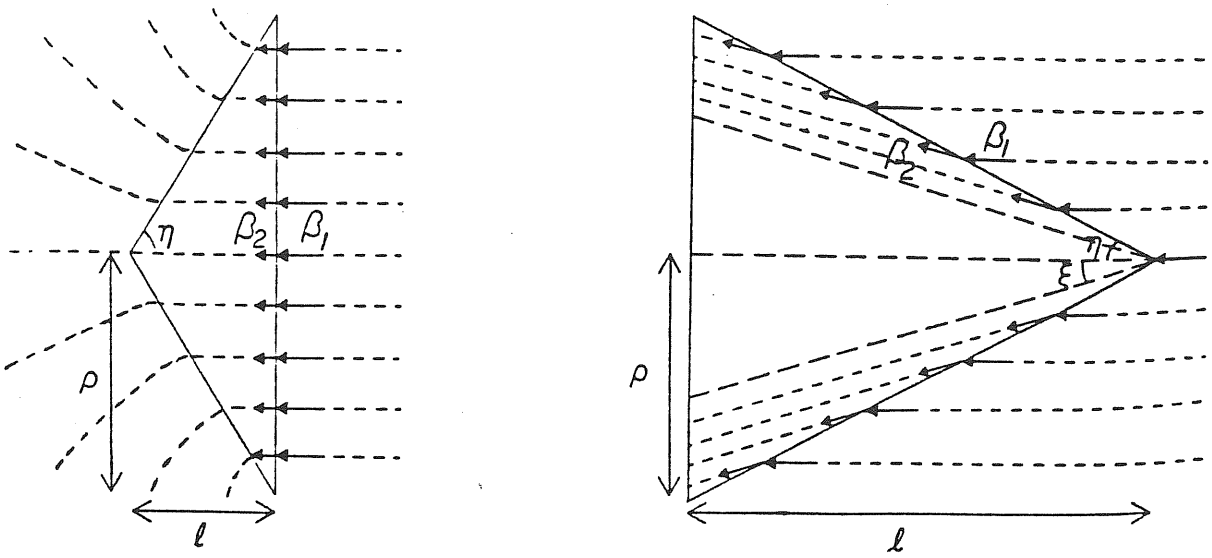

Figure 3.3: The two geometries of the shocks are shown in the frame of the shock. In both models β_1 and β_2 are the preshock and postshock fluid velocities in the shock frame and η is the cone opening angle. (a) The plane shock model has a cone angle η fixed by the sound speed and the preshock velocity. (b) The conical shock model may have a range of opening angles η, the angle of the interior cone ξ is given according to the oblique shock jump conditions

In this case the emission should be calculated considering the variation of the optical depth, because the source can not be assumed optically thin for all the viewing angles. For low frequencies the spectrum is optically thick to synchrotron radiation, however at intermediate frequencies since the optical depth varies as $\mathcal{D}^{5/2+\alpha}$ the source may be optically thick for small viewing angles and optically thin for larger angles.

Lind and Blandford'85 calculated the emission coming from different values of the optical depth at the whole range of orientations.

In these models where numerical calculation is needed to establish the dependence of observed flux with the orientation angle it is not easy to give an expression for the probability of observing a source with flux exceeding a given value S due to beaming effects. They should be calculated numerically. However in this work (Lind and Blandford'85) the curves are constructed by connecting the emission observed at different angles and identifying the angle of observation with the probability P(S) of observing the flux of the source exceeding the value S (see figure 3.4). This idea works only in the case that a monotonic behaviour is shown by the flux increasing with decreasing angle. The only inconvenient is that for optically thick postshock emission (small angles with the line of sight implies high values of D and hence high optical depth) the flux may increase because

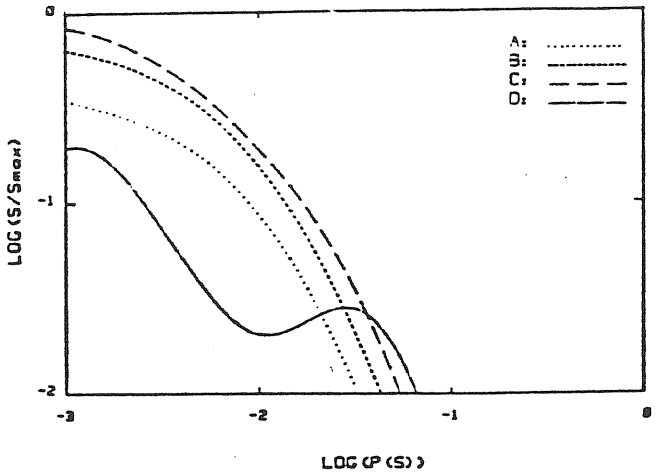

Figure 3.4: Probability distribution for plane shock models at different frequencies corresponding to different optical depths (A: $\tilde{\tau} \simeq 0.01$; B: $\tilde{\tau} \simeq 0.1$; C: $\tilde{\tau} \simeq 1$; D: $\tilde{\tau} \simeq 10$), from Lind and Blandford (1985). The curves P(S) versus S/S_{max} should be monotonic but in the case D, optically thick, to get a monotonic curve one should calculate the angle (solid angle) for which the flux exceeds the value S and this is the probability.

when the angle with the line of sight increases the projected area of the emitting region also increases and this effect could superate the decreasing of the Doppler boosting.

The second model involving shock waves considers a conical oblique shock; for simplicity we assume that the velocity behind the shock is constant and therefore emissivity is also constant in the shock frame (see fig 3.3 .b). The optical depth decreases with increasing viewing angle more slowly than in the plane perpendicular shock , this is reflected in the variation of the flux density with the viewing angle (see figure 3.5)[5]. This occurs because the angle between the postshock velocity direction and the observer is not a single value but a certain range for each inclination of the jet axis and hence there is still Doppler boosting for large values of the viewing angle.

In this conical shock model it is possible to obtain a still lower decrease of the probability function if the preshock flow velocity is not consider low as it was implicitly done in the previous results. If the preshock velocity is higher then a wider range of postshock velocities is obtained since the postshock velocity is spread out from the axis of the jet.

It is interesting to look at the calculated brightness distribution for a conical shock in the frame of the observer (see figure 3.6). From the figure

[5]One must be present that $P(S)$ versus S is interpreted as *viewing angle* versus S.

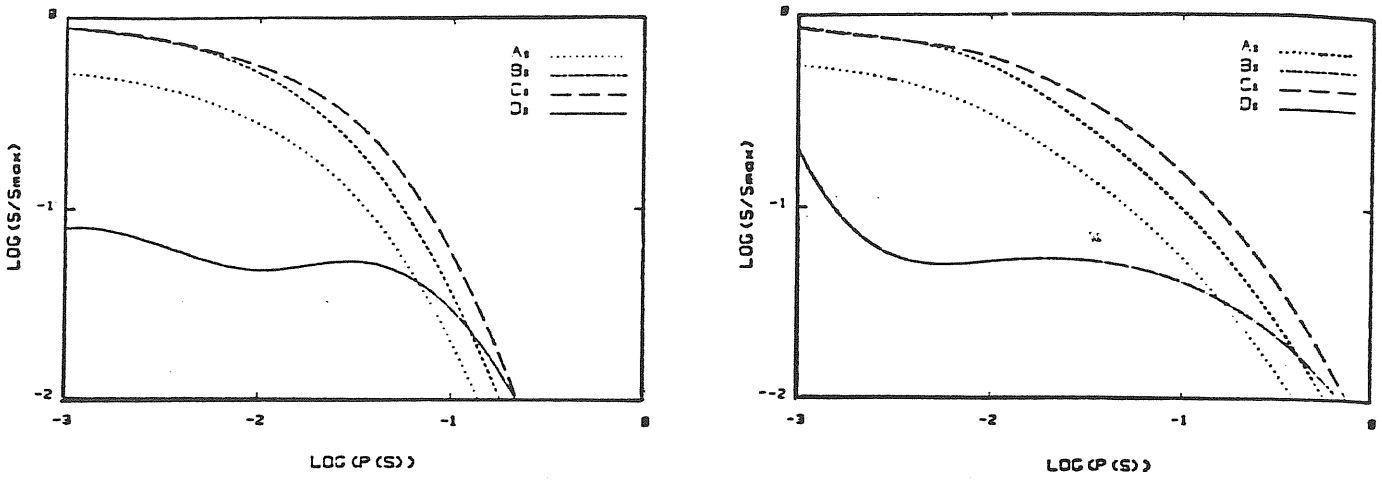

Figure 3.5: Probability distribution for conical shocks models calculated at differents frequencies as in the previous figure (figure 3.4) and two different opening angles. At the left wide conical shock ($\eta = 30°$), at the right narrow conical shock ($\eta = 10°$). From Lind and Blandford (1985)

one can see that the brightness distribution is sharper for smaller optical depths, broadens for larger than unity optical depths and it is close to be uniform in the optically thick models.

This behaviour is expected since the optically thick case is not reflecting as much as the optically thin case the beaming effects.

There is a third model with shock fronts, in this case the jet is passing an obstacle and the conical shock will extend downstream. The difference with the previous models is that the velocity of the shock front and that of the emitting plasma are in the same direction and therefore the beaming is stronger, the probability $P(S)$ is more peaked at small viewing angles. This model is called *inverse conical shock.*

It is important to compare the models according to the decreasing flux with the viewing angle increasing, in the optically thin limit. The beaming effect for optically thick sources is small and the structural details become important.

A rough classification of the models could be done according to the degree of beaming:

The highest beamed models are the inverse conical shock, the narrower the opening angle of the cone the stronger the beaming.

After it could classified the plasmoid model, with less degree of beaming are the blob or plasmoid model, the plane perpendicular shock and the continuous jet.

From the analized models those which present less degree of beaming are

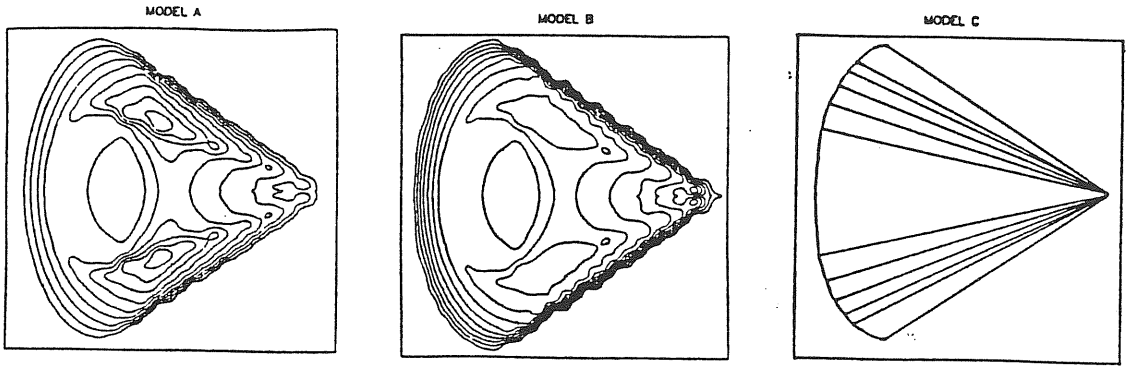

Figure 3.6: Brightness distribution for a conical shock model in the frame of the observer at three different optical depths (A: $\tau = 0.1$; B: $\tau = 1.$; C: $\tau = 10.$), from Lind and Blandford (1985)

the conical shock and the propagation of an excitation pattern. The conical shocks present more beaming when they are wider because the postshock velocity is higher for higher values of the opening angle.

The conclusion is that the postshock velocity or better the velocity of the emitting fluid in the patern frame are the dominant factors in determining the dependence of the flux on the viewing angle. Furthermore in the conical shock models the fact that the velocity behind the shock fans out instead of being parallel to the symmetry axis also contributes to the decrease of the beaming.

Another interesting comparison is made by taking the models corresponding to continuous jet, plasmoid with finite and infinite lifetime for a value of the bulk Lorentz factor $\gamma = 5$ and spectral index $\alpha = 0$, which corresponds to the *standard unified* model discussed before, Orr and Browne'82, and the results obtained with shock models for two values of the bulk Lorentz factor, $\gamma = 2$ and $\gamma = 7$. Looking at the probability distributions functions one sees that the same observed statistical relations could be fitted by different models with different values of the Lorentz factor. From this result one can assert that statistical predictions are not good to establish whether a beaming model is a realistic model or is not. Only with further information as knowledge of the component spectra or intensity distributions one should be able to discriminate between different models. However they could be used as estimation of the model parameters, to put limits on those values.

An important and notorious fact of the models involving shock waves,

especially conical shock fronts is the possibility to have relativistic beaming effects within a wide range of source orientation angles and in this manner reduces the strict conditions under which simple ballistic models operates.

Later on other statistical studies (*e.g.* the presence of superminal motion in weak cores of extended double radio sources) implores for relativistic beaming occuring at a wide range of orientation angles.

3.3 Other interesting statistical results

In this section we will review some results concerning the statistical properties of the relativistic beaming hypothesis.

The main problem which presents a test of the relativistic beaming hypothesis is to select a sample which is free of orientation effects, the most usual criterion is to select the sources according to a minimum flux in the extended lobes. Since they should appear to have a steep spectrum, the selection will be preferentially done at low frequencies. An important warning was given by Scheur (1986): the large scale structure could be also relativistically beamed and in that case the suppossed unbiased samples are not really unbiased.

Hough an Reahead (1986) selected a sample of 26 double lobed quasars from the 3^{rd} Cambridge Revised Catalog (3CR Laing, Riley and Longair, 1983) with the criterion that the density flux at 178 GHz exceeds 10 Jy but only in the lobes emission.

The sample was separated in two groups according to the redshift, because sources with high reshift will be probably beamed towards us and actually a correlation between linear size and redshift is found for values of z higher than 1.3, indicating that a selection effect is present at high redshifts.

Another sample which has been selected to be free of orientation effects is presented by Zensus and Porcas (1986). They selected 30 quasars from the Jodrell Bank survey at 966 MHz under the conditions that the flux exceeds 0.7 Jy, the extended structure is larger than 10 arcsecond and the maximum visual magnitude is about 19.

The first aim of these works is to study the occurrence of superluminal motions mapping the nucleus with the resolution of VLBI measurements at different times. But the inconvenient is the weakness of those nucleii and therefore only particular results have been derived by the authors since most of the sample has not been mapped with VLBI at different times to observe structural changes.

Anyway from 5 sources under study in the second sample (Zensus and Porcas'86) superluminal motion is found in 3 of them and probably in 1 more. In the first sample, Hough and Readhead'86 have studied two sources

at different times with evidence for superluminal motion in both.

Apart from the study of superluminal motions in unbiased samples, other predictions of the relativistic beaming hypothesis can be tested from those kinds of samples.

A different approach is to take samples of bright radio sources or furthermore sources which show relativistic effects as superluminal motion and to study the properties comparing to the unbeamed sources.

Examples of this kind of approach are undertaken by Browne (1986), Witzel (1986) and Impey (1986) among others.

Browne (1986) studied the extended structure of superluminal sources with the aim of clarifying the scenario where relativistic motion close to the line of sight is present.

Witzel (1986) chose a sample of flat spectrum quasars from the S5 survey (Kühr et al. 1981), which includes objects selected at 5 GHz with a low limit flux of 250 mJy, and studied the ocurrence of superluminal motions and the evidence for relativistic beaming using independent observations.

Impey (1986) studied the distinctive properties of superluminal sources at a wide range of wavelenghts from infrared to X-rays.

We will combine the two different approaches to study statistically the simple relativistic jet model.

One of the most conclusive tests is the distribution of the apparent transverse velocities.

Considering the continuous jet model with a maximum bulk velocity $v \sim c$ the probability of finding a value of v_{app} exceeding a certain value should be less than the probability to find the source within an angle θ with $v = c$ and then:

$$P(> v_{app}) < 1 - \cos\theta,$$

where $v_{app} = \sin\theta/(1 - \cos\theta)$.

If an unbiased sample of 100 sources have more than 10 sources with apparent transverse velocity larger than 5c the simple relativistic model is in trouble [$P(> 5c) < 7.5\%$]. The statistics still are not sufficient feasible to rule out any model.

However there is a tendency to observe, as measurements extends to weaker cores lower values of the apparent transverse velocity, the statistics could confirm the expected behaviour.

Hough and Reahead (1986) measured the separation velocity in two well resolved cores of their unbiased sample. The values of apparent velocities of $1.3 \pm 0.4c$ and $3.1 \pm 1.1c$ were measured for 3C 263 and 3C 245, respectively; moreover the projected linear size of 3C 263 is about 192 pc and its core is of medium brightness, whereas 3C 245 has a linear size of 34 pc and its core is rather bright. A possible explanation for this fact is that the objects are intrinsically similar but the difference is in the orientation angle, the source

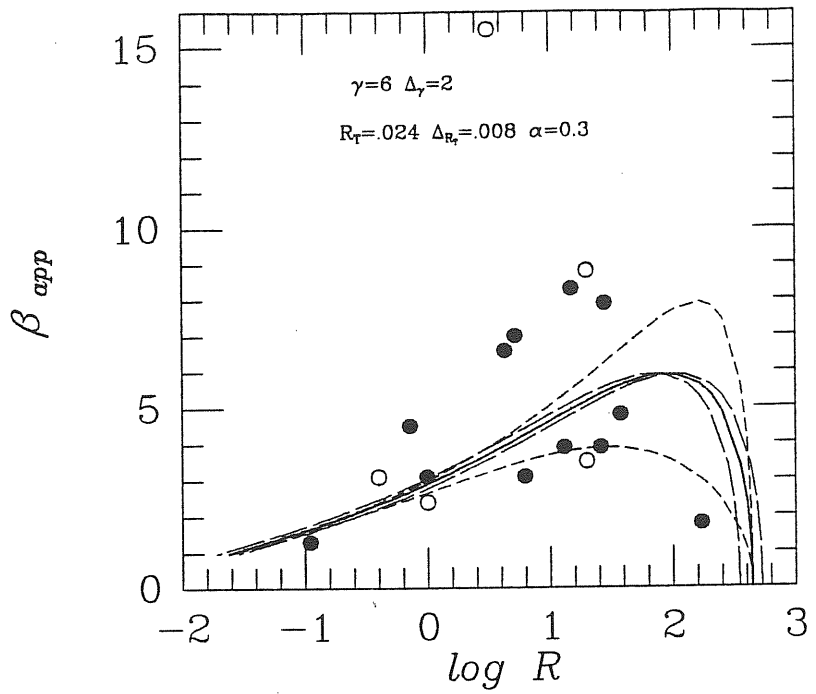

Figure 3.7: Distribution of apparent for velocities versus core strenght, the data are from Hough and Readhead (1986) and Browne (1986). Short dashed lines represent the variation in γ, long dashed lines represent the variation in ΔR_T

3C 245 is pointing closer to the line of sight than 3C 263. Another classical double source which shows superluminal motion in its core is 3C179 (with $v_{app} \sim 4.5c$).

These sources should not be oriented at small angles to the line of sight, they should form a fairly large angle. If one considers the bulk Lorentz factor to be common for all the sources and taking the minimum value for the maximum apparent transverse velocity $\gamma \sim 5$ (see the beginning of the previous chapter), the sources 3C 245, 3C 263 and 3C 179 result to be oriented with the angles $18°, 32°$ and $70°$ respectively. This is consistent with the presence of double large scale structure.

In this direction one may look at the distribution of apparent velocities versus core strenght in superluminal sources samples (see figure 3.7). Hough and Readhead'86 observed that the average apparent velocity of the core dominated quasars are twice ($v_{app} \sim 6c$) that of the lobe dominated quasars ($v_{app} \sim 3c$); using a simple relativistic model one could constrain the values of γ and R_T. In the figure we plotted R versus β_{app} using a relation for $R = R_T 1/(1 - \beta \cos\theta)^2$ and $\beta_{app} = \beta \sin\theta/(1 - \beta \cos\theta)$ with different values of γ as a parameter, this is done eliminating the angle θ from the two expressions. We found that a large range of the bulk Lorentz factor is needed to comprises the observations, the range of γ is between 4 and 8 (see the figure 3.7); however a small range of R_T is sufficient to fit the observations.

A similar correlation is found by Browne (1986): stronger cores have

higher values of the apparent velocity; moreover he pointed out that the absence of sources with vaues of β_{app} lower than $\sim 3c$ could be explained because the cores of those sources will be so weak that VLBI measurements are not yet available.

An interesting source is BL Lac, it shows the strongest value of R in the sample but its apparent transverse velocity is very low, $\beta_{app} \sim 1.8$. This fact could be interpreted if this source is oriented very close to the line of sight ($\theta \sim 13°$ for $\gamma \sim 5$) and the location in the graph is consistent with the predictions of the beaming model.

3.3.1 Misalignments

In the line of elucidating whether the extended emission corresponds to a prolongation of the milliarsecond structure supposed to be relativistic beamed, one should look at the aspect of both structures in the same objects. Anyway misalignments and bending of the jets at both large and small scale could be observed. The presence of relativistic motions along the line of sight may amplify the curvature of the jet producing an extra bending of the structure (Readhead et al., 1978) by a factor as much as γ.

An application of this effect is briefly discussed by Scheuer (1986), he took a wavy jet (it can be simulated by imposing a sinusoidal pertubation to the simple ballistic model, precession effects are also consider in the literature and they seem to have the same effect, for instance see the works of van Groningen, Miley and Norman, 1980; Linfield, 1981) and looked at the kinematics effects which can modify the appearance of the jet. The results confirmed that when considerable bends are produce in the jet very large variations of the brightness are consequently obtained, but also that long straigh bright portions are alternating with invisible parts seen at different angles.

The idea is that relativistic beaming could produce misleading in the observed patterns and *we are seeing irregularities in the flow* rather than a uniform and universal pattern.

Following from the previous discussion, Browne (1986) concluded from his study of the extended structure in superluminal sources that extended structures always appear around the core, the motions occurr towards the brighest part of the extended structure and where a large scale jet is present the small scale jet looks like to join up.

The misalignment between the arsecond structure and the milliarsecond structure is found to be concentrated at small angles but also a second peak is found around 90°.

On the other hand Hough and Readhead'86 confirmed the same result in the double lobed quasars: asymmetries always lie in the same side of the core.

Hough and Readhead'86 found a correlation between the curvature defined as the supplement of the angle made by the vectors which connect the core with each of the lobes. This correlation is also found between the curvature and the parameter R (ratio of the core strenght to the lobes).

With these results it is possible to estimate that an intrinsic misalignment less than 10° is consistent with the observations, based on the uniform distribution of values of the R parameter.

Furthermore an average angle of 9° is found by Hintzen, Ulvestad and Owen (1983) for a sample of quasars selected at radio frequency.

Therefore one should not expect to have intrinsic misalignments in the extended structure of strong radio sources (Faranoy-Riley class II) larger than 10°. The importance of this result should be clear in the next subsection.

3.3.2 Linear size of relativistically beamed sources

An evident consequence of the special orientation of the relativistically beamed sources is that the projected linear size should decrease with the angle to the line of sight decreasing if one assumes that the linear size of the sources does not differ too much from source to source. Hence for large values of the ratio R small projected linear sizes of the sources are expected.

This result is confirmed by Hough and Readhead (1986), an anticorrelation between the value of R and the linear projected size is found.

However it has been pointed out by several people (de Bruyn and Schilizzi, 1986; Barthel et al., 1986) that if one deprojects by using the small angle required by the relativistic jet model the extended radio structure around superluminal sources will result too big.

Barthel (1986) concluded that the sources which present relativistic motion are between the largest quasars once deprojected (see figure 3.8). To ilustrate this conclusion he took the quasar 4C 34.37, which is one of the largest known quasar ($560h^{-1}kpc$ with $h = H_o/100, q_o = 0.5$). It exhibits a one-sided jet with a brightness ratio ($jet\ to\ counterjet \approx (1+\beta\cos\theta/1-\beta\cos\theta)^2$) around 10:1 and therefore is supposed to be oriented not very close to the line of sight ($\theta \lesssim 60°$).

This quasar 4C 34.37 shows superluminal motion of this source with an apparent velocity around $3.1c$ which implies a minimum angle with the line of sight $\theta \sim 36°$. The probability to find a source within an angle of 36° is about 20%. Therefore at least five sources should be found that are as large as 4C34.47. But these sources have been not found up to now.

A more significative set up of the large linear size problem of the relativistic beamed sources is made by Browne (1986).

A comparison sample is selected by matching for each superluminal

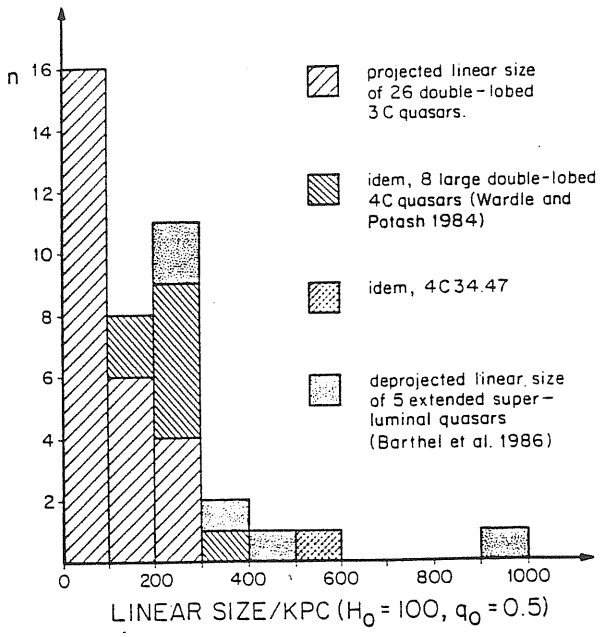

Figure 3.8: Linear size of superluminal quasars compared to the distribution of unbiased sources, from Barthel (1986)

source two or more quasars in similar redshift and similar extended emission.

The projected linear sizes of the superluminal is found to be smaller than those in the comparison sample.

The problem begins when we tried to choose a deprojection factor. From the apparent superluminal velocity one gets a maximum value for the angle with the line of sight, but it is not clear where this should be the right orientation angle; on the other hand many works adopt the value which minimizes the bulk Lorentz factor, a possible solution is to take an intermediate value.

But from the previous subsection the result that an intrinsic misalignment lower than 10° is permisible, we will consider that when a source is to be oriented within an angle less than 10° as deduced from the apparent motion, then the source should be deprojected using the intrinsic misalignment angle.

The conclusion obtained from the comparison of the deprojected linear size distribution of superluminal sources is that these sources are in fact larger than the "normal" sources.

Another interesting result is mentioned by Browne (1986): Murphy in his Ph. D. Thesis (the Victoria University of Manchester) compared the linear sizes of core selected quasars with those of the lobe selected quasars and found that for a relativistic jet model with $\gamma \sim 7$ the core selected sources are larger than the predictions of the model, he concluded that large misalignments should be observed between the core and the lobes (larger than 30°) to reconcile with the beaming theory, but those large

misalignments angles are not seen.

Browne'86 claimed that a correlation between linear size and bulk Lorentz factor may exist, faster jets produce larger sources. A similar correlation is found in the large scale structure of the radio sources: Faranoy-Riley class II are larger sources than Faranoy-Riley class I[6].

A second possibility is that a wider range of orientation angles in the emitting fluid would produce Doppler boosting at different angles than the actual orientation angle of the large scale structure; by the way Browne'86 rejected this hypothesis based on the narrow range of misalignments with the large scale structure observed in superluminal sources.

3.3.3 Independent evidences for relativistic motions

An independent (of the observations of the radio morphology) test of relativistic beaming models could be done looking at other expected features of the models. For instance, to compare the calculated inverse self-Compton radiation with the observed flux at X-rays. Since the predicted flux depends on the inverse of the Doppler factor (for an homogeneous source) in the following way:

$$S_\nu^C \propto S_{\nu_m}^{2(\alpha_o+2)} \nu_m^{-(3\alpha+5)} \theta^{-2(2\alpha_o+3)} \nu^{-\alpha_o} \mathcal{D}^{-2(\alpha_o+2)}$$

a minimum Doppler factor is obtained because other mechanisms could also contribute to the X-rays flux. However in this expression there are two quantities which are not always well espicified: the maximum frequency and the angular size of the source which is frequency dependent and should be precisely determined at the maximum frequency that is often not known.

Another lower limit in the Doppler factor can be put by using the observations at low radio frequencies. We spoke in the first chapter about the inverse Compton problem: the brightness temperature should not exceed by much the value $10^{12}\ ^\circ K$, however one can lower the observed value,

$$T_B \propto \left(\frac{1}{t_{var}}\right)^3,$$

by changing t_{var} by $t_{var}\mathcal{D}$ and if the source is relativistically expanding and $\mathcal{D}$ is the Doppler factor. Therefore the new value for the brightness temperature is given as:

$$T_B \propto \left(\frac{1}{t_{var} > \mathcal{D}}\right)^3;$$

[6]Large luminosity sources, FR-II, implies large internal energy at the end of the jet and therefore large velocity through the jet, whereas low luminosity sources, FR-I, have lower internal energy at the lobes and therefore lower velocity through the jet. We assumed that the internal energy at the end of the jet comes from the conversion of the bulk kinetic energy present along the jet.

the minimum value of $\mathcal{D}$ needed to lower T_B down to the value 10^{12} ° is a lower limit for $\mathcal{D}$.

Witzel (1986) chose a subsample (13 sources) from the S5 survey as we mentioned above and he studied the structural changes at $\lambda \simeq 6cm$ (5 GHz) for 12 sources and the result is that superluminal motion is found for most of the sources with known redshift and at least there are strong candidates among those without known redshift.

Furthermore Witzel'86 obtained lower limits of the Doppler factor using the two previously described methods (see figure 3.9). He obtained evidence for bulk relativistic motion using the self-Compton prediction in the 13 sources, with only one exception: the source 1803+78 does not show structural changes but the Doppler factor predicted by the self-Compton and variability arguments indicate bulk relativistic motion. This fact is not surprising since some sources do not show structural changes during a long period and in other times they show superluminal motions, then the source 1803+78 is a good candidate to superluminal source.

In general lower values of $\mathcal{D}$ are obtained from the variability argument (see figure 3.9). The values of the Doppler factor obtained by the variability and self-Compton arguments are fairly well correlated, however the values derived from superluminal motion are in general larger than the others, this could mean that the value of the Doppler factor is overestimated because the projection angle is larger than the adopted value.

A similar work was done by Madau, Ghisellini and Persic (1987). They consider a sample of about 40 objects with known VLBI size and X-rays flux. They calculated the minimum Doppler factor by the argument of the maximum self-Compton scattering flux.

The result is that for BL Lac objects the Doppler factor calculated in this way ranges from the value 0.01 to 15 and half of the sources have $\mathcal{D} < 1$. On the other hand high polarized quasars (HPQs) show values of $\mathcal{D}$ larger than unity up to a value around 19.

The fact that Doppler factors are less than unity for BL Lac objects does not imply neccesary misaligned beaming of the radiation, since the X-rays flux could have a different origin than self-Compton scattering.

Ghisellini (1987) argued that there is evidence for some BL Lacs being oriented at large angles to the line of sight from a certain correlation observed between the R parameter (ratio of core component to extended emission) and $\mathcal{D}$, however this argument could not be valid from the large observed values of the parameter R, characteristics of BL Lac's. Misclassified objects could be a reason for this discrepancy.

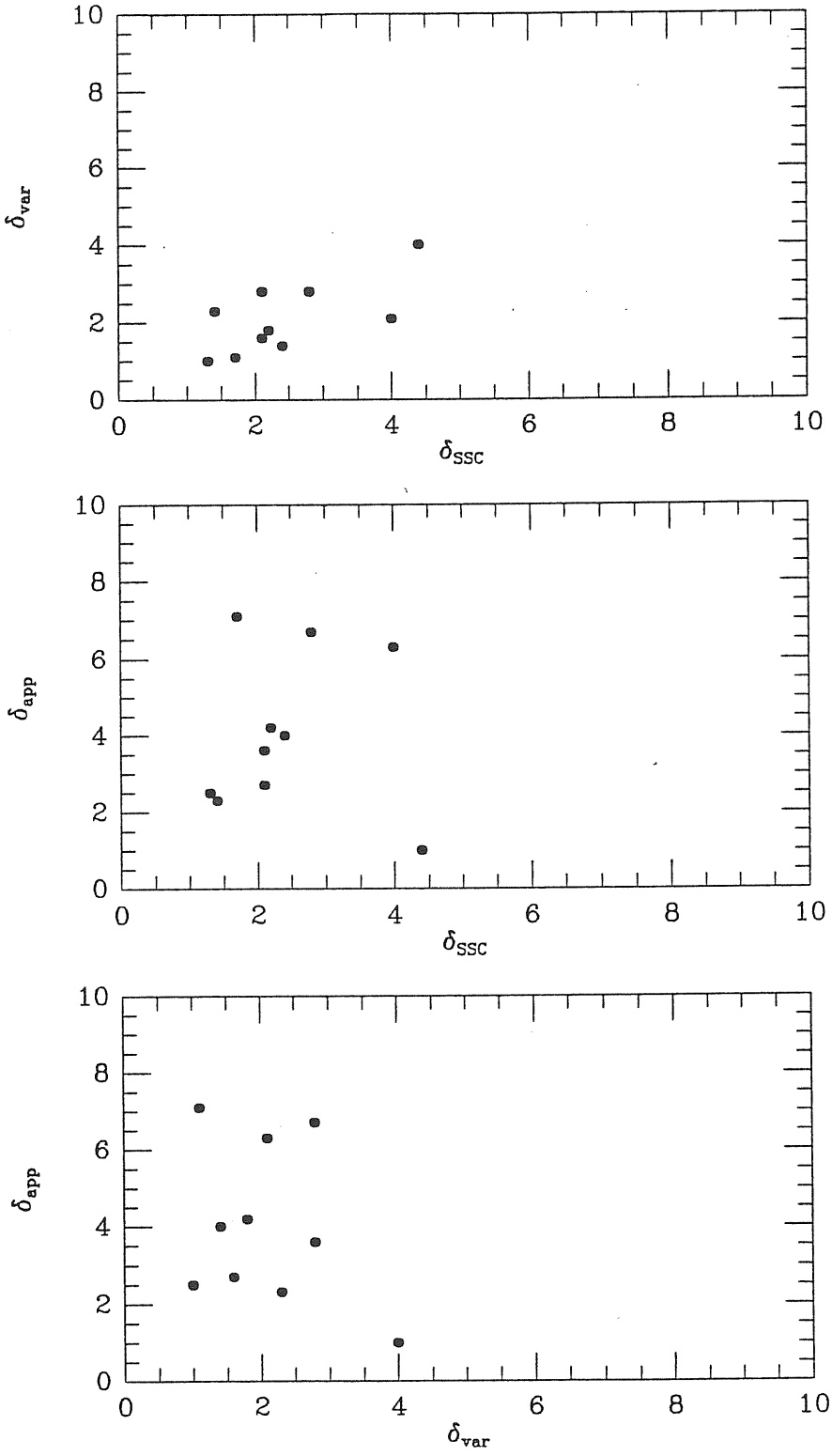

Figure 3.9: Different values of the Doppler factor obtained by the different estimations, the data are taken from Witzel (1986)

3.3.4 Infrared, Optical and Ultraviolet properties

The extension of measurements to optical infrared and UV bands permits to build up new tests of the relativistic jet models. Spectroscopic measurements could also reveal to be powerful tests. The line emission could be well supposed to be free of beaming effects (the Narrow Line Region is believed to be located at $10^4 pc$ and then very far from from the base of the relativistic jet). Therefore the ratio of the line emission to continuum emission is a good indicator of beaming. One could tries to plot curves of this ratio versus beaming parameters and expects for correlation or even try to put constrains on the models. To compare with the observations is not an easy task since the measurements are done with different sensibilities and therefore difficult to calibrate absolutely.

Moreover an isotropic component could be present at infrared, optical or UV frequencies. The parameter f will account for this unbeamed component, f is defined as the ratio beamed component to unbeamed component when the source is oriented perpendicularly to the line of sight (the parameter f is very similar to the value R_T in the Orr and Browne'82 model).

The observed line to continuum ratio L/C is then given by the expression:

$$\frac{L}{C} = \left(\frac{L}{C}\right)_o \frac{1+f}{\mathcal{D}^2 f + 1}.$$

As the factor f is lower the beamed component is less important and the ratio L/C decreases slower with the Doppler factor increasing.

In realistic models a range of values in f should be present as a range in L/C.; larger values of $\mathcal{D}$ should be needed to blank more the lines when the isotropic component is dominant. Using these statistics one could be able to constrain values of the Doppler factor for different classes of objects (which may be classified according to the ratio line to continuum emision).

Another important correlation is found from the indication that low polarization sources shows higher L_{opt}/L_{radio} ratios than high polarization sources (if high polarization sources are relativistically beamed whereas low polarization sources are not); supporting evidence for this is the fact that Hough and Readhead (1986) found no correlation between the optical luminosity and the parameter R. This seems to indicate that the optical flux is not beamed in low polarization sources.

In this direction one could expect some connections between optical polarization properties and radio observations. In fact measuring the differences between the polarization angle at optical wavelenghts and the position angle of the milliarsecond structure, the distribution is found to be peaked around 0°, but there is also a peak at 90°. This could be explained by different emission mechanisms. From further disecting the statistics Impey (1986) discovered that radio galaxies do not show a preferred alignment

of the VLBI structure with the optical polarization, however quasars and blazars show a strong alignment. This is consistent with the fact that in blazars and quasars the synchrotron radiation is producing the polarization whereas in radio galaxies other mechanisn could be responsible for the polarization as electron scattering and therefore lower degree of polarization should be observed.

3.3.5 Asymmetry in the polarization properties

A possible confirmation of the special orientations expected in sources showing relativistic effects is coming from the work of Laing (1988) and Garrington, Leahy, Conway and Laing (1988).

A sample is selected among strong radio sources among those which present a *double structure* but in which *only one jet* is seen.

Garrington et al'88 obtained the maps of the polarization for 25 of the those sources and look at the degree of polarization occurring at two different radio wavelenghts ($\lambda 20\ cm$ and $\lambda 6\ cm$), to look for depolarization effects.

From the differential Faraday rotation the flux at larger wavelenghts will be less polarized proportionally to the thermal plasma found by the radiation in its path to reach the observer[7]; the important result from this work is that depolarization occurs for all the sources in the side which does not contain the jet, whereas in the side containing the jet depolarization is less marked (see figure 3.10).

The stronger depolarization is occuring in the direction of more matter presents in the viewing line, therefore in the jet side there is less matter than in the opposite side.

The thermal plasma which is depolarizing the radiation may be located either within the radio components or around the source.

In the first possibility the jet is intrinsically one sided, the differences in Faraday depolarization are intrinsics to the source.

Whereas in the second possibility the jet is relativistically beamed and the counter jet is always seen (when it is seen) through a larger amount of thermal plasma.

The way to distinguish between these two possibilities is to make high resolution polarization measurements; at higher resolution the depolarization should be less pronounced and not correlated with the features of the radio emission, as observed in 3C130 and other edge darkened sources

[7]The amount of rotation of the polarized flux is given by $\Delta\phi = RM\lambda^2$, where the quantity $RM = 810 \int n_e B dl_{kpc.}\ rad\, m^{-2}$ is called rotation measure. A depolarization is observed because we should add in projection the rotation suffered by emission coming from parts farther back in the source with the less rotated from the closer parts .

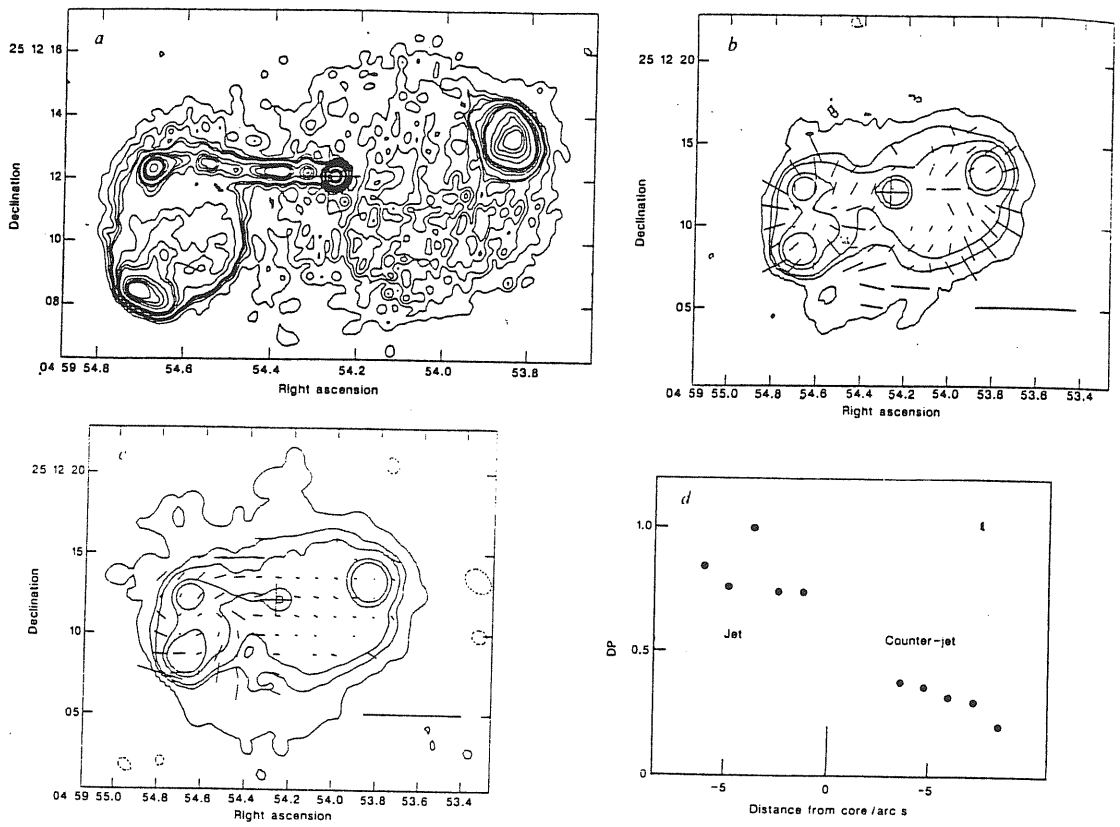

Figure 3.10: Maps of the source 3C133: (a) VLA map at 4.9 GHz; (b),(c) Polarization vectors imposed to the intensity distribution at 4.9 GHz and 1.4 GHz, respectively; (d) depolarization profile averaged perpendicularly to the direction of the jet. The lenght of the vectors indicate the degree of polarization; from Laing (1988)

(Jägers et al.), but only with the running of the gradients in the Faraday rotation as observed in Cygnus A and NGC 6251.

Chapter 4

Shocks as the origin of radio variability

4.1 Introduction

At the beginning of chapter 1 we spoke about jets as channels which allow to transport energy from the central active nucleus to the outer lobes. Therefore the jets will contain with a large bulk kinetic energy.

If the channel of the jet were perfect and non dissipative the jet will remain invisible. Since jets are observed and they present rather high surface brightness, dissipation mechanisms should be invoked. Besides the structures seen in the jet are neither homogeneous or smooth or continuous but they are complex and inhomogeneous.

Certain dissipation will occurr at the interface between the jet channel and the ambient medium and probably a turbulent region will be formed. Furthermore in the central parts of the jet shock fronts could form. The origin of these shocks could be varied, for instance if the flow finds an obstacle in the way to the outer parts a bow shock will form close to that obstacle. Wilson and Scheuer (1983) calculated the intensity distribution and flux of a hot spot of a midly relativistic jet in the optically thin limit.

In other case if the flow is unsteady, supersonic and propagating in a decreasing density medium, a perturbation of pressure or density which is propagating down at the same time it will steepen, perhaps forming shocks waves. Shocks waves constitute a particurlarly natural method of introducing dissipation in the flow, hence converting bulk kinetic energy in internal energy. By the way they have a desiderable fact: the acceleration of particles by Fermi processes operates effectively at the shock fronts (see for instance Blandford and Ostriker, 1978). Acceleration of particles at the outer parts of the radio sources is usually invoked because the synchrotron lifetime of the elctrons is in general shorter than the radiative lifetime of

the source.

The aim of this chapter is to describe the expected features seen in the brightness distribution and flux coming from an emitting flow with shock waves. The shock wave will propagate through a preexisting jet. Therefore the conditions through the jet will be given a priori and the shock will not modify them.

In the first section I will present a model which permits to calculate the brightness distribution and the integrated flux of a perturbation injected up in the base of the channel. This perturbation will propagate down through the jet and at the same time it will undergo adiabatic losses due to the expansion of the beam. Then the emitting electrons will loose energy and the emission will progressively dim. At the end of the section an application to the blazar AO 0235+164 is presented. The observations are made in a long period over 5 yr and at a large range of frequency.

In the second section I will described a more sophisticated model. This model is based on the existence of a piston (enhanced density perturbation) producing shocks in the propagation down through the jet. The shocks will compress the magnetic field (a random magnetic field is existing in the jet) and then produce outbursts in the degree of polarization simultaneously with outbursts in the total flux. This model is based on the observations of BL Lac in total and polarized flux during the period 1980 to 1984.

In the third section I will present a model very similar to the one presented in the first section. The difference is basically in the more qualitative predictions of the present model compared with the more quantitative predictions of the former. For the rest the model considers how the structure of the shock evolves during the propagation through the jet and what are the relevant emission processes at each stage of the evolution of the shock. The interesting observations for this model are made at high radio frequency and specifically the model is applied to the radio quasar 3C 273 during a flare exhibited at millimeter wavelenghts in 1983.

In the models described in the sections 1-3 the shocks are imposed *ad hoc* to the jet and the problem is to follow the propagation downstream through the given jet conditions. However in the last section I will mention about models in which the shock appears naturally and evolves perhaps modifying the downstream flow.

4.2 Adiabatically evolving structures

In this section I will describe a simple model which does consider the adiabatic evolution of a structure injected at a certain radius at the base of a jet. This model is described in O'Dell et al.(1988) and O'Dell (1988). Our discussion is largely based on these references.

The basis of the model is the observation of some pattern which is introduced in the base of the jet close to the central object, and to follow it propagating through the jet.

Let us consider a narrow jet, oriented at an angle θ with respect to the line of sight and with a constant bulk Lorentz factor. The distance along the jet is parametrized by a dimensionless parameter ζ defined as $r = r_1\zeta$ where r is the distance along the jet and r_1 is the point at which the injection occurs. The transverse radius is parametrized in the same way by $R = R_1\zeta^\epsilon$ where ϵ gives the geometry of the jet ($\epsilon = 1$, conical free jet;$\epsilon < 1$, elongated confined jet).

The model is constructed in such a way that the initial conditions at the base of the jet are known and specify as functions of the time. These initial conditions fix the consequent evolution of the jet flux density. Therefore the conditions at a certain position in the jet are conveniently parametrized by the elapsed time for the flow element to reach that position starting from the injection place.

At a given time to calculate the emitted flux one should integrate along the whole extension of the jet. The conditions at a certain radius are known for extrapolating back in time, up to the moment in which that structure was introduced in the base of the jet; moreover one should take into account the evolution of the physical quantities through the jet. Nevertheless there is an effect of time delay in the radiation coming from inner regions of the jet due only to geometrical effects and finite signal propagation speed.

Then the radiation observed at time t is emitted by fluid elements which have been injected in the base of the jet at time t'':

$$t'' = t' - (r - r_1)/\beta c$$

t' is the retarded time corresponding to the difference of propagation time from the base of the jet:

$$t' = t + (r - r_1)/c\cos\theta.$$

The radiation coming from a fluid element at position r takes less time than the radiation coming from the base of the jet. Therefore at the observing time t the radiation was emitted at the position r at the time t', later than at the base. Then the expression for the time at which one should extrapolate back the conditions is:

$$t'' = t - (\zeta - 1)(r_1/\beta c)(1 - \beta\cos\theta) = t - (\zeta - 1)t_1,$$

where t_1 is the apparent transit time scale and corresponds to the minimum variability time scale observed for the source and is corrected for the shortening of the time due to Doppler effect:

$$t_1 \equiv r_1/\beta c(1 - \beta\cos\theta).$$

The fluid element injected at the base of the jet will evolve according to the number density, energy and magnetic flux conservation as in the majority of the models. Using the previous parametrization for the position along the jet channel those quantities can be written in the frame of the jet as:

$$n(r,t^{'}) = n_1(t^{''})\zeta^{-2\epsilon}$$
$$\gamma_e(r,t^{'}) = \gamma_e(t^{''})\zeta^{-2\epsilon/3}$$
$$B(r,t^{'}) = B_1(t^{''})\zeta^{-m\epsilon},$$

where the subscripts 1 indicates values of the quantities at the base of the jet.

In deriving the above expression the following considerations are done: a volume element varies as $R^2 \propto \zeta^{2\epsilon}$, the individual electron energy is decreased adiabatically, $\gamma_e \propto R^{-2/3}$, and the magnetic field changes as R^{-m}.

A dimensionless frequency f is defined by the expression $f = \nu/\nu_1$, where ν_1 is a reference frequency.

The emissivity and absorptivity for synchrotron radiation are parametrized in this way as:

$$\epsilon_\nu(r,t^{'}) = \epsilon_1(t^{''})f^{-\alpha}\zeta^{-\epsilon[2(1+2\alpha/3)+m(1+\alpha)]}$$

$$k_\nu(r,t^{'}) = k_1(t^{''})f^{-5/2-\alpha}\zeta^{-\epsilon[2(1+2\alpha/3)+m(3/2+\alpha)]}$$

and the source function:

$$l_\nu(r,t^{'}) \equiv \frac{\epsilon_\nu(r,t^{'})}{k_\nu(r,t^{'})} = l_1(t^{''})\zeta^{\epsilon m/2}\, f^{5/2}.$$

The optical depth through the width of the jet is:

$$\tau_\nu(r,t^{'}) = \tau_1(t^{''})\zeta^{-\epsilon[(1+4\alpha/3)+m(3/2+\alpha)]}\, f^{-5/2-\alpha}.$$

The total flux is obtained from the integration upon the lenght of the jet:

$$S_\nu = \int_0^{\chi_{max}} l_\nu(\chi)(1-\exp(-\tau(\chi)))2\Theta(\chi)d\chi,$$

where Θ is the tranverse angular extension of the jet and χ is angle giving the projected position on the jet. Then with the temporal parametrization introduced above the expression for the flux results as:

$$S_\nu(t) = \int_1^\infty \Phi_1(t^{''})\zeta^{\epsilon(m/2+1)} f^{5/2} \times$$
$$\left[1-\exp\left(-\tau_1(t^{''})\zeta^{-\epsilon[(1+4\alpha/3)+m(3/2+\alpha)]}\, f^{-5/2-\alpha}\right)\right] d\zeta,$$

$\Phi_1(t'')$, $\tau_1(t'')$ represent the source function and the optical depth at radius r_1 and the reference frequency ν_1. These functions could be estimated from the evolution of the source flux at the higher frequencies where the source could be considered optically thin.

The evolution of the flux density is completely determined from the specification of the two time dependent functions Φ_1 and τ_1 and the two parameters ϵ and m.

The upper limit of the integral is only valid when the energy distribution of relativistic electrons is a power law extended up to arbitrarily large energies. But in the general case there is a break at high energies due to radiative losses. The upper break in the energy distribution of electrons is given by $\gamma_u = \gamma_{u_1}\zeta^{-2\epsilon/3}$, where γ_{u_1} is the break of the energy distribution at the base of the jet and the energy of the electrons is decreasing due to adiabatic losses. The break in the frequency is given by the expression:

$$f_u = f_{u_1}\zeta^{-\epsilon(m+4/3)}$$

and therefore the maximum distance for a given frequency at which the integral should carry out is given by:

$$\zeta_u(f) = (f/f_{u_1})^{-1/\epsilon(m+4/3)}.$$

However in most cases the contribution comes mainly from the regions close to the base of the jet and the integral could be calculated from 1 to ∞.

Let us first consider what is the expected emission from a stationary jet, hence τ_1 and Φ_1 are not functions of the time.

At frequencies for which the jet is transparent at the base $\tau_1 f^{-5/2-\alpha} \ll 1$, the integral giving the flux is easily evaluated and the result is:

$$S_\nu^{thin} \propto \Phi_1\tau_1 f^{-\alpha},$$

where convergence at infinity has been assumed.

At frequencies where the jet is optically thick $\tau_1 f^{-5/2-\alpha} \gg 1$ at the base but it could be optically thin in the outer parts, the flux is given by the expression:

$$S_\nu^{thick} \propto f^{-\alpha_p},\ \alpha_p = -\frac{\epsilon\left[(7\alpha/3) + m\,(5/2 + 2\alpha)\right] - (5/2 + \alpha)}{\epsilon\left[(1 + 4\alpha/3) + m\,(3/2 + \alpha)\right]}.$$

For the case in which the jet is conical ($\epsilon = 1$) and with dominant transverse magnetic field ($m = 1$) the spectral index becomes:

$$\alpha_p = \frac{-20\alpha}{15 + 14\alpha}$$

which produces a spectrum flatter than the self-absorbed spectrum.

Returning to the time dependent behaviour, important differences are obtained from the way in which the outbursts are produced. For a single outburst there are basically two different ways of injection at the base of the jet: prompt or continuous injection.

Let us consider a single outburst with an observed duration Δt_o, the maximum radius which can reach before extinction is given by:

$$\Delta\zeta_o = \frac{\Delta t_o}{t_1}.$$

However if at the base of the jet the injected plasma is opaque at a given frequency ν, it will not be observed at this frequency until the position $r_m(f)$ is reached. This distance is calculated by the expression:

$$\tau_\nu(r, t^{'}) = 1 \text{ or } \tau_1 f^{-5/2-\alpha} \zeta_m^{-\epsilon[(1+4\alpha/3)+m(3/2+\alpha)]} = 1.$$

So the outburst at this frequency will be detected with a delay with respect to the high frequencies outburst (where the base of the jet is transparent). Turning to the parametrization with the time, this delay time is given by the expression:

$$t_m(f) = (\zeta_m(f) - 1)t_1$$

Therefore the maximum flux density near the time $t_m(f)$ at the frequency f has a value:

$$S_m(f) \approx \Phi_1[\zeta_m(f)]^{-\epsilon(m/2+1)} f^{5/2} \Delta\zeta,$$

where $\Delta\zeta$ is the minimum between the values $\Delta\zeta_o$ and ζ_m. The distinction between prompt and prolonged injection is reflected in these two time scales. For prompt injection the flux is limited by $\Delta\zeta_o$ while the continuous injection the minimum $\Delta\zeta$ is ζ_m. There are important differences for these two cases in the behaviour of the peak flux with the frequency.

For prompt injection the extent of the emitting region is independent of frequency and therefore:

$$S_m(f) \propto f^{k_o},$$

where $k_o = [7\alpha/3 + m\,(5/2 + 2\alpha)] \,/\, [(1 + 4\alpha/3) + m\,(3/2 + \alpha)]$, and $k_o = [13\alpha/3 + 5/2] \,/\, [5/2 + 7\alpha/3]$ for $\epsilon = 1$ and $m = 1$, which is a rather strong dependence on frequency.

However for a prolonged injection the variation of the peak of the flux density with the frequency is:

$$S_m(f) \propto f^{-\alpha_p},$$

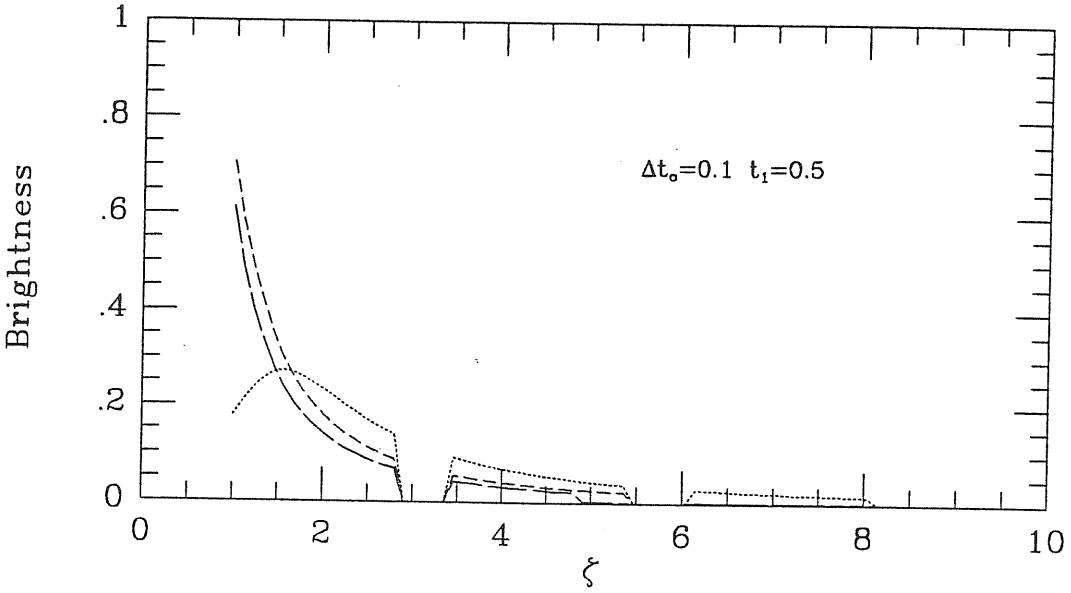

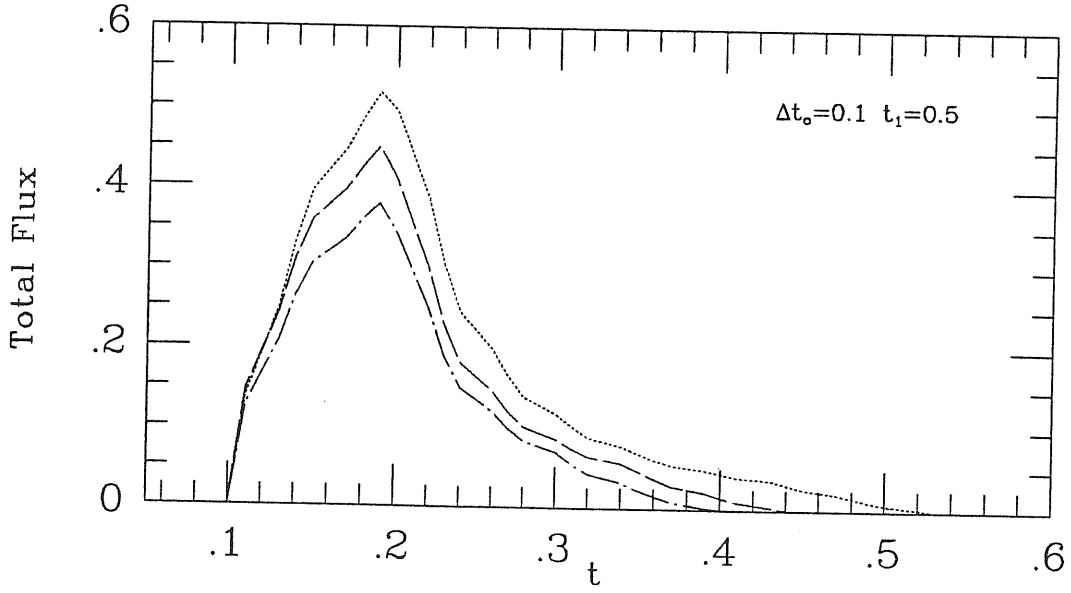

Figure 4.1: Propagation of a rectangular pulse of duration 0.1. Top figure: Brigthness distribution at three different times (t=0.19,0.45,0.71). Dotted, short dashed and long dashed lines correspond to the frequencies f=0.5, 1.5,2.5, respectively. Bottom figure: Time evolution of the total flux at three different frequencies (dotted, dashed and dot-dashed lines correspond to f=0.88,1.91,2.48, respectively)

being α_p the same as the one given above for optically thick stationary jets, which is a rather weak dependence on the frequency.

along the jet axis for three different times With these prescriptions it is possible to think about what is the response to the injection of a wide pulse (see figure 4.1). At high frequencies where the base of the jet is transparent the emission will be dominated by those internal parts and plateaus of emission are obtained. Instead at low frequencies where the base of the jet is opaque the flux will rise when the pulse has propagated at outer regions therefore it will be observed with a certain delay and furthermore the increase of the flux will be longer and smoother but with smaller plateaus. When the injection terminates the trailing edge of the pulse is moving outward and emission from the inner region declines while the emission from the outer regions remains constant and the shock declines later at lower frequencies.

In fact this behaviour is commonly observed in the radio outbursts of compact variable radio sources. The same kind of behaviour is expected from a expanding cloud model but in this case the amplitude should change strongly with the frequency which is not observed.

4.2.1 Comparison with observations

O'Dell et al. (1988) reported the results from monitoring the flux of the source AO 0235+164 during the period between 1980 and 1984 at eight frequencies covering the range between 318 MHz and 14.5 GHz.

The flux density variations are correlated over the whole range of frequencies showing that even low frequency variability should correspond to intrinsic variability.

There are other sources which show the same kind of behaviour, variability correlated over a wide range of frequencies including the low frequencies. BL Lac and OJ 287 are in this category also other three sources are found by Padrielli et al. (1987). The same analysis could be applied to these sources and check out that the model is basically right and could be used to predict behaviour at different times and frequencies.

AO 0235+164 exhibited at the highest observed frequencies series of well marked outbursts. These outbursts rise and fall in a short time scale (about few weeks), but they stand at the high flux level for a longer time (about a year). Moreover the outbursts at the highest frequencies show a non inverted spectrum and appear almost simultaneously. This indicates that the source should be transparent at those frequencies, although a rather flat spectrum is observed (spectral index $\alpha \approx 0.3$).

O'Dell et al (1988) were able to predict the flux at the lowest observed frequencies (as low as 318 MHz) taking the time series for $\tau_1(t'')$ and $\Phi_1(t'')$

from the highest observed frequencies 14.5 GHz and 8 GHz. The free parameters to adjust the observations are the apparent transit time scale t_1, the transparent spectral index and the exponents ϵ and m, modelling the geometry and magnetic field structure, respectively.

The model fits reasonably well the basic features of the observations (see fig 4.2). The important fact is the large range of frequency which is covered by the model. However there is a period in which the spectral behaviour is different. The spectrum is inverted at high frequencies and then self-absorbed but at low frequencies the spectrum is not so inverted. An explanation for this anomalous behaviour is the ocurrence of the enhancement of the emission at regions far from the base of the jet and therefore the flux at low frequencies is increased over the expected valued. The model does not account for events which originates in regions different from the base of the jet, to account for this effect one should consider an injection function with a dependency on the position in the jet. But at this point the complications of this semiempirical model are increasing so much that it seems more interesting to build up a model in which the hydrodynamics is treated more carefully and therefore those perturbations should appear more naturally.

Anyway this model has some more advantages. It permits to do predictions about the radio structure of the source. The angular structure is given by the integrand in the expression for the total flux. O'Dell et al. (1988) produced a linear brightness distribution which seems consistent with the observed VLBI maps at the same period and frequency.

The interest of this model is the interpretation of VLBI maps; suppose that an increase in the total integrated flux is detected and the previous model can be applied because measurements at sufficiently high frequencies have been done to well establish the time functions needed to specify the model. Then the evolution of new emerging components could be predicted and adjusted to the observations of the small scale structure and analyze the dynamics of the components. Certainly it can not account for bending effects or new features appearing in the middle of the jet but otherwise it can give a good tool to fit radio observations.

4.3 A piston driven shock

4.3.1 Observations

BL Lacertae exhibited during the period between 1980 and 1984 a series of well separated outbursts, offering a good chance to individuate the development of each event (see fig 4.3). These outbursts are reported by Aller,Aller and Hughes (1985). The observations are done at three differ-

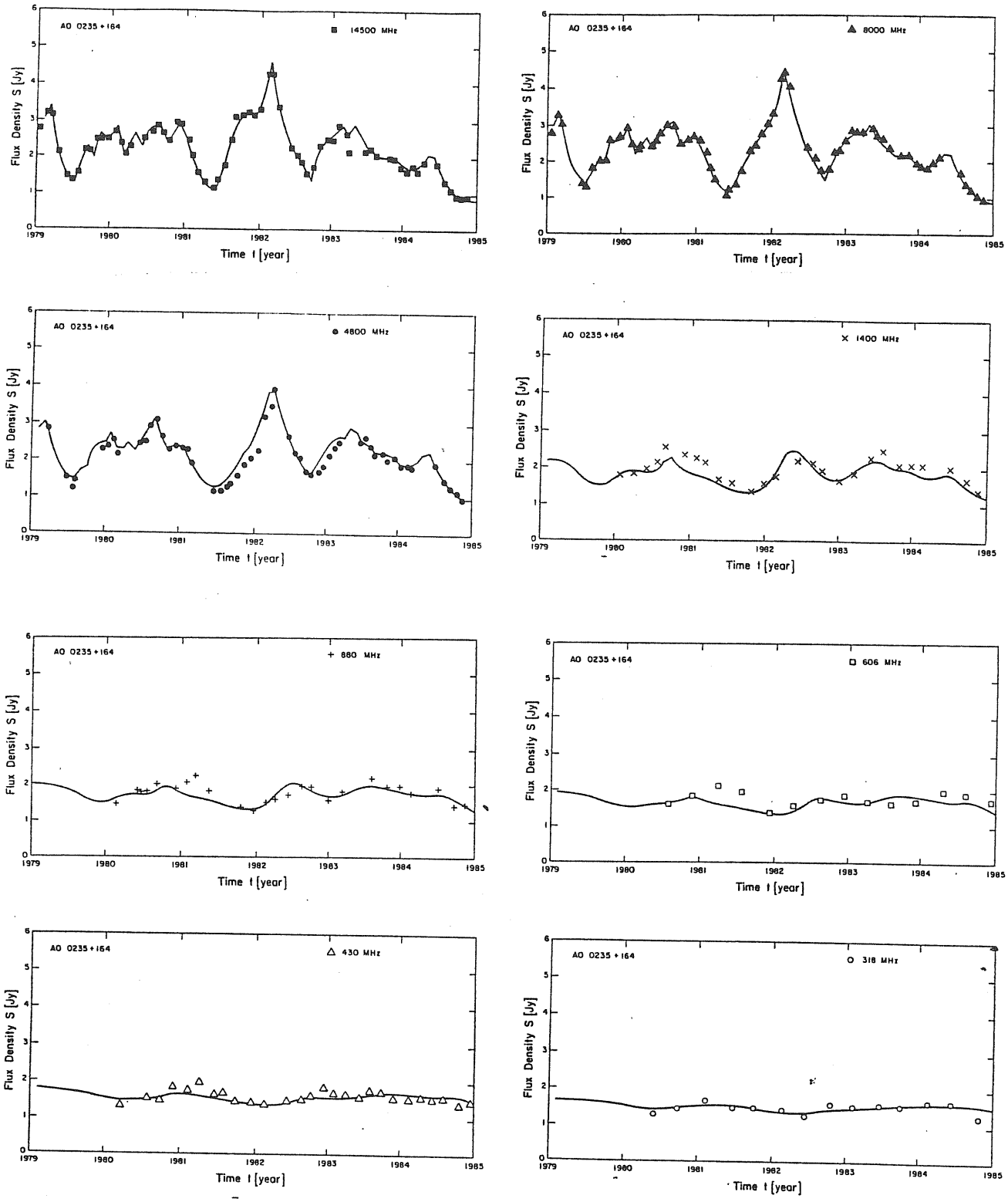

Figure 4.2: Flux densities history of AO 0235+164 at different radio wavelenghts; from O'Dell et al, 1988

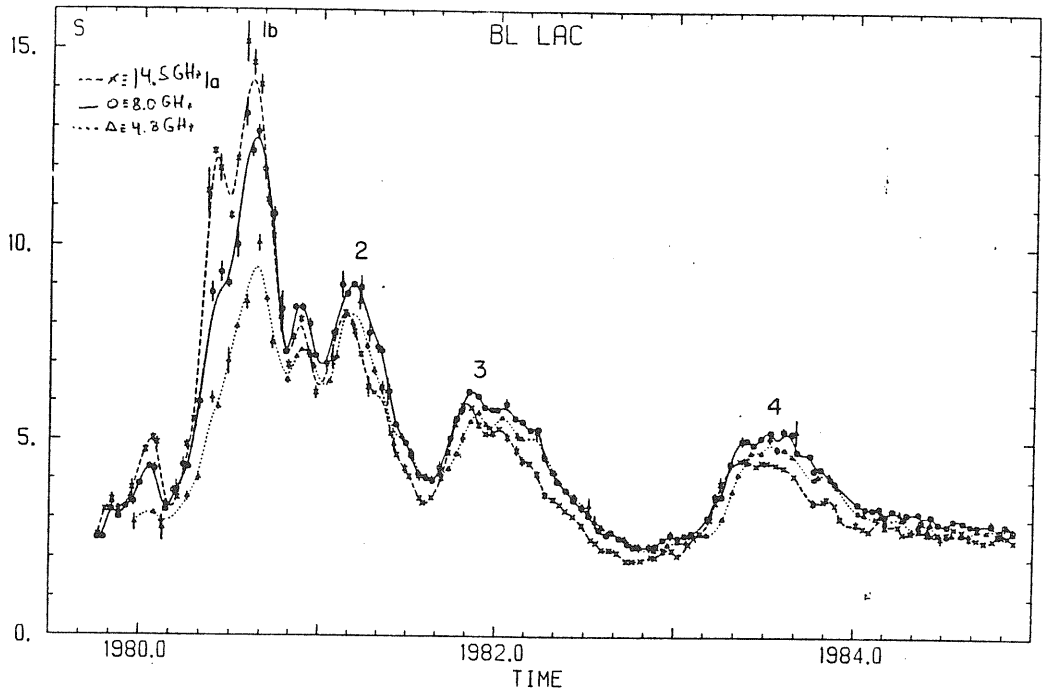

Figure 4.3: Total flux density of BL Lac at 4.8, 8.0 and 14.5 GHz, indicated by triangles, circles and crosses, respectively. The continuous curves are fitting to the data; from Aller, Aller and Hughes (1985)

ent radio wavelenghts in both total and polarized flux.

I will first consider the main features of these observations and after I will expound the model developed in Hughes, Aller and Aller (1985) to explain these observations.

An important coincidence is found between these outbursts and the simultaneous observed motion by VLBI measurements. Superluminal motion is observed from the emerging components at the same time that outbursts are observed (Mutel and Philips, 1984). The outburst 3 and 4 are identified with two components which show superluminal motion but both give evidences for a deceleration when they are far from the core. The third component has a curved trajectory and when it reaches a separation distance of 2 *m.a.s* from the core decreases its velocity (Mutel and Philips, 1986). The fourth component shows a decreases in the velocity at a distance 1.4 *m.a.s.* from the core but its trajectory is not curved. This is not an enormous problem if the observed components are not real blobs of fluid which are moving but shock fronts which can change the apparent velocity of the components depending on the frequency, as I will mention in the last part of this section.

Except for the first outburst (1980) in which only a rotation of the polarization angle is observed, all the outbursts show a considerable increase

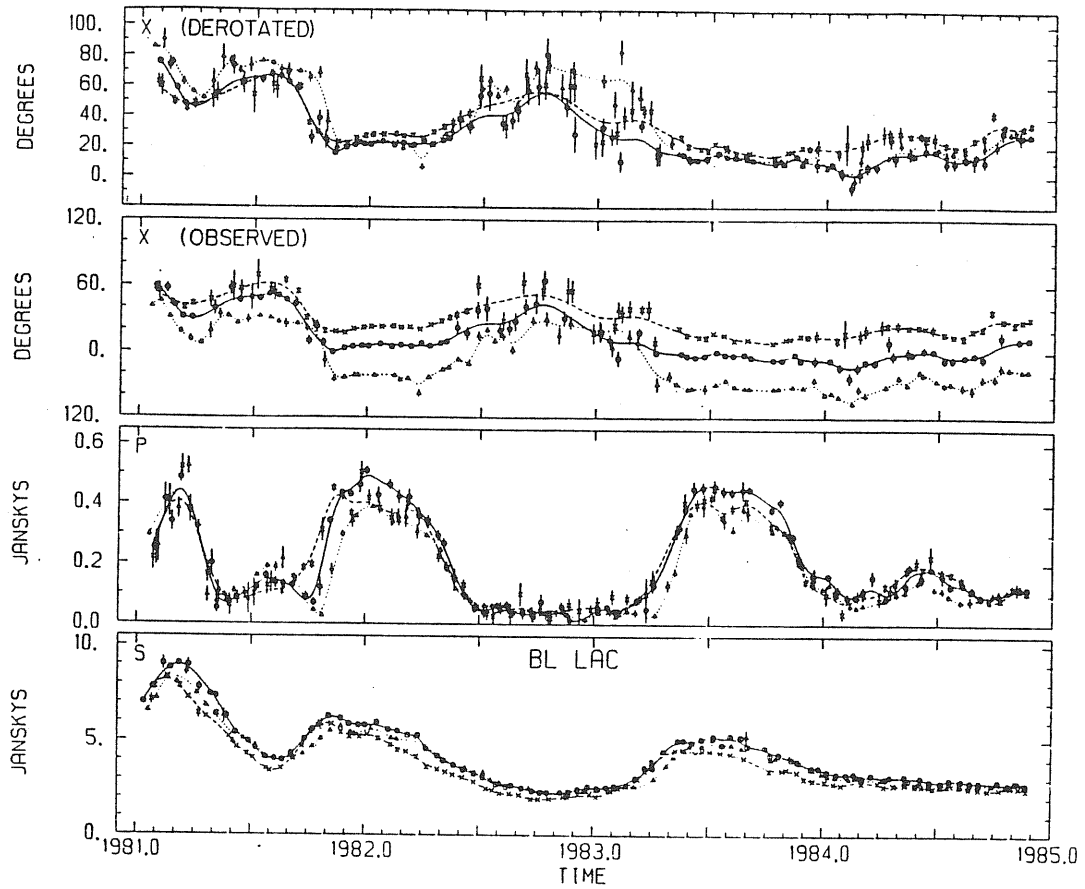

Figure 4.4: Total flux density, polarized flux density, observed and derotated polarization angle, for the period between 1982 and 1984; from Aller, Aller and Hughes (1985).

in the degree of polarization (see fig4.4).

Looking at the variations of the flux at the different observing frequencies the presence of an opaque emitting region with inverted spectrum is appreciated for the first outburst. In later outbursts a larger flux at the intermediate frequency indicates a partially opaque emitting region.

Comparing the total flux outbursts with the polarization outbursts we see that they do not exactly correspond. While the polarized flux rises sharply and then remains for a certain time at high level and finally decays quickly, the total flux density increases and decreases less abruptly, in a longer time scale.

The relevant point is that the same behaviour is observed in two of the outbursts, explicitly outbursts 3 and 4. The outburst 2 could be contamined by the slow declining of the first outburst and then it should not be taken as an individual event.

Moreover Aller et al.'85 observed that a Faraday rotation measure due to internal depolarization about $-228\,rad\,m^{-2}$ and $-234\,rad\,m^{-2}$ for the outbursts 3 and 4 is consistent with the observations. However if Faraday rotation due to our Galaxy is included then no plausible internal depolarization is consistent with the observations. Therefore the derotated value

of the polarization angle is obtained with the Faraday rotation due only to our Galaxy (see fig 4.4).

The derotated polarization angle at the outbursts is very close to the orientation angle of the VLBI structure.

Moreover the low polarization degree observed between the outbursts could be explained by a random magnetic field.

With these details we can understand the ingredients used by Hughes, Aller and Aller'85 to developed the model.

4.3.2 The model

The main ingredient of the model is to rely the enhancement of the polarization degree on the compression of the random magnetic field by shocks propagating down in the flow. At the shock location, the perpendicular component (to the jet axis) of the initially random magnetic field is dominant upon the paralell component, therefore the polarization angle will be oriented parallel to the jet axis. This compression of the magnetic field should be the cause of the rises in the polarization degree.

However from the different runnings of the polarization degree and the total flux the simple model with a single shock seems not sufficient. At the outbursts an optically thick unpolarized component is also contributing to the total flux and diluting the polarized component. This component is associated in the model with a piston of material corresponding to an increasing of the core activity or some perturbation of the outflow. This piston is the cause of the formation of the shock: when a sound wave is propagates along the jet and finds a gradient of pressure the slope steepens and a shock is formed.

In adition, a background flow with the random magnetic field giving rise to the observed quiescent emision should be included in the model.

In general the shock structure propagating down in the beam should consist of a constant discontinuity, which is the head of the piston and two shock fronts at both sides of it. One of these is assumed to be much stronger. When the particles find a shock front they are accelerated and the resultant energy distribution of the particles is flatter when the shock is stronger. Hence a higher number of particles at high energy will contribute more to the emitted energy and therefore only the stronger shock will be considered.

A Mach number will characterized the shock. The geometry assumed for this shock is a thin disk.

Therefore the total observed flux is the sum of three components: shock, piston and beam or quiescent emission. Then:

$$S_{obs} = S_S + S_P + S_B.$$

Furthermore if a constant Lorentz factor is taken for the whole jet and therefore Doppler beaming is the same everywhere the terms of relativistic beaming could suppresed of the equations.

The magnetic field changes with the jet width as $B \propto r^{-n}$. The propagation down in the jet can be parametrized by the time t and hence the jet width is related to the time by the expression $r \propto t^m$ for an expanding jet ($m > 0$). A power law distribution is taken for the energy of the electrons, including adiabatic losses (the energy per electron decreases as $r^{-2/3}$, and then K varies as $r^{-2(p+2)/3}$).

With this parametrization the flux coming from a portion (a thin disk perpendicular to the jet axis) in the jet is given by the expression:[1]

$$S_d \propto t^{mn/2+2m} \left[1 - \exp\left(-const\, \nu^{-(p+4)/2} t^{m(1-n(p+2)/2-2(p+2)/3)}\right)\right] \nu^{5/2}$$

Therefore the flux coming from an extended structure will be calculated by integration the above expression upon the appropiate extension which is parametrized in the time by t varying between $t' = 0$ and $t' = T$. The expression is:

$$S_{ext} \propto \int_0^{t \text{ if } T>t \text{ or } T \text{ if } T<t} S_d(t - t')dt'.$$

Both piston and shock are assumed to be evolving from an optically thick to an optically thin synchrotron emission as they emerge from the core.

The shock front is believed to be geometrically thin and therefore the time scale in which it becomes optically thin is shorter than the evolution time scale of the outburst. This is confirmed from the inspection of the polarized flux at the beginning of each outburst (see fig 4.4). The polarized flux at 14.5 GHz is larger than at 8 GHz at the rising of the polarization, when the high level is reached the flux at 8 GHz is larger as corresponds to an optically thin source at frequencies higher than 8 GHz.

---

[1]The flux is given by the expression

$$S_d \propto r^2 S_m \left[1 - \exp \tau_\nu\right],$$

being S_m the flux at the maximum frequency:

$$S_m \propto B^{-1/2} \nu^{5/2}$$

and τ_ν the optical depth:

$$\tau_\nu \propto r B^{(p+2)/2} \nu^{-(p+4)/2} K_o \propto r^{1-2(p+2)/3-n(p+2)/2} \nu^{-(p+4)/2}$$

Obeying these conditions a good functional form for the shock flux is given by the expression:

$$S_s = \left(1 + \frac{p_s}{q_s}\right) 2^{-\beta_s} \left[\nu^{-\beta_s} (t/t_{I2})^{-p_s} + (p_s/q_s)\, 2^{-(\alpha_s+\beta_s)} \nu^{\alpha_s} (t/t_{I2})^{-q_s}\right]^{-1},$$

where t_{I2} is the time scale in which S_s has reached the maximum for $\nu = 2$ (the frequency is scaled in such way that $\nu = 1, 2, 4$ correspond to the three observations frequencies).

However the piston flux has two different time scales: a rising time scalet_l and a decaying time scale t_u. In between a plateau is expected if the piston structure is long enough to fill the emitting region. With these expected characteristics the flux could be given in a functional form:

$$S_p = S_p^o \frac{(t/t_u)^{-q_p}\, \nu^{-\alpha_p}}{\left[\nu^{-\beta_p} (t/t_l)^{-p_p} + 1\right] \left[\nu^{-\alpha_p} (t/t_u)^{-q_p} + 1\right]}.$$

The piston is a more extended region than the shock and therefore has a flat spectrum given by β_p at the initial times because it is the integrated flux of a partially opaque emitting region. At the latest stages the spectrum is optically thin but with an steeper slope because it is a non homogeneous emitting region. The flux S_p^o is calculated from the normalization to unity of the maximum of the polarized emission, the peak flux of total density is dominated by the piston emission at early stages of the outburst.

The quiescent emission is described by a convex spectrum with a maximum at ν_c and a power law β_B and α_B for the optically thick and optically thin part of the spectrum, respectively:

$$S_B = S_B^o \nu_c^{\alpha_B} \left(1 + \frac{\alpha_B}{\beta_B}\right) \left[\nu^{\alpha_B} + \alpha_B/\beta_B \nu_c^{\alpha_B+\beta_B} \nu^{-\beta_B}\right]^{-1},$$

where S_B^o is the maximum quiescent emission at ν_c.

A similar calculation should be done for the polarization.

The piston and the quiescent emission have a low constant polarization. This emission could be produced by a turbulent optically thin region. However for the piston could be more appropiate a partially opaque emitting region at the rising of the outbursts. Anyway most of the polarization will come from the shock and the constant low polarization for both beam and piston is a good approximation. The value adopted is taken from the measurements at quiescent states, hence $P_{P,B} \lesssim 0.02$.

The situation for the shock is a little bit more complicated because the evolution passing from optically thick to optically thin of the shock structure should be considered.

When the emission comes from an optically thick region the polarization is zero and jumps to the maximum value when the emission becomes optically thin. This is expressed by the following condition:

$$P_d(\nu) = \begin{cases} P_o & \nu > \nu_d \\ 0 & \nu < \nu_d \end{cases}$$

being ν_d the peak of the emission.

For an element of the shock propagating along the channel this frequency is given as $\nu_c^t \approx 6(t-t')^{-2\Gamma/(\delta+4)}$, this expression is obtained from the above formula for the optical depth when equals unity.

The polarization should be obtained by integrating upon the whole extension of the shock:

$$P_S(\nu,t) = \frac{\int_0^{t \ if \ t<T \ or \ T \ if \ t>T} P_d^t(\nu) S_S(\nu,t)_{|(t-t')} dt'}{\int_0^{t \ if \ t<T \ or \ T \ if \ t>T} S_S(\nu,t)_{|(t-t')} dt'}.$$

From the above formula three different stages are obtained for the polarization: a first stage in which the polarization is zero, this stage will be present while the shock has not progressed along the channel of the jet enough to become optically thin at the highest observed frequency. A second stage in which the polarization is increasing coresponding to the emission becoming optically thin when the shock is going further. A third stage in which the polarization reachs the maximum and stand there.

This behaviour is well reflected in the following functional representation:

$$P_S(\nu,t) = \begin{cases} 0 & \text{if } \nu^F < (t/t_{Q1})^{-G} \\ \frac{\nu^F - (t/t_{Q1})^{-G}}{1/P_o \nu^F - (t/t_{Q1})^{-G}} & \text{otherwise,} \end{cases}$$

where

$$F = \frac{G/2\,[(p+4)/(p+2)]}{mn/2 + 2m/3}; \quad G = \frac{mn}{2}(p+1) + \frac{2m}{3}(p-1) - 1.$$

The time t_{Q1} is the time scale in which the maximum of the polarization is reached.

The maximum value of the polarization is in the range $0.3 - 0.4$, as derived from measured values and this is the corresponding value for P_o.

The angle for the polarization vectors is taken from the observations. The piston and the quiescent emission should have the same orientation angle.

It is possible to estimate the values for the different parameters doing considerations about the evolution of each component.

The value for m is constrained by the collimation of the beam and therefore if one considers that jets are collimated m should be less than 1.

The value for n is as usually limited by the two extreme configurations of the magnetic field perpendicular or parallel to the flow $n = 1$ or $n = 2$, respectively.

The asymptotic behaviour of the total flux gives an indication for the declining of the shock and the piston component when they are optically thin. The dependence is given by:

$$t^{-[mn(p+1)/2+2m(p-5/2)/3]}$$

when $t \rightarrow \infty$. Since the decay observed for the polarized flux is sharper than that of the total flux and the values of m and n should be the same for piston and shock it is derived that the energy distribution of the electrons in the shock is steeper than the one for the piston. The value for p_{piston} could be obtained from the spectral index in the optically thin phase hence at the latest moments in the outburst. Therefore from this expression above it is possible to have an estimation of the parameters $q_{S,P}$.

Moreover an estimation for the parameters G and F can be obtained from the rising of the degree of polarization.

However the parameters governing the rising of the flux are not so easily estimated. The spectral indices for both the piston and the shock are taken to be equal to zero supposing they are passing from optically thick to optically thin.

The piston component is an extended one but at the initial stages the flux rising is more associated with the piston becoming optically thin and the temporal evolution is not as important as the previous fact. Hence the expected value for p_S is around unity.

However for the shock component if it is a thin component one could use the asymptotic behaviour of the flux and the time dependence is given by $(t/t_{I2})^{3.5}$. But if the shock spectrum exhibits a flattening the rise of the polarized flux is controlled as in the piston emission from the part which is becoming optically thin and the rising flux will be faster with a lower value of p_S.

The conclusion is that if the fit is better with low values of p_S this means that the shock structure has a non negligible extension, because the flux coming from a thin structure should rise rather quickly and then high values of p_S.

The spectral index for the shock is taken to be $\alpha_S = 0$ because at the time when the shock is optically thin the emision is dominated by the piston component and therefore it is not relevant which value is adopted for the spectral index.

The piston component is all the time showing a flat spectrum in the lowest frequencies and steepening at higher ones. An spectral index which

depends on the frequency is adopted: $\alpha_P = \alpha_P^\circ(\nu - 1)/3$, where $\alpha_P^\circ = (p-1)/2$.

It remains to specify the beam component which is easily identified at quiet periods. It shows a convex spectrum: flat at lower frequencies, $\beta_B = 0$ and a small steepening at higher frequencies $\alpha_B = 0.2$; the maximum frequency is fixed at 2.

The relative contribution of the components is estimated to be $S_B \sim S_S \sim 0.5 S_P$, hence the dominant component is the piston. This should be always the case when the shocks are not enormously strong.

The parameters which the model leaves free to adjust with the observations are all the time scales t_{Q1}, t_{I2}, t_u and t_l.

There should be a relation between t_{Q1} and t_{I2} but it could also leave free to adjust wiht the observations, the only requirement is that t_{Q1} should be less than t_{I2}, because the polarization degree will rise suddenly when the structure becomes optically thin.

Hughes et al.'85 found that the model fit is not altered by small changes in the values of the parameters. However the spectral indices of the components are rather critical to reproduce the data. This implies that the opacity and the geometry are critically determining the shape of outbursts.

The assumption of a geometrically thin shock structure could be the cause of the discrepancy between the maximum in the polarized flux observed at 8 GHz and the predicted at 14.5 GHz. A second indication for this fact is the close time scales observed for the rising of the shock and piston components.

The encouraging fact of these models is that two outbursts, 3 and 4, are fitted by very close values of the parameters, only changing the time scaling and the relative contribution of the components. This seems to indicate that the outbursts were very similar and produced in close regions.

Another interesting fact is the presence of a fith burst, a standing at high level of the total flux is seen when the fourth outburst is slowly decaying, while the polarized flux is firmly increasing. Probably a lot of outbursts are too weak in total flux that they are not detected except in the polarized flux.

Hughes et al (1986) calculated the propagation of a shock along a jet solving the transfer of polarized radiation through a magnetized plasma. An interesting feature found in their calculations for a series of three shocks (see figure 4.5) is that the apparent expansion speed changes in a rather arbitrarily manner. Furthermore the apparent distance between components can be frequency dependent and by the way the separation speed.

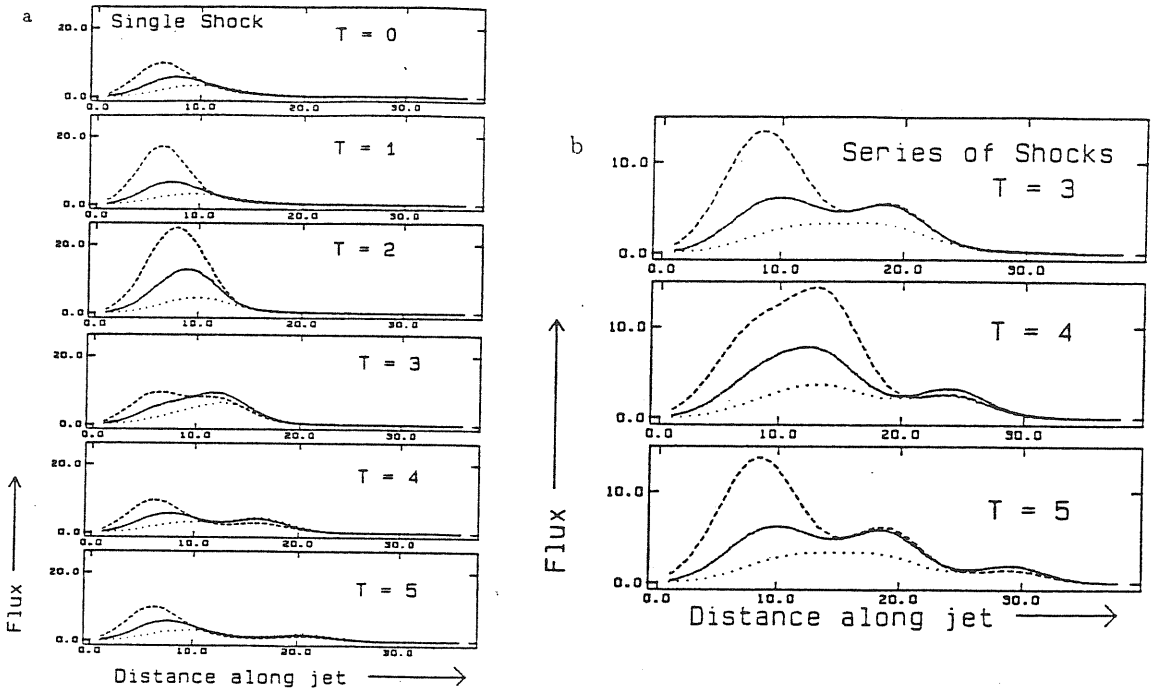

Figure 4.5: Time evolution of the brightness profiles for shocks propagating in a magnetized jet at the frequencies:dotted line, 5 GHz; continuos line, 10 GHz;dashed line, 15 GHz. In the cases of: (a) a single shock, (b) a sequences of three shocks.

4.3.3 Extension of the model to other sources

BL Lac was an exceptional source showing the outburst so well resolved and clearly identified in the polarized flux, many sources show activity in both total and polarized flux but without changing the polarization angle appreciably , these sources if showing shocks according to this model they should not be dominant in the polarization.

However for a number of sources some evidence can be found about the presence of shocks moving in the flow. Hughes, Aller and Aller (1986) discussed the activity seen in 3C 446 as one of these sources.

Let us consider a very simple model with two components for the polarization that could be assumed $P_{\perp}$ and $P_{||}$ which are identified with the quiescent emission and the outburst or shock emission. It is possible to imagine and then explain qualitatively the changes in polarized flux and polarization angle. For instance in a weak shock, and therefore a small polarization produced by compression, the observed behaviour is a decreased in the degree of polarization with a small change in the polarization angle. This behaviour is the observed in many sources as I mentioned above.

Another source which exhibits outbursts with simultaneous increases in the polarization degree is 3C 279. The outbursts in this source are very closely spaced in time and they are not so well resolved as in BL Lac.

The same model was applied to this source by Hughes et al. (1986). The

parameters of the model can be adjust with the outbursts in polarized flux density and then the evolution of the total flux density could be predicted. A relatively good fit to the observations was obtained.

4.4 High frequency outbursts. Flare models

The reason to look at short wavelenghts is that at high frequencies one is able to observe inner regions and therefore the outburst is seen at the initial stages of the evolution. The model which I described before can be exactly applied at these frequencies.

4.4.1 Observations

In 1983 an outburst in the millimeter to infrared emission was observed from 3C 273 (reported by Robson et al., 1983). In the following I will describe the characteristics of this outburst.

To better study this event Marscher and Gear (1985) substracted the supposed quiescent emission (as it is given by Clegg et al. 1983), then obtained the spectrum of the flare, free of other emission.

The spectrum of the flare is well fitted by a power law with spectral index $\alpha \approx 1.2$ and no break at near-infrared is seen. This contrasts with the quiescent spectrum in which the spectral index is $\alpha \approx 0.7$ and a break is observed at 10^{14} Hz. It is noted the fact that the spectral index has increased by a factor 0.5 as it is expected from synchrotron losses.

Between the two observations periods the spectrum has evolved. The peak flux increases from 14 to 26 Jy and the frequency of the maximum decreases from 370 to 300 GHz. At later time the peak flux density remained constant while the maximum frequency still was decreasing. Two months later the flux at near-infrared was found in the quiescent state.

This behaviour is consistent with a flare component which is becoming optically thin progressively at larger wavelenghts, the model proposed by Marscher and Gear'85 considers a shock wave which is evolving in this sense. The difference of this model with the one described before is in the details of the calculations rather than the idea itself.

4.4.2 The flare evolution model

The basis of the model is a shock wave which is propagating down in a non homogeneous jet and this affects how the population of radiating electrons changes.

Basically the same assumptions as the previous model considers should

be done. The magnetic field behaves as r^{-m} and the electron energy distribution varies as $r^{-2(p+2)}$.

However in this case the shock has an extended structure. The simplified structure consists of a constant distribution of the dynamical quantities (*e.g.* the density, the pressure) up to a certain distance which is called x_{max}. Further on this distance all those quantities drops and the shock dilutes in the jet without producing more enhancement of the radiation[2]. The highest energy electrons suffer substantial synchrotron and Compton radiation losses when they have travelled a distance x much less than that maximum distance. The expression for this distance x is:

$$x \propto \nu^{-1/2} B^{-3/2} \text{ for } \nu > \nu_*,$$

where ν_* corresponds to $x = x_{max}$.

The emission of the shock in the optically thin case is given by the expression :

$$S_\nu \propto K B^{(p+1)/2} R^2 x \nu^{-(p-1)/2}$$

and the maximum frequency ($\tau = 1$) is given by:

$$\nu_m \propto [K B^{(p+2)/2} x]^{2/(p+4)}$$

and then the peak flux at the maximum frequency is obtained as:

$$S_m \propto [K^5 B^{2p+3} x^5]^{1/(p+4)} R^2.$$

Three cases could be considered depending on which is the dominant mechanism for the electron energy losses in the region behind the shock: adiabatic losses, synchrotron and Compton emission losses.

The Compton radiative losses dominates upon the synchrotron losses when the radiation energy density exceeds the magnetic energy density, this occurs for $u_{ph} > B^2/8\pi$. The radiation energy density is given by $u_{ph} \propto K[B^{3p+7} R^{p+5}]^{1/8} \propto R^{-U}$, being $U = [(13p + 17) + 3m(3p + 7)]/24$, therefore the Compton losses will dominate for small values of R.

Moreover the synchrotron losses will become less important in the outer regions and the value of x will be close to the the maximum size of the shock structure. In this situation the electrons will mostly undergo adiabatic losses.

So the picture is consistent with the propagation of such shock wave along the channel of the jet. First electrons are cooling by Compton emission, further out synchrotron emission becomes dominant and only very far out the adiabatic losses are important.

[2]The higher density in the region of the shock does not mean that more electron will be radiating. The density of high relativistic electrons, responsible for the synchrotron radiation, does not increase by the compression but for acceleration process that could be acting in the shock

Moreover this picture is at least qualitatively consistent with the evolution of the peak density and the maximum frequency observed at the two periods. I will justified this in the following.

When the synchrotron losses dominates, the flux is given by the following expression:

$$\begin{aligned} S_\nu &\propto R^{-[4(p-1)+3m(p-2)]/6}\nu^{-p/2} \\ &\propto R^{-1.13}\nu^{-1.2} \qquad (p=2.4,\ m=1), \end{aligned}$$

and the maximum frequency is given as:

$$\begin{aligned} \nu_m &\propto R^{-[4(p+2)+3m(p-1)]/6(p+5)} \\ &\propto R^{-0.98} \qquad (p=2.4,\ m=1). \end{aligned}$$

Hence the peak flux is given by:

$$\begin{aligned} S_m &\propto \nu_m^{[(2p-5)(2+3m)]/[4(p+2)+3m(p-1)]} \\ &\propto \nu_m^{-0.05} \qquad (p=2.4,\ m=1). \end{aligned}$$

For the case of dominant Compton losses the equivalent expressions are[3]:

$$\begin{aligned} S_\nu &\propto R^{-[(11-p)-m(p+1)]/8}\nu^{-p/2} \\ &\propto R^{0.65}\nu^{-1.2} \qquad (p=2.4,\ m=1), \end{aligned}$$

the maximum frequency is given by:

$$\begin{aligned} \nu_m &\propto R^{-(m+1)/4} \\ &\propto R^{-0.5} \qquad (p=2.4,\ m=1). \end{aligned}$$

and the peak flux:

$$\begin{aligned} S_m &\propto \nu_m^{(11-m)/[2(m+1)]} \\ &\propto \nu_m^{-2.5} \qquad (p=2.4,\ m=1). \end{aligned}$$

When the adiabatic losses are dominant, the extension of the emitting region reachs the maximum extension of the shock. Then the shock is assumed to be self-similar, this maximum extension is proportional to the distance along the jet. Therefore $x = x_{max} \propto R$.

Then the expressions for the flux and the maximum frequency are:

$$\begin{aligned} S_\nu &\propto R^{-7(p-1)/6}\nu^{-(p-1)/2} \\ &\propto R^{-1.63}\nu^{-0.7} \qquad (p=2.4,\ m=1), \end{aligned}$$

[3]The expression for the distance x now should be change by

$$x \propto u_{ph}^{-1} B^{1/2}\nu^{-1/2}$$

and $u_{ph} \propto R^{-U}$ as given above.

$$\begin{aligned} \nu_m &\propto R^{-(7p+8)/6(p+4)} \\ &\propto R^{-1.29} \qquad (p = 2.4,\ m = 1). \end{aligned}$$

The peak flux is therefore given by:

$$\begin{aligned} S_m &\propto \nu_m^{10(p-1)/(7p+8)} \\ &\propto \nu_m^{0.56} \qquad (p = 2.4,\ m = 1). \end{aligned}$$

From the previous formulae the model is consistent with the interpretation that during the two observations periods the shock was in the phase of Compton losses. The peak flux is increasing with time and the maximum frequency is decreasing.

After the second period the flux does not increase apreciably but the maximum frequency is still decreasing as expected if the shock goes in the phase of synchrotron losses.

In order to test the aplicability of this model Marscher and Gear'85 estimates the parameters intervening in the model from the data. I will mention the values of these parameters for the purpose of illustration and to confirm the plausibility of the model.

The distance at which relativistic electrons are supposed to be initially accelerated (by shock fronts or because they are injected there) is around 2 pc, but the distance to the central source could be larger. The magnetic field at that distance is around 0.4 G.

The location of the shock at the time of the observations is estimated to be close to the place of injection at the time 1 and about 2.7 pc at the time 2 (the time between the two observations is 1 month).

Assuming an homogeneous model for the shock it is possible to derive values for the magnetic field electron number density and extension of the shock. These values are $B_S \sim 10\,G$, $K_S \sim 5 \times 10^{-3}(cgs)$ and $x(\nu_m \sim 2 \times 10^{-4} pc$ being $\nu_m \sim 300\,GHz$. The compression of the shock is found to be in the range 2 to 20 as derived from the magnetic field amplification.

It will be interesting to know about the polarization measurements at submillimeter and infrared frequencies and try to find outbursts as appear in the model of Hughes et al.'85 for BL Lac.

Another interesting prediction of the model concerns to the quenching of stable fluxes observed for several sources at millimeter wavelenghts (Epstein et al., 1982). Let us consider the shock at the latest stages of the evolution. The shock structure should be very extended then the flux density is obtained by integrating over all the zone and it is found that this spectrum has the same spectral dependence that the quiescent jet at frequencies below the maximum frequency. Moreover it coincides with the dependence of the peak flux with the maximum frequency in the adiabatic stage. Then when

the maximum frequency decreasing with time reachs a particular frequency the flux seems to decrease mantaining the same spectral slope.

The fact that the structure of the shock is extended should also explain the broadening of the peak of the flux density with respect to an uniform synchrotron source, this is the effect of a non homogeneous source.

In a later paper Gear et al. (1986) the variability in the region of millimeter to infrared wavelenghts was reported for a sample of ten blazars. The observed behaviour of these sources was shown to be consistent with the predicted from the above model. An observed feature is that the infrared fluxes increase at once at all the range of frequencies hence the emission at those frequencies should come from the same region, the region which is near behind the shock.

This model would also have implications with the superluminal motion because the centroids of the brightness distribution will not move together with the shock. During the synchrotron phase the shock front will move at a fairly uniform velocity but the leading edge, ahead of the shock, will move with a higher velocity since it is an expanding limit (electrons have longer synchrotron emitting lifetime when the shock is at outer regions). Then the brightness centroid will move at an intermediate velocity. However when the shock reachs the adabiatic stage the whole extension of the shock will expand uniformly and the brightness centroid will move suddenly, this moment would correspond to the superluminal expansion.

According to this theory one should see a new component appearing after a flare is detected in the submillimeter wavelenghts. In fact predictions for new superluminal knots to emerge from 3C 273, OJ 287, 3C 279 and 3C 345 are found in Gear et al.'86.

In the initial stage of the development of the flare when Compton losses are dominant the X-rays flux should undergo an increase. But when the flare is detected at submillimeter wavelenghts the X-rays flux should be already in declining, because the Compton losses decreases very fast with time[4]. Hence a flare at submillimiter or infrared wavelenghts should be first detected by a month as an X-ray flare.

[4]Looking at the ratio Compton losses to synchrotron losses

$$\frac{P_{Comp}}{P_{synch}} \approx \frac{u_{ph}}{u_B} \propto R^{-U+2m}$$

and the exponent is close to 2.

4.5 Modelling flows with shock waves. Calculating the spectrum

The numerical simulations of jets as done by Norman et al. (1982) suggests that the formation of internal shocks in the structure of the jets is a normal feature[5]. Therefore if these internal shocks are produced in a natural way in the numerical simulations it is direct to think to calculate the flux emitted by these shocks and then to build up models of radio jets predicting the extended brightness structure.

Jones (1982) presents numerical simulations of non steady flows in relativistic jets and then calculate the brightness enhancements and flux variations due to the presence of transverse shocks (Unfortunately I did not find a more explicit reference that a short abstract from that work).

I believe that numerical simulations of non steady flows with conditions similar to those found in extragalactic jets could be very interesting to compare with the observed motions seen in VLBI scales. Moreover in this way the shocks will appear and evolve in consistency with the dynamics of the flow. Therefore a smaller number of parameters will specify the model. The major inconvenient of the models presented in the sections 2-3 is the high number of parameters which models the fit to observations, or rather the arbitrariness to constrain those parameters. A similar intent is outlined in Aller, Hughes and Aller (1986): the propagation of weak shocks through a randomly oriented magnetic field is considered by using numerical simulations.

Several authors (Webb, Drury and Biermann, 1984; Bregman, 1985; Perez Fournon, 1985; Biermann and Strimatter, 1987) have treated the problem of calculating in a self-consistent way the emission coming from shock waves allowing for acceleration process and synchrotron radiative losses. This problem consists in solving the kinetic transport equation for the electrons including energetic synchrotron losses (and Compton losses in Biermann and Strimatter, 1987). Then, once the electron energy distribution is obtained, the synchrotron spectrum could be calculated.

The synchrotron spectra obtained by these calculations have a spectral cutoff at millimeter frequencies due to the synchrotron losses dimming the number of electrons at high energies.

A critical test of these theories should come from high resolutions observations at frequencies other than radio bands (Perez Fournon et al, 1988). The objects more interesting for it are the jets seen in visible as the one of M 87 and 3C 273.

[5]Internal shocks are formed as the result of reflection of an incident shock converging towards the axis of the jet and then reflected forming a Mach disk for sufficiently high Mach numbers.

Summary and conclusions

The hypothesis that relativistic outflows directed towards us are present in the core of radio sources producing such spectacular effects as superluminal motions has been largely criticized from its birth. However there is a very general conclusion that we have been implicitly assuming through this work, that relativistic beaming is important in compact radio sources and our ideas to understand those sources should consider that as a working hypothesis. The reasons to say that are based on the large number of observations which seem to be logically interpreted in the relativistic jet scenario.

Let us quickly review some of these evidences, considering that probably a strong generalization is made and particularly counterexamples will not be the exception.

First of all we will dedicate few words to the *brightness jet model* (we want to do reference merely to the brightness distribution through the extension of the jet). The inhomogeneous jet models are able to explain rather satisfactorily the flattening of the radio spectrum at long wavelenghts and the steepening at shorter wavelenghts. Those models give some discrepancies when they try to explain the different variability time scales at different regions of the spectrum. But this needs to be checked with a high number of observations.

The presence of superluminal motions in the core of the brightest radio sources is a rather common feature. However more relevant is that the superluminal motions, when observed in weak cores, are apparently slower; possibly indicating that these sources will be oriented a little farther from our line of sight. Moreover the presence of asymmetries in the small (milliarsecond) scale and large (arsecond) scale seems always to be in the same sense.

It seems to us particularly important to mention the recent results of Laing (1988) and his collaborators confirming that depolarization always occurs in the counter-jet side. The favorite interpretation of this result is that there is a larger amount of matter in the light path from the counter-jet side than from the jet side, this is believed to be a pure geometrical

effect due to the orientation of the source, which is pointing towards us.

In spite of the rather coherent interpretation of observed features as produced by relativistic beaming of the emitting flow, we found that there is a statistical problem: the expected high number of unbeamed sources by each beamed source is not seen. A way of escaping this problem is to think of the possibility that beaming of the radiation is occurring in a wider range of angles than the range expected from the narrow relativistic jet model.

In this line of thought a model of jet containing emitting homogeneities will be the solution to our problem. In a real jet the flow will find obstacles, undergo compressions and have shear near the boundaries, therefore a diversity of dissipative processes will originate during the jet propagation. This will guarantee that a rather wide range of directions and velocities are implicated in the emission of the jet. Our impression is that these structures could be responsible for the presence of relativistic beaming in a high number of sources.

To illustrate this proposal we will look at a simple calculation (it is taken from Phinney, 1985), which reveals how a small relativistcally moving blob could block up the emission from a larger emitting volume. Let us take a volume V_r of fluid at rest and suppose a small blob of volume V_m moving with a speed βc at an angle θ with the line of sight. Now we calculate the observed flux coming from both components. If the emissivity (supposing an optically thin emitting source) is given in the rest frame of the source by $j_\nu \propto \nu^{-\alpha}$, then the ratio of observed flux coming from the small blob to that coming from the larger volume is given as:

$$\frac{S_m}{S_r} = \frac{\gamma V_m}{V_r - V_m}\mathcal{D}^{3+\alpha} \sim \gamma \mathcal{D}^{3+\alpha}\frac{\gamma V_m}{V_r}.$$

From this formula we obtain that a blob oriented precisely in our line of sight and with a Lorentz factor $\gamma \sim 5$ needs to occupy only 1 part in 15000 of the rest volume to dominate the emission of the source. However a blob, occupying the same fraction of the rest volume but moving in a direction perpendicular to our line of sight, will emit a fraction of the total flux smaller than 0.01%.

The meaning of this simple calculation is that perhaps what we are seeing from relativistically beamed sources is only an insignificant fraction of its emitting volume, which is able to blur out the dominant component in the rest frame. Therefore our observations of compact radio sources could be reflecting irregularities in the source rather than uniform and universal emission patterns.

We conclude saying that the dynamical study of non steady flows in jets could give us a lot of information about the appearance of radio sources once we will be able to establish a good stage to base the models on. In this direction we expect that numerical simulations of the radiation processes

present during the jet propagation would help to clarify the ideas about compact radio sources. Why numerical simulations? Because it could be the fastest (the unique?) way to study non steady flows propagating in jets. In this thesis we commented on models involving propagating shocks, but we saw that these models do not manage with the dynamics of the problem and then they are constructed with a high number of parameters, which in general are not well constrained by the fitting with observations.

Appendix A

Synchrotron radiation

A.1 Synchrotron emission

A relativistic electron of energy γmc^2 spiraling in a magnetic field B emits a power:

$$P(\gamma,\theta) = 2\sigma_T c u_B \gamma^2 \beta^2 \sin^2\theta,$$

where σ_T is the Thomson cross section, θ is the pitch angle and u_B is the magnetic energy density.

The spectrum is continuous for $\gamma \gg 1$ and for an isotropic distribution of electrons and it is given by the expression:

$$P(\nu,\gamma) \propto B(\nu/\nu_c)\int_{\nu/\nu_c}^{\infty} K_{5/3}(x)dx$$

where

$$\nu_c = \frac{3}{2}\nu_B\gamma^2,\ \nu_B = \frac{eB}{2\pi mc} \text{ and } F(x) = x\int_x^{\infty} dsK_{5/3}(s)$$

and $K_{5/3}$ is the modified Bessel function of order 5/3. The function $F(x)$ has a maximum for the value $x = 0.29$, which means that at the frequency $\nu = 0.29\nu_c$ the spectrum will have a maximum. The asymptotic behaviour of the function F(x) is as follows:

$$F(x) \propto \begin{cases} x^{1/3} & x \ll 1 \\ e^{-x}x^{1/2} & x \gg 1 \end{cases}$$

For the case that instead a single electron there is a power law distribution of emitting electrons the spectrum is calculated by integrating over the whole range of energy of the electrons. If $N(\gamma) = K\gamma^{-p}$ for $\gamma_{min} \leq \gamma \leq \gamma_{max}$ then the emissivity is given as:

$$\epsilon_\nu = \int d\gamma N(\gamma)p(\gamma,\nu)$$

$$\epsilon_\nu \propto K\,(\nu/\nu_B)^{-(p-1)/2}\,\nu_B$$

and written in terms of the spectral index α:

$$\epsilon_\nu \propto K\nu^{-\alpha}B^{\alpha+1/2} \text{ with } \alpha = \frac{p-1}{2}$$

A.1.1 Synchrotron self-absorption

Synchrotron emission is accompanied by absorption, the same electrons which emit the synchrotron radiation can absorb those photons when the density of these is high enough. Moreover stimulated emission is another process which can occur.

The absorption coefficient is calculated by means of the Einstein coefficients:

$$k_\nu = \frac{h\nu}{4\pi}\sum_{E_1}\sum_{E_2}[n(E_1)B_{12} - n(E_2)B_{21}]\phi_{21}(\nu).$$

For a power law electron energy distribution the result is given by the formula:

$$k_\nu \propto K\nu_B^{(p+2)/2}\nu^{-(p+4)/2}.$$

Then the source function for a synchrotron emitting source is:

$$S_\nu = \frac{j_\nu}{k_\nu} = f(p)\nu^{5/2}\nu_B^{-1/2}$$

The important result is the overall spectrum for a power-law distribution of electrons. From the shape of the absorption coefficient it is evident that self-absorption will be important at low frequencies therefore there will be a turnover in the spectrum in which the source passes from the optically thick regime to the optically thin. The observed intensity for the optically thick emission is proportional to the emission function $I_\nu \propto \nu^{5/2}$. While for the optically thin emission the intensity is proportional to the emissivity and then $I_\nu \propto \nu^{-(p-1)/2}$. The overall shape of the spectrum is dependent on the particular conditions in the emitting source, but in general the shape should be close to the one given in the figure A.1. At low frequencies the emission is optically thick and it has a low frequency end of the spectrum given by the rising of the single electron spectrum, that is a power law ($\nu^{1/3}$). At the turnover frequency the optical depth is close to unity, for frequencies higher than this value the source becomes optically thin with the described power law spectrum ($\nu^{-\alpha}$ and $\alpha = (p-1)/2$). The upper fall down of the spectrum is the corresponding to the single electrons with the maximum energy.

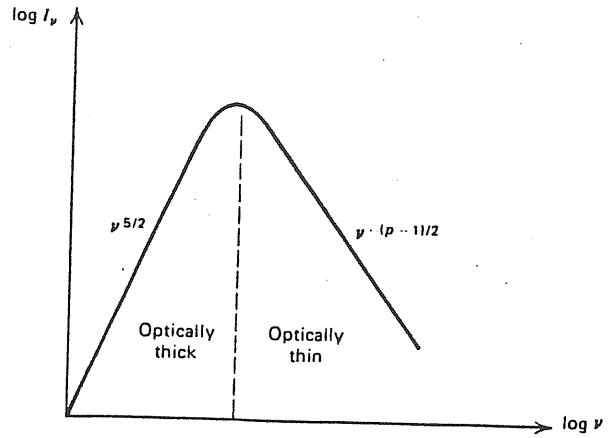

Figure A.1: Overall spectrum of a synchrotron emitting source

A.1.2 Polarization of the synchrotron radiation

The synchrotron radiation coming from a single emitting electron is elliptically polarized. However for an isotropic distribution of emitting particles this elliptical polarization is cancelled and the radiation will remain partially linearly polarized.

The degree of linear polarization for a single electron is given by the expression:

$$P(\nu) = \frac{P_{\|} - P_{\perp}}{P_{\|} + P_{\perp}} = \frac{G(x)}{F(x)},$$

where $G(x) = xK_{2/3}(x)$ and $F(x) = x\int_x^\infty K_{5/3}(l)dl$. The degree of polarization increases from 0.5 at low frequencies to 1 at very high fequencies. At the critical frequency, where the maximum of the emission is produced then $P(\nu_c) \sim 0.7$

In the case of a power law energy distribution of the electrons the degree of polarization is given by the expression:

$$P = \frac{p+1}{p+7/3}$$

This formula is only valid for frequencies higher than the peak frequency, this is the optically thin case. At low frequencies the source becomes optically thick and the polarization is very low, it is given by the formula:

$$P = \frac{3}{6p+13}.$$

A.2 Compton scattering

The collisions of fast electrons with the synchrotron photons could produce under certain conditions a redistribution of the radiation spectrum. Electrons will loose energy and the photons will gain that energy. This process could change the energy of the photons by factors of the order of γ^2.

Let us consider a photon of energy γ which is moving at an angle θ with respect to the incident photon of energy ϵ in the lab frame.

The photon energy in the frame of the electron is given by the expression:

$$\epsilon^{'} = \gamma\epsilon(1 - \beta\cos\theta),$$

treating the collision of the photon with the electron as two particles collision and solving for the conservation of energy and momentum, the energy of the scattered electron is after the collision:

$$\epsilon_1^{'} = \frac{\epsilon^{'}}{1 + \epsilon^{'}/mc^2(1 - \cos\Theta)},$$

where $\Theta = \theta_1^{'} - \theta_1$ is the angle between the original incident direction of the photon in the electron frame and the scattered direction in the same frame.

Once the energy of the scattered particle is known one must transform again to the lab frame, then the resulting energy is given as:

$$\epsilon_1 = \gamma\epsilon_1^{'}(1 + \beta\cos\theta_1^{'}).$$

In the case of relativistic electrons the energies of the photon before the scattering in the lab frame, in the rest frame of the electrons and after the scattering are in the rate $1 : \gamma : \gamma^2$. Therefore the process converts a photon of energy ϵ in a photon of energy $\epsilon\gamma^2$.

In the case that the energy of the photons in the electron frame is less than the rest mass the scattering process reduces to the Thomson scattering and the change of energy for the photons is negiglible in the collision. When the energy of the photons is high enough there is an effect of reduction of the cross section, the Klein-Nishina cross section should be used, but in most cases is not considered.

The total radiated power due to Compton scattering is given by the expression:

$$P_{Comp} = 4/3\sigma_T c\gamma^2\beta^2 u_{ph},$$

where u_{ph} is the photon energy density.

The ratio of Compton losses to synchrotron losses is obtained comparing the above formula with the corresponding for synchrotron losses:

$$\frac{P_{Comp}}{P_{sync}} = \frac{u_{ph}}{u_B}.$$

This expression indicates that the ratio of the Compton losses to synchrotron losses is equal to the ratio of the photon energy density to the magnetic energy density, therefore Compton losses will dominate only when the radiation energy density dominates upon the magnetic energy density and viceversa for the synchrotron losses.

A.2.1 Compton spectrum

The energy distribution of a monoenergetic distribution of photons after the scattering with monoenergetic electrons is given by the expression:

$$j(\epsilon_1) \propto f(x)/\gamma^2,\ x = \frac{\epsilon_1}{4\gamma^2\epsilon}$$

$$f_T(x) = 2x\ln x + x + 1 - 2x^2$$

valid for the range $0 < x < 1$ and for the Thomson regime ($\gamma h\nu < mc^2$). This function $f_T(x)$ is monotonic and decreases from 0 to 1.

The total scattered power of an arbitrary initial spectrum ($I_\nu = v(\epsilon)c/4\pi$) by a power law of relativistic electrons can be calculated now by the expression:

$$\epsilon_{scat}(\nu) = 4\pi\epsilon_1 \int d\epsilon v(\epsilon)/\epsilon \int_{\gamma_{min}}^{\gamma_{max}} d\gamma\gamma^{-p-2} f(\epsilon_1/4\gamma^2\epsilon),$$

changing the variable of integration from γ to x the resultant expression is:

$$\epsilon_{scat}(\nu) \propto \nu^{-(p-1)/2} \int d\epsilon\epsilon^{(p-1)/2} v(e) \int_{x_1}^{x_2} dx x^{(p-1)/2} f(x)$$

If the maximum and minimum energy of the electrons differs by several orders of magnitude and the photon distribution function has a peak then the last integral is independent of the value of ϵ and can be removed as a constant. Therefore the Compton spectrum in the Thomson regime is calculated by the formula:

$$\epsilon_{scat}(\nu) \propto \nu^{-(p-1)/2} \int_{\epsilon_{min}}^{\epsilon_{max}} d\epsilon\epsilon^{(p-1)/2} v(\epsilon).$$

In this formula $\epsilon_{min} = max\{h\nu_{s_{min}}, h\nu/\gamma^2_{max}\}$ and $\epsilon_{max} = min\{h\nu_{s_{max}}, h\nu/\gamma^2_{min}, (mc^2)^2/h\nu$. Therefore the resultant spectrum of the scattering by a power law of relativistic electrons is a power law with the same spectral index that the synchrotron radiation.

For values of ν higher than $4\gamma^2\nu_s$ the Klein-Nishina regime is reached and the spectrum for arbitrary initial radiation field is calculated in a similar way. The exact formula for the inverse Compton emissivity has been

derived by Jones (1968) and it is also reported in Blumenthal and Gould (1970). In the extreme Klein-Nishina limit the emissivity is given as:

$$\epsilon_{KN}(\nu) \propto \nu^{-p},$$

a steepening of the spectrum is observed in this regime and this regime will be important only when $\alpha > 1$, because the steepening of the spectrum is less pronounced than the spectrum in the Thomson regime.

Appendix B

Emission from relativistically moving emitting sources

B.1 Beaming Effect

Let us consider a frame K' moving with a velocity β with respect to a frame K.

Suppose a photon emitted in the frame K' at an angle θ' with the direction of motion. Then the angle θ in which the obsever at the frame K sees the radiation is given by the expressions:

$$\tan\theta = \frac{\sin\theta'}{\gamma(\cos\theta' + \beta)}$$

$$\cos\theta = \frac{\cos\theta' + \beta}{1 + \beta\cos\theta'}$$

The effect of these transformations is that electrons emitted at large angles at the emitting rest frame will be detected at small angles at the observer frame. This effect is also called *relativistic aberration.* For instance if the angle of emission in the frame K' is $\theta' = \pi/2$ then the observed angle in the frame K is given as $\theta = \arctan 1/\beta\gamma$ which is a very small angle for highly relativistic speeds. Therefore the photons in the frame K are concentrated in a cone of semi-aperture $1/\gamma$ and very few photons will be at angles larger than $1/\gamma$. This is called *beaming effect.*

B.2 Doppler effect

Each periodic event which is occurring in the frame K' will appear to have a longer period in the frame K by a factor γ, as deduced from the Lorentz transformations. If moreover an observer measures the arrival times of

pulses then there will be an additional effect due to the propagation time delays. This is the *Doppler effect.*

Combining these two effects the frequency in the rest frame is given by the expression:

$$\nu = \frac{\nu'}{\gamma(1 - \beta \cos\theta)} = \mathcal{D}\nu',$$

where $\mathcal{D}$ is the Doppler factor and θ the direction of emission in the observer frame.

Therefore the time interval measured in the rest frame is given as:

$$\Delta t = \Delta t'/\mathcal{D},$$

$\Delta t'$ is the interval of time as measured in the rest frame of the emitting fluid. Then the result is a shortening of the time interval when the emitting source is pointing in a direction close to our line of sight.

B.3 Lorentz transformations of the radiation field

Because the transformation of the frequency between the two frames involves the direction of emision the quantities which determine the radiation field could be isotropic in the frame of emission but highly anisotropic in the observer frame. Let us derive how the quantities giving the radiation field change.

A volume element in the phase space will be invariant under Lorentz transformations. This could be applied to a distribution of photons; the phase space density is given by $f = dN/d\mathcal{V}$, which is also an invariant because dN is the number of photons in the volume element and therefore invariant. Relating this function to the specific intensity it is possible to determine the transformation of that quantity. This is done evaluating the energy density per unit solid angle per frequency as given by using the phase space density:

$$h\nu f p^2 dp d\Omega = \frac{I_\nu}{c} d\Omega d\nu$$

$$p = \frac{h\nu}{c},$$

therefore it results that I_ν/ν^3 is a Lorentz invariant.

The transformation for the source function should be the same since l_ν appears in the transfer equation in the same way that I_ν. Then l_ν/ν^3 is another Lorentz invariant.

To find the transformation of the absorption coefficient one could consider that the optical depth, τ, is an invariant since it is the probability

that a photon is absorbed and this probability should be a number. In the slab approximation the optical depth is written as:

$$\tau = \frac{l k_\nu}{\sin\theta},$$

now considering that quantities in direction transverse to the motion are not changed by the Lorentz transformations, then l and $\nu \sin\theta$ (perpendicular component of the photon momentum) are also invariant. Therefore νk_ν is a Lorentz invariant.

The transformation for the emission coefficient comes from the definition of the source function $S_\nu = j_\nu / k_\nu$ and then the result is that j_ν / ν^2 is invariant.

Once the transformations of these quantities are known the flux for each particular geometry could be calculated.

First I will give the expressions for the case in which synchrotron processes are the relevant emission mechanisms.

Let us consider a reference frame K' in which the emitting plasma has isotropic emission and absorption coefficients. For the case of synchrotron radiation they are given by the expressions:

$$j'(\nu') \propto \nu'^{-\alpha}$$

$$k'(\nu') \propto \nu'^{-\alpha-5/2}.$$

The same quantities in the observed frame are given as:

$$j(\nu) = \mathcal{D}^2 j'(\nu') \propto \mathcal{D}^{2+\alpha} j'(\nu)$$

$$k(\nu) = \mathcal{D}^{-1} k'(\nu') \propto \mathcal{D}^{3/2+\alpha} k'(\nu)$$

The observed specific intensity is then given by the expression:

$$I_\nu(\vec{n}) = \int j_\nu(\vec{n}) \exp[-\int_0^x dl\, k_\nu(\vec{n}, l)]\, dx$$

and the flux is obtained by integrating over the emitting surface:

$$S_\nu = \int I_\nu d\Omega.$$

For the optically thin case when $\tau \ll 1$ then the specific intensity is given by:

$$I_\nu = \int_0^x j_\nu dx$$

and the flux:

$$S_\nu = \int I_\nu d\Omega$$

and then the integral is done over the volume in the emitting source ($d\Omega = d\Sigma^{'}/D^2$):

$$S_\nu \propto \int \mathcal{D}^3 j^{'}(\nu^{'}) dV^{'} \propto \mathcal{D}^{3+\alpha} \int j^{'}(\nu) dV^{'}.$$

However in the optically thick limit $\tau \gg 1$ and the specific intensity is given as:

$$I_\nu = \frac{j_\nu}{k_\nu}$$

and then the flux:

$$S_\nu = \int \frac{j_\nu}{k_\nu} d\Omega$$

which is calculated by integrating over the transverse surface of the source:

$$S_\nu \propto \int_{\Sigma^{'}} \frac{j^{'}(\nu^{'})}{k^{'}(\nu^{'})} \mathcal{D}^3 d\Sigma^{'} \propto \mathcal{D}^{1/2} \int_{\Sigma^{'}} \frac{j^{'}(\nu)}{k^{'}(\nu)} d\Sigma^{'}.$$

From the expressions for the optically thin and optically thick sources is evident that the Doppler beaming is more important in optically thin sources ($\mathcal{D}^{3+\alpha}$)than in optically thick ($\mathcal{D}^{1/2}$) sources. Moreover the flux in optically thin sources is rather independent of the shape of the source while in the optically thick sources the opposite is true.

Nevertheless the optical depth is a strong function of the Doppler factor of the emitting source:

$$\tau_\nu = \int_0^{x^{'}} k^{'}(\nu^{'}) dl^{'} \propto \mathcal{D}^{5/2+\alpha} \int_0^{x^{'}} k^{'}(\nu) dl^{'},$$

where $l^{'}$ is the coordinate along the path of the light ray in the frame $K^{'}$. The implication of this strong dependence of the optical depth on the Doppler factor is that a given source has a wide range of values for the optical depth depending on the orientation angle.

Bibliography

[1] Aller H. D., Aller M. F. and Hughes P. A., 1985 *Ap. J.*, **298**, 296

[2] Aller H. D., Hughes P. A., Aller M. F., 1986 in *Superluminal Radio Sources*, ed. J. A. Zensus and T. J. Pearson, p. 273

[3] Angel J. R. P. and Stockman, 1980 *Ann. Rev. Astr. Ap.*, **18**, 34

[4] Barbieri C. *et al.*, 1988 *Preprint, submited to Astr. Ap. Suppl. Ser.*

[5] Barthel P., 1986 in *Superluminal Radio Sources*, ed. J. A. Zensus and T. J. Pearson, p. 148

[6] Barthel P. *et al.*, 1986 *Ap. J. (Letters)*, **310**, L7

[7] Begelman M.,Blandford R. and Rees M., 1984 *Rev. Mod. Phys.* vol. 56, n. 2, part 1

[8] Biermann P. and Strittmatter P. A., 1987 *Ap. J.*, **322**, 643

[9] Björnsson C., 1982 *Ap. J.*, **260**, 855

[10] Blandford R. and Königl A., 1979 *Ap. J.*, **232**, 34

[11] Blandford R. and McKee C. F. , 1977 *M.N.R.A.S.*, **180**, 343

[12] Blandford R. and Ostriker J. P., 1978 *Ap. J. (Letters)*, **221**, L29

[13] Bregman J. N., 1985 *Ap. J.*, **288**, 32

[14] Bregman *et al.*, 1986 *Ap. J.*, **301**, 708

[15] Bregman *et al.*, 1988 *Ap. J.*, **331**, 746

[16] Bridle A. H., Perley R. A., 1984 *Ann. Rev. Astr. Ap.*, **22**, 319

[17] Browne I., 1986 in *Superluminal Radio Sources*, ed. J. A. Zensus and T. J. Pearson, p. 129

[18] Clegg P. E. *et al.*, 1983 *Ap. J.*, **273**, 58

[19] Cohen M. H. *et al.*, 1971 *Ap. J.*, **170**, 207

[20] Cotton W. D. *et al*, 1980 *Ap. J. (Letters)*, **238**, L123

[21] de Bruyn A. G. and Schilizzi R. T., 1986 *I.A.U. Symp* n.119, p. 203

[22] de Ruiter H. R. *et al.*, 1986 *I.A.U. Symp* n.119, p. 197

[23] Eckart A. *et al*, 1985 *Ap. J. (Letters)*, **296**, L23

[24] Epstein E. E. *et al.*, 1982 *Astron. J.*, **87**, 449

[25] Garrington S. T., Leahy J. P., Conway R. G., Laing R. A., 1988 *Nature*, **331**, 147

[26] Gear W. *et al.*, 1985 *Ap. J.*, **304**, 295

[27] Ghisellini G., 1987 *Ph D Thesis* SISSA

[28] Ghisellini G., Maraschi L., Treves A., 1985 *Astr. Ap.*, **146**, 204

[29] Ghisellini G. *et al.*, 1986 *Ap. J.*, **310**, 317

[30] Hintzen P. *et al*, 1983 *Astron. J.*, **88**, 709

[31] Hough D. H. and Reahead A., 1986 in *Superluminal Radio Sources*, ed. J. A. Zensus and T. J. Pearson, p. 114

[32] Hughes P. A., Aller H. D. and Aller M. F., 1985 *Ap. J.*, **298**, 301

[33] Hughes P. A., Aller H. D. and Aller M. F., 1986 *Can. J. of Phys.*, **64**, 466

[34] Impey C., 1986 in *Superluminal Radio Sources*, ed. J. A. Zensus and T. J. Pearson, p. 233

[35] Jägers W. J., 1987 *Astr. Ap. Suppl. Ser.*, **71**, 75

[36] Jones T. W., 1982 *Bull. Am. Astron. Soc.*, **14**, 963

[37] Jones T. W., O'Dell S. L. and Stein W. A., 1974 *Ap. J.*, **188**, 353

[38] Jones T. W. and Tobin W., 1977 *Ap. J.*, **215**, 474

[39] Kapahi V. K., Kulkarni V. K., 1986 *I.A.U. Symp.*, n.119, p. 207

[40] Kellerman K. I., 1966 *Ap. J.*, **146**, 621

[41] Kellermann K. I., Pauliny-Toth I. I. K., 1981 *Ann. Rev. Astr. Ap.*, **19**, 373

[42] Kikuchi S. *et al*, 1988 *Astr. Ap.*, **190**, L8

[43] Königl A., 1981 *Ap. J.*, **243**, 700

[44] Kühr H. *et al*, 1981 *Astron. J.*, **86**, 854

[45] Laing R. A., 1988 *Nature*, **331**, 149

[46] Laing R. A. *et al.*, *M.N.R.A.S.*, **204**, 151

[47] Ledden J. E. and Aller H. D., 1978 *Pittsburgh Conference on BL Lac objects* ed. A. M. Wolfe, p. 60

[48] Lind K., Blandford R., 1985 *Ap. J.*, **295**, 358

[49] Madau P., Ghisellini G., Persic M., 1987 *M.N.R.A.S.*, **224**, 257

[50] Maraschi L., 1987 *X-Ray Variability on Galactic and Extragalactic Sources* ed. A. Treves, p.101

[51] Marcaide J. M. and Shapiro I. I., 1984 *Ap. J.*, **276**, 56

[52] Marscher A., 1978 *Ap. J.*, **219**, 392

[53] Marscher A., 1980 *Ap. J.*, **235**, 386

[54] Marscher A. and Gear W., 1985 *Ap. J.*, **298**, 114

[55] Morisawa K., Takahara F., 1987 *M.N.R.A.S.*, **228**, 745

[56] Norman M. L., Smarr L., Winkler K.-H. A. and Smith M. D., 1982 *Astr. Ap.*, **113**, 285

[57] O'Dell S. L., 1988 *Ap. J.*, **327**, 60

[58] O'Dell S. L. *et al.*, 1988 *Ap. J.*, **327**, 668

[59] Orr M. J. L., Browne I. W. A., 1982 *M.N.R.A.S.*, **200**, 1067

[60] Pacholczyk A. G., 1970 *Radio Astrophysics* (San Francisco:W. H. Freeman)

[61] Padrielli L. *et al*, 1987 *Astr. Ap. Suppl. Ser.*, **67**, 63

[62] Pearson T. J. and Readhead A., 1984 *I.A.U. Symp.* n. 110, p. 15

[63] Pearson T. J. and Readhead A., 1988 *Ap. J.*, **328**, 114

[64] Pearson T. J., Perley R. A. and Readhead A., 1985 *Astron. J.*, **90**, 738

[65] Perez Fournon I., 1985 *Tesis Doctoral* Universidad de La Laguna, Spain

[66] Perez Fournon *et al.*, 1988 *Ap. J. (Letters)*, **329**, L81

[67] Phynney E. S., 1985 *Astroph. of Active galaxies and quasi-stellar objects* ed. J. S. Miller p. 453

[68] Porcas R., 1985 *Active Galactic Nuclei* ed. Dyson p. 20

[69] Porcas R., 1986 in *Superluminal Radio Sources*, ed. J. A. Zensus and T. J. Pearson, p. 12

[70] Rees M., 1967 *M.N.R.A.S.*, **135**, 345

[71] Reynolds S. P., 1982 a,b *Ap. J.*, **256**, 13,28

[72] Roberts D. H. and Wardle J. F. C., 1985 *I.A.U Symp.* n. 119, p. 141

[73] Robson E. I. *et al.*, 1983 *Nature*, **305**, 194

[74] Romney J. *et al*, 1984 *Astr. Ap.*, **135**, 289

[75] Rybicki G., Lightman A., 1979 *Radiative Processes in Astrophysics* (John Wiley & sons)

[76] Scheuer P., 1986 in *Superluminal Radio Sources*, ed. J. A. Zensus and T. J. Pearson, p. 104

[77] Scheuer P., Readhead A., 1979 *Nature*, **277**, 182

[78] Sieber W., 1982 *Astr. Ap.*, **113**, 311

[79] Unwin S. C. *et al*, 1983 *Ap. J.*, **271**, 536

[80] Urry M., Mushotzky R., 1982 *Astron. J.*, **253**, 38

[81] Webb G. M., Drury L. O'C. and Biermann P., 1984 *Astr. Ap.*, **137**, 185

[82] Wilson M. J. and Scheuer P. A. G., 1983 *M.N.R.A.S.*, **205**, 449

[83] Witzel A., 1986 in *Superluminal Radio Sources*, ed. J. A. Zensus and T. J. Pearson, p. 83

[84] Zensus A. and Porcas R., 1986 in *Superluminal Radio Sources*, ed. J. A. Zensus and T. J. Pearson, p. 126